

Thermoactive Smart Electrospun Nanofibers

Anna Liguori, Stefano Pandini, Chiara Rinoldi, Nelsi Zaccheroni, Filippo Pierini, Maria Letizia Focarete, and Chiara Gualandi*

The recent burst of research on smart materials is a clear evidence of the growing interest of the scientific community, industry, and society in the field. The exploitation of the great potential of stimuli-responsive materials for sensing, actuation, logic, and control applications is favored and supported by new manufacturing technologies, such as electrospinning, that allows to endow smart materials with micro- and nanostructuring, thus opening up additional and unprecedented prospects. In this wide and lively scenario, this article systematically reviews the current advances in the development of thermoactive electrospun fibers and textiles, sorting them, according to their response to the thermal stimulus. Hence, several platforms including thermoresponsive systems, shape memory polymers, thermo-optically responsive systems, phase change materials, thermoelectric materials, and pyroelectric materials, are described and critically discussed. The difference in active species and outputs of the aforementioned categories is highlighted, evidencing the transversal nature of temperature stimulus. Moreover, the potential of novel thermoactive materials are pointed out, revealing how their development could take to utmost interesting achievements.

sensing, actuation, logic, and control are required. In the category of smart materials, stimuli-responsive systems, capable of altering their chemical and/or physical properties upon exposure to external stimuli (e.g., temperature, electric or magnetic field, pH, light, etc.), have a primary role. Undoubtedly, the world of polymers includes the widest variety of stimuli-responsive systems, able to “read” different physical, chemical, or biological stimuli and to “respond” by changing one or more of their properties.^[1,2] A library of stimuli-responsive polymeric systems has been developed, including thermoplastic and thermosetting polymers,^[3,4] elastomers,^[5] hydrogels,^[6] micro-nanoparticles,^[7] vesicles,^[8] supramolecular polymers,^[9] and hyperbranched polymers.^[10] Compared to other classes of materials, polymers possess enormous advantages in terms of processability, thus allowing the preparation of stimuli-responsive polymers with

a variety of shapes and morphologies, from the macro- to the nanodimensions.

Since smart materials perform their functions by communicating with the environment, nanotechnologies and miniaturization ensure a high surface-to-volume ratio to efficiently sense the surrounding. In this frame, an established technology is the electrospinning (ESP), which uses electrostatic forces

1. Introduction

A great challenge in today's material research is to develop functional smart materials that can actively self-adapt and/or sense changes occurring in the surrounding environment. This topic is of extreme interest for any kind of application where


A. Liguori, N. Zaccheroni, M. L. Focarete, C. Gualandi
 Department of Chemistry “G. Ciamician” and INSTM UdR of Bologna
 University of Bologna
 via Selmi 2, Bologna 40126, Italy
 E-mail: c.gualandi@unibo.it

S. Pandini
 Department of Mechanical and Industrial Engineering and INSTM UdR
 of Brescia
 University of Brescia
 via Branze 38, Brescia 25123, Italy

C. Rinoldi, F. Pierini
 Department of Biosystems and Soft Matter
 Institute of Fundamental Technological Research
 Polish Academy of Sciences
 5B Pawińskiego Str., Warsaw 02-106, Poland

M. L. Focarete
 Interdepartmental Center for Industrial Research on Health Sciences and
 Technologies
 University of Bologna
 Via Tolara di Sopra 41/E, Ozzano dell'Emilia 40064, Italy

C. Gualandi
 Interdepartmental Center for Industrial Research on Advanced
 Applications in Mechanical Engineering and Materials Technology
 University of Bologna
 Viale Risorgimento, 2, Bologna 40136, Italy

 The ORCID identification number(s) for the author(s) of this article can be found under <https://doi.org/10.1002/marc.202100694>

© 2022 The Authors. Macromolecular Rapid Communications published by Wiley-VCH GmbH. This is an open access article under the terms of the Creative Commons Attribution License, which permits use, distribution and reproduction in any medium, provided the original work is properly cited.

DOI: 10.1002/marc.202100694

to produce continuous nanometric and micrometric fibers, typically assembled into nonwoven mats.^[11] ESP obtained its first patents awarded in 1902^[12,13] but only in the 1990s this technology began to receive great attention from academia and industry.^[14–18] At first, research was devoted to understanding the effect of ESP parameters in successfully obtaining electrospun fibers^[19–21] and very soon their unique properties over their bulk and microscopic fiber counterparts have emerged. Among those, their large specific surface area and high porosity, as well as anisotropy,^[22] mechanical properties,^[23–25] and thermal conductivity^[26] have been highlighted. Nowadays, this technology is well established, allowing the production of multicomponents and multifunctional nonwovens with controlled fiber dimension, orientation,^[27,28] and functionalization,^[29–31] both at the lab and at the industrial scales.^[32–35] Electrospun materials are currently under investigation for applications that span from air and water filtration,^[36,37] to the biomedical field,^[38–40] catalytic systems,^[41,42] sensors,^[43,44] structural composites,^[45,46] and energy storage and harvesting.^[47–49] Thus electrospun platforms are expected to significantly impact socioeconomic aspects in the next few years.

This short digression on ESP aimed not only to introduce this technology but, above all, to underline once again its versatility that, for example, allows to electrospun inorganic species together with a polymer, a key point of fundamental importance for the preparation of smart nanofibers and textiles with different stimuli responsiveness. In this framework, it is important to mention the work by Duan and their co-workers^[50] that provides an updated overview of smart electrospun fibers capable of actively interacting with the environment by capturing stimuli, such as temperature changes, electrical field, light, and pH changes.

Within all the possible physical stimuli, in this review we want to focus the attention on temperature stimulation, due to its transversal and widespread applications; as it is well known, temperature variations play a crucial role in regulating the biological activities, the physical state of matters and the environment. Similarly, also in the field of smart materials, temperature-responsiveness induces macroscopic effects that can involve phase transitions,^[3] changes in supramolecular structures,^[51] conformational changes,^[52] and changes in molecular architecture.^[53,54] A great advantage of using smart materials sensitive to temperature is that the thermal stimulus can also be indirectly induced by light (i.e., photothermal effect), magnetic field (magnetothermal effect), and electrical field (Joule effect), upon the addition of proper additives that act as internal heating sources. This creates the possibility to apply a spatial and time-dependent stimulation with good resolution in space and time.^[55–59] Above all, electrospun fibers, being characterized by high surface-to-volume ratio and high porosity, display enhanced sensitivity to the temperature changes of the environment and fast responsiveness when compared to their bulk counterparts.^[60–63]

Fascinated by the versatility and potentialities of this area, in this review, we aim at presenting a comprehensive picture of the state of the art of electrospun fibers that actively respond to a change of temperature with different outputs. For illustrative simplicity, the discussion is arranged by dividing thermoactive materials into specific categories (**Figure 1**): i) thermorespon-

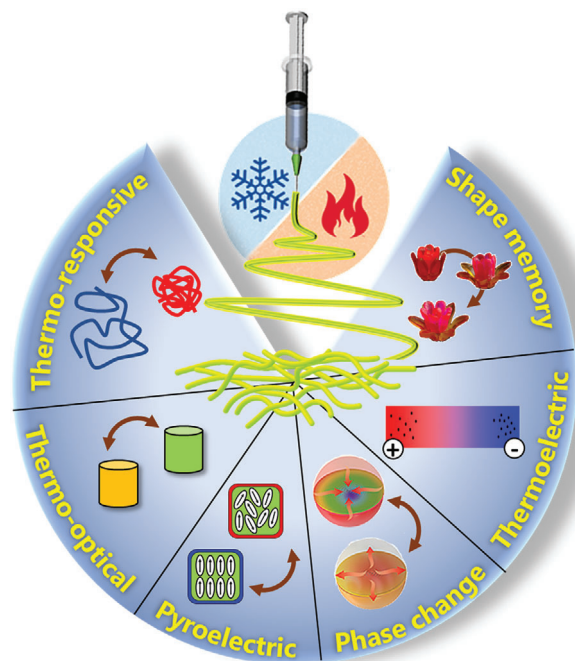


Figure 1. Overview of thermoactive electrospun smart materials.

sive systems; ii) shape memory polymers; iii) thermo-optically responsive systems; iv) phase change materials; v) thermoelectric materials; vi) pyroelectric materials. In particular, thermoresponsive systems work in the presence of a solvent (typically water) by changing their solubility and swellability as a function of temperature, while shape memory polymers modify their shape, among two or more. Materials that change their optical properties are generally called thermo-optically responsive systems, comprising both thermochromic and thermoluminescent materials, and their processing into electrospun fibers is not yet widely explored. We have included in this review also electrospun fibers containing phase change materials, able to actively accomplish functions like thermal regulation and heat storage, by exploiting their capability to absorb and release heat. Electrospun fibers constituted by thermoelectric and pyroelectric components are also of high interest due to their promising role in converting waste heat into electricity. All these categories are very different and we have preferred, for each of them, to briefly introduce the working principles and, by reviewing the main specific literature, we have analyzed in detail the different ESP approaches adopted for their processing into fibers, highlighting, when applicable, the pros and cons. Finally, wide space is given to the possible applications with the intent to inspire scientists and engineers for the rational design of thermoactive electrospun fibers with properties tuned to a specific use.

2. Thermoresponsive Electrospun Fibers

Thermoresponsive nanofibers able to show a drastic volume change in water upon temperature variation are generating considerable interest as smart materials. This particular attitude is due to the presence, in the fiber composition, of polymeric chains showing either a lower critical solution temperature

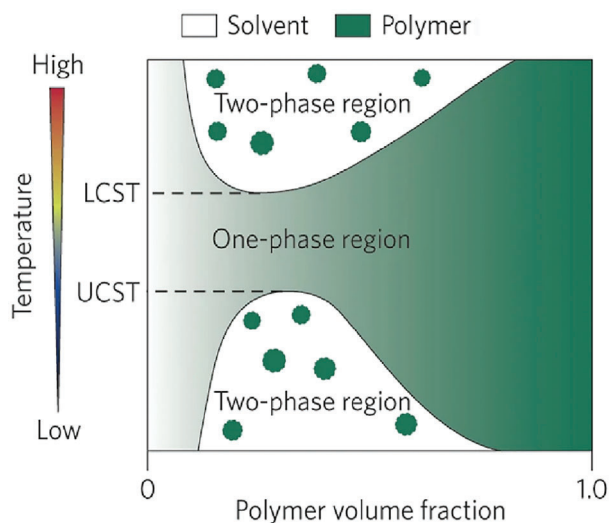


Figure 2. Scheme presenting phase transitions connected to LCST and UCST behavior of thermoresponsive polymer chains in liquid. Reproduced with permission.^[65] Copyright 2015, Nature Publishing Group.

(LCST) behavior or an upper critical solution temperature (UCST) behavior. In this chapter, a general description of LCST- and UCST-type polymers will be provided, followed by a focus on the crosslinked polymeric systems showing a volume phase transition temperature (VPTT). The most common methods employed for the production of thermoswellable nanofibers will be described and eventually an overview of the proposed applications will be presented (Table 1).

2.1. LCST, UCST, and VPTT in Thermoresponsive Polymers

The term “thermo-responsive polymers” defines those polymers possessing temperature-dependent miscibility, which determines exceptional sol–gel transition above and/or below a specific temperature; when these polymer chains are dissolved in solutions they assume a well-solvated coil conformation that, depending on the temperature, can agglomerate and/or precipitate in collapsed globule, thus creating typical colloidal systems stabilized by polymer–polymer hydrophobic interactions.^[64] Such a kind of smart polymers are classified into two different groups according to their behavior: the first group includes macromolecular chains that experience coil-to-globule transition above a temperature defined as lower critical solution temperature (LCST); contrarily, the second group shows coil-to-globule transition below a specific temperature, called upper critical solution temperature (UCST) (Figure 2).^[65]

The first class of thermoresponsive polymers is generally well dissolved in water at room temperature, but their solubility suddenly drops when overcoming the LCST. Poly(N-isopropylacrylamide) (PNIPAAm) is undoubtedly the most studied and applied LCST polymer, with a LCST value equal to 32 °C.^[66] On the other hand, UCST polymers, such as polyacrylamide and poly(acrylamide-co-butyl methacrylate), precipitate when the temperature of the solution drops below UCST.^[67,68] Moreover, it is worth mentioning that some polymers may show both LCST and UCST behaviors.^[69]

Most of the thermoresponsive polymers are amphiphilic and their unique behavior can be explained, from the thermodynamic point of view, by considering both the enthalpic and the entropic contributions to polymer dissolution; for both LCST and UCST polymers, the precipitation at the transition temperature is due to polymer–polymer interactions becoming more thermodynamically favored than polymer–water interactions. In a simplified view, LCST polymers precipitate when polymer–water interactions, which are favored in the coil conformation, become unstable as temperature rises, since the negative enthalpy of mixing is compensated by the entropic term. Conversely, in UCST systems polymer–polymer H-bonds and ionic interaction are favored at low temperature, resulting in a globule conformation, and solubilization is obtained upon heating by destroying these interactions. According to this thermodynamic explanation, it is not surprising that LCST and UCST systems are strongly affected by several system parameters such as the polymer concentration,^[70] molecular weight,^[71] the inclusion of a second monomer into polymer chains,^[72] as well as the presence of additional substances into the systems, as surfactants,^[73] salts,^[74] or a second solvent.^[75] More details on the thermodynamic aspects and on the possibility to properly design the response of thermoresponsive polymers can be found in an article published by Zhao et al.^[76] Such versatility opens the way to finely tune the temperature range of responsivity, an extremely important aspect for biomedical applications since transition should take place close to the body temperature.^[77]

The thermodynamics at the basis of LCST and UCST behavior can be exploited also in crosslinked systems to form hydrogels with a thermoresponsive degree of swelling.^[78] Hydrogels are 3D networks of either hydrophilic or amphiphilic polymers able to host water in their structure. Hydrogels made of crosslinked thermoresponsive polymers show a drastic variation in their volume when the environmental temperature overcomes the typical volume phase transition temperature (VPTT). In particular, thermophobic hydrogels, based on LCST-type behavior, collapse with the increase of the temperature and the water contained in the polymeric material is ejected out from the structure,^[79] while UCST-type hydrogels show the opposite behavior.^[80] Thus, VPTT hydrogels can change their water content,^[81] structure morphology,^[82] mechanical,^[83] and optical properties,^[84] which make them one of the most studied stimuli-responsive polymer systems.

2.2. Electrospinning Approaches for the Production of Thermoresponsive Fibers

2.2.1. Direct Electrospinning of Thermoresponsive Polymers

Pure PNIPAAm has been successfully electrospun from several solvents such as water, acetone, tetrahydrofuran,^[85] methanol,^[86] and hexafluoroisopropanol (HFIP).^[87] However, to avoid fiber dissolution below LCST, a post-crosslinking treatment is necessary. In one case, thermal crosslinking has been applied on PNIPAAm fibers containing a polyhedral oligomeric silsesquioxane (POSS) and a catalyst previously added to the starting solution.^[88] More often, chain crosslinking is accomplished by polymerizing NIPAAm with N-methylolacrylamide (NMA), whose methylol groups self-condense at high temperature generating methy-

Table 1. Types of thermoresponsive electrospun systems, classified in terms of ESP approach, material, class, cloud point, and applications (n.a.: not available).

Fabrication strategy	Material	Thermoresponsive class	Cloud point [°C]	Application	Refs.
Direct ESP	Uncrosslinked PNIPAAm	LCST	n.a.	Basic research	[85–87]
Direct ESP	PNIPAAm crosslinked with POSS	LCST	30–32	Basic research	[88]
Direct ESP	Crosslinked P(NIPAAm-co-NMA)	LCST	37–39	Basic research	[89]
Direct ESP	Crosslinked P(NIPAAm-co-NMA-co-rhodamine derivative)	LCST	30–45	Sensor of pH, temperature, and Hg ²⁺	[90]
Direct ESP	Crosslinked P(NIPAAm-co-NMA) + Fe ₂ O ₃ NPs	LCST	43	Magnetic field assisted drug release	[91]
Direct ESP	P(MMA-co-NIPAAm-co-AA) Poly(methyl methacrylate-co-N-isopropylacrylamide-co-acrylic acid)	LCST	38–52	Drug delivery	[92]
Direct ESP	P(MMA- <i>b</i> -NIPAAm)	LCST	n.a.	Oil/water separation	[63]
Direct ESP	Crosslinked P(NIPAAm-co-stearyl acrylate)	LCST	30–32	Basic research	[93]
Direct ESP	Crosslinked P(NIPAAm-co-NMA-co-AA)	LCST	31–43	Drug delivery	[95]
Direct ESP	Crosslinked P(VCL-co-NIPAAm)	LCST	31.5–37.4 °C	Drug delivery	[97]
Direct ESP	Crosslinked P(VCL-co-MMA)	LCST	33–37.2 °C	Drug delivery	[98]
Direct ESP	Crosslinked poly(acrylamide-co-acrylonitrile)	UCST	20–48 °C	Actuators	[99]
Direct ESP	Crosslinked P(NIPAAm-co-NMA) + magnetic NPs	LCST	48 °C	Drug delivery	[128]
Direct ESP	Crosslinked P(NIPAAm-co-NMA) + Ag NPs	LCST	n.a.	Basic research	[126]
Direct ESP	Crosslinked poly(hydroxyethylacrylate-co-coumaryl acrylate-co-ethylmethacrylate)	LCST	20–40 °C	Drug delivery	[127]
Direct ESP	Crosslinked P(NIPAAm-co- benzophenone)	LCST	18 °C	Cell capture	[61]
Direct ESP	Polyfluorene- <i>b</i> -PNIPAAm- <i>b</i> -PNMA	LCST	35.9–39.1 °C	Sensors	[125]
Direct ESP	Crosslinked P(NIPAAm-co-NMA)	LCST	39.2–52.9 °C	Sensors	[131]
Direct ESP	Crosslinked P(NIPAAm-co-NMA-co-4-rhodamine hydrazonomethyl-3-hydroxy-phenyl methacrylate)	LCST	55–62 °C	Sensors	[132]
Blend ESP	P(2,7-(9,9-dihexylfluorene)- <i>b</i> -NIPAAm) + PMMA	LCST	30–32 °C	Sensors	[130]
Blend ESP	PNIPAAm+PCL	LCST	n.a.	Cell sheet	[100]
Blend ESP	PCL (core)/PNIPAAm (shell)	LCST	32 °C	Basic research	[115]
Blend ESP	PCL (core)/crosslinked PNIPAAm conjugated with BSA (shell)	LCST	32 °C	Blood erythrocyte capture	[116]
Blend ESP	P(NIPAAm- <i>b</i> -LLA) + PLLA	LCST	n.a.	Drug delivery	[133]
Blend ESP	PNIPAAm + PLLA	LCST	29 °C	Basic research	[101]
Blend ESP	PNIPAAm + PEO	LCST	n.a.	Drug delivery	[102]
Blend ESP	PNIPAAm + PAN	LCST	n.a.	Oil/water separation	[103]
Blend ESP	PNIPAAm + PU	LCST	31–45 °C	Drug delivery	[104]
Blend ESP	P(NIPAAm-co-AA) + PU	LCST	34–38 °C	Drug delivery	[105]
Blend ESP	Crosslinked PNIPAAm + gelatin	LCST	37–40 °C	Drug delivery	[106]
Blend ESP	Crosslinked P(NIPAAm-co-NMA) + chitosan	LCST	37.2–28.1 °C	Metal ion removal	[107]
Blend ESP	Crosslinked PNIPAAm + PEKc	LCST	n.a.	Basic research	[108]
Blend ESP	PVCL + cellulose	LCST	40–50 °C	Basic research	[109]
Blend ESP	P(D,L)LA + PDEGMA/SH	LCST	22 °C when heated; <18 °C when cooled	Cell expansion and phenotype support	[110]
Coaxial ESP	Crosslinked PNIPAAm (core)/PEG ³ + PCL (shell)	LCST	34–50 °C	Drug delivery	[111]
Coaxial ESP	Crosslinked P(NIPAAm-co-NMA) (core)/PLCL (shell)	LCST	37 °C	Drug delivery	[112]
Coaxial ESP	PAN (core)/crosslinked P(VCL-co-AA) (shell)	LCST	34–38 °C	Water capture	[113]
Core-shell fibers	Cellulose acetate (core) /crosslinked PNIPAAm (shell)	LCST	34 °C	Water capture	[114]
Surface functionalization	Crosslinked PMMS/PS functionalized with maleimide-terminated poly(N-isopropylacrylamide)	LCST	n.a.	Basic research	[117]

(Continued)

Table 1. (Continued).

Fabrication strategy	Material	Thermoresponsive class	Cloud point [°C]	Application	Refs.
Surface functionalization	Regenerated cellulose functionalized with crosslinked PNIPAAm	LCST	32 °C when heated; <29 °C when cooled	Oil/water separation	[118]
Surface functionalization	PET functionalized with crosslinked PNIPAAm	LCST	32 °C	Basic research	[119]
Surface functionalization	PHBV functionalized with crosslinked PNIPAAm	LCST	32 °C	Cell passaging	[120]
Surface functionalization	PCL functionalized with crosslinked PNIPAAm	LCST	32 °C	Drug delivery	[121]
Composites	Crosslinked P(NIPAAm-co-NIPMAAm) + gold nanorods hydrogel encapsulated between two nanofibrous PLLA + rhodamine B layers	LCST	37 °C	Drug delivery	[122]
Composites	Electrospun PMMA fibers attached to flexible PET substrates, encapsulated in PET foils, and covered with crosslinked PNIPAAm hydrogel sheets	LCST	n.a.	Drug delivery	[123]
Composites	Crosslinked 3D printed PNIPAAm + clays deposited on crosslinked PNIPAAm fibers	LCST	32 °C	Thermal actuators	[124]
Composites	Crosslinked P(NIPAAm-co-AA) fibers embedded within a passive thermoplastic PU matrix	LCST	12 °C	Multiresponsive actuators	[94]

^{a)} PEG: poly(ethylene glycol).

lene bridges. Depending on crosslinking conditions and NMA content, fibers with tunable swelling degree and cloud point can be produced.^[89–91] In particular, the increase of NMA content induces the formation of a dense crosslinked network that contributes to limit fiber solubility but decreases the mat shrinkage above LCST and increases the cloud point.^[90]

Thermoplastic PNIPAAm-based copolymers have also been electrospun, with the aim of gaining stable thermoresponsive fibers in water. In this case, the type and the amount of the counit provide stable hydrophobic interactions that limit polymer solubilization and tune the swelling degree and cloud point, some examples being poly(methyl methacrylate-co-N-isopropyl acrylamide) [P(MMA-co-NIPAM)],^[63,92] poly(methylmethacrylate-*b*-N-isopropylacrylamide) [P(MMA-*b*-NIPAAm)]^[63] and poly(N-isopropylacrylamide-co-stearyl acrylate).^[93] The inclusion of acrylic acid units in PNIPAAm-based copolymers, stabilized either by chemical crosslinks or by hydrophobic interactions, is largely exploited to tune the LSCT of the resulting copolymer, as well as to couple its thermoresponsivity with pH sensitivity.^[92,94,95]

ESP was also applied to poly(vinyl caprolactam) (PVCL), another well-studied thermoresponsive polymer with LCST in the range 32–34 °C.^[96] Similar to P(NIPAAm-co-NMA), P(VCL-co-NMA) fibrous hydrogels were produced by ESP followed by thermal crosslinking, to study the effect of NMA content on polymer solubility and volume changes. In this frame, the increase of NMA units and curing time determines an increment in the cloud point temperature and a concomitant decrease of solubility in water and of shrinking degree.^[97] Counits of methyl methacrylate have been also copolymerized with VCL to obtain uncrosslinked P(VCL-co-MMA) whit tunable solubility, cloud point, and swelling degree.^[98]

The first example of UCST-type electrospun fibers was presented by Liu et al.,^[99] as a series of terpolymers of acrylamide (AAm), acrylonitrile (AN), and 4-acryloyloxybenzophenone

(BPA) prepared via RAFT polymerization, that could be electrospun and subsequently photocrosslinked via UV irradiation.

2.2.2. Thermoresponsive Fibers from Blend Electrospinning

Blending thermoresponsive polymers with electrospinnable polymers is a possible approach for successfully fabricating thermoresponsive polymer-based fibers, widely adopted due to its simplicity. Thermoresponsive PNIPAAm homopolymer and copolymers can be blended with other polymers, such as polycaprolactone (PCL),^[100] polylactic acid (PLA),^[101] poly(ethylene oxide) (PEO),^[102] polyacrylonitrile (PAN),^[103] vv polyurethane (PU),^[104,105] gelatin,^[106] and chitosan.^[107] More specifically, it was shown that the addition of a second polymer did not negatively affect the thermoresponsivity of PNIPAAm, since the wettability test revealed the hydrophilic behavior of the constructs at room temperature and their switch to hydrophobic behavior at high temperature.^[101,103–105] Furthermore, PNIPAAm has also been blended with reinforcing polymers in order to improve its mechanical properties. In this frame, Wang et al. electrospun poly(aryl-1-ether ketone-cardo) (PEKc) mixed with PNIPAAm, obtaining fibrous structures with enhanced mechanical and thermoresponsive characteristics.^[108] Despite the simplicity of the blending approach, a partial PNIPAAm loss from the blended fibers due to polymer dissolution below LCST was reported,^[100,104] albeit in most studies this aspect is not explored.

Other temperature-responsive polymers, e.g., PVCL and poly(di(ethylene glycol) methyl ether methacrylate) (PDEGMA), have been explored to create thermoresponsive blended electrospun fibers. In this frame, PVCL was blended with cellulose and electrospun in order to fabricate tunable thermoresponsive nanofibers.^[109] On the other hand, the blending of PDEGMA with PLA reveals an excellent potential for producing temperature-responsive fibrous architectures.^[110]

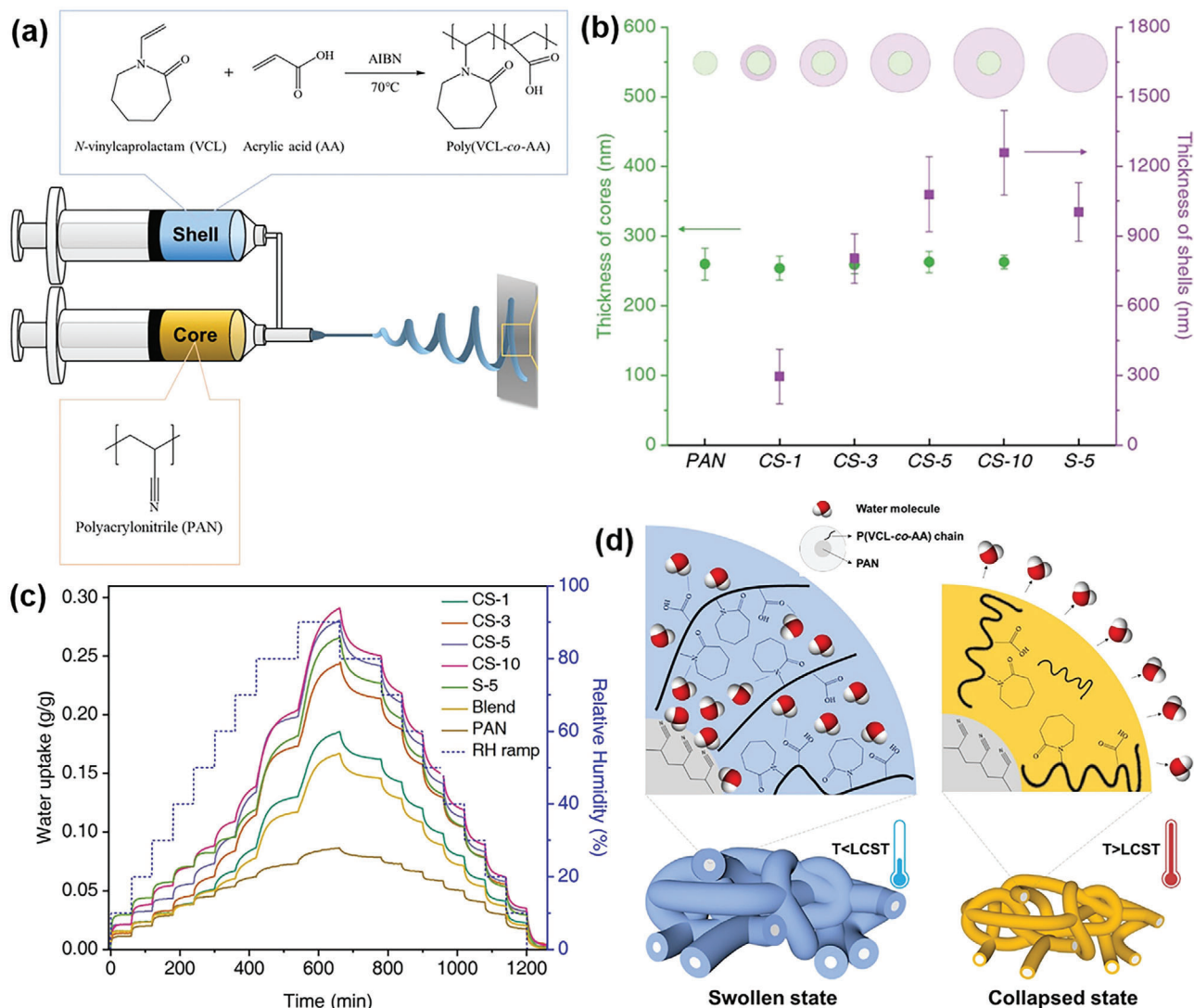


Figure 3. a) Preparation of thermoresponsive P(VCL-co-AA)/PAN core-shell nanofibers by coaxial electrospinning; b) core and shell thickness of nanofibers obtained by changing shell flow rate; c) water uptake kinetics of the investigated nanofiber at 25 °C and at various relative humidity; d) illustration of water collection and release by the thermally responsive core-shell nanofiber. Reproduced with permission.^[113] Copyright 2019, American Chemical Society.

2.2.3. Core-Shell Thermoresponsive Fibers

Thermoresponsive polymers have been also employed in the realization of core-shell fibrous architectures. In this frame, the thermoresponsive polymers have been applied either as the core of the fibrous structure^[111,112] or as the fibers' shell.^[113,114] In regard to confining thermoresponsive polymers into the fiber core, Pawłowska et al. developed a temperature-sensitive fibrous system composed of a core of poly(*N*-isopropylacrylamide-*co*-*N*-isopropylmethacrylamide) P(NIPAAm-*co*-NIPMAAm) copolymer and a shell of poly(*L*-lactide-*co*-caprolactone) (PLCL). In order to spin the fibers, the solutions flowed into a coaxial needle during the ESP process, allowing the production of hydrogel-based core-shell nanofibers upon in situ crosslinking.^[112] An example of thermoresponsive polymer located at the shell was reported by Kim and Choi.^[113] By using a coaxial needle, they fab-

ricated temperature-responsive core-shell nanofibers made by a core of PAN surrounded by a shell of poly(*N*-vinylcaprolactam-*co*-acrylic acid) P(VCL-*co*-AA), where VCL units provide thermoresponsiveness, AA units self-crosslink at high temperature and increase the shell hydrophilicity, PAN provides high mechanical, thermal, and chemical resistance (Figure 3a). By changing the flow rate of the shell fluid, it was possible to finely tune the shell thickness (Figure 3b) and, consequently, the wettability and the water absorption capability of the fibers (Figure 3c,d).

Some groups reported the obtention of core-shell PCL/PNIPAAm fibers by using single-spinneret ESP thanks to the phase separation occurring during fiber solidification that drives the PNIPAAm either to fiber surface^[115,116] or to fiber core,^[100] depending on the solvent used for the process and on PNIPAAm molecular weight. In particular, when a low molecular weight PNIPAAm ($M_n = 20\text{--}25$ kDa) was electrospun

from a dimethylformamide chloroform mixture, fibers with PNIPAAm-enriched surface were obtained, while the use of a high molecular weight PNIPAAm in a mixture of methanol and chloroform led to fibers where the thermo-responsive polymer was preferentially located in the core.

2.2.4. Fibers Surface Functionalized with Thermo-responsive Polymers

Another interesting approach to obtain temperature-sensitive nanofibers consists in postfunctionalizing the electrospun fiber surface with thermo-responsive polymers. In this frame, Yang et al.^[117] electrospun poly((3-mercaptopropyl)methylsiloxane) (PMMS) fibers carrying thiol groups at the surface from a photocurable mixture of polystyrene (PS), with PMMS, a crosslinking agent and a photoinitiator, obtaining continuous fibers by in situ photopolymerization during ESP. PMMS fibers were then surface functionalized with a maleimide-terminated PNIPAAm via thiol-ene click chemistry by following a “grafting to” approach. The presence of PNIPAAm coating was verified by Fourier-transform infrared spectroscopy (FTIR) and X-ray photoelectron spectroscopy (XPS), while the temperature responsiveness was assessed by water contact angle measurements at different temperatures. A “grafting from” approach was instead applied by Wang et al.^[118] to functionalize the surface of regenerated cellulose electrospun fibers with PNIPAAm brushes. More in detail, cellulose acetate electrospun fibers were subjected to hydrolysis in a strong base that allowed the attachment of initiator molecules on the surface, thus permitting the grafting of PNIPAAm brushes on the cellulose nanofibers by surface-initiated atom transfer radical polymerization (SI-ATRP). The obtained mat shows temperature-switchable superlyophilic/superlyophobic properties. In another study, SI-ATRP was used to prepare thermo-responsive poly(ethylene terephthalate) (PET) fibers coated with PNIPAAm brushes.^[119]

Ko et al. developed a poly(3-hydroxybutyrate-co-3-hydroxyvalerate) (PHBV) fibrous structure functionalized with thermo-responsive PNIPAAm grafted by electron beam irradiation. FTIR spectroscopy confirmed the achievement of surface functionalization, while contact angle measurements proved the temperature-responsive properties of the developed fibrous architecture.^[120] In another research, a PCL nanofibrous surface was functionalized by coating the fibrous matrix with thermo-responsive PNIPAAm crosslinked in situ under UV light.^[121]

2.2.5. Hybrid Systems

Recent promising strategies for the fabrication of thermo-responsive platforms include the combination of thermo-responsive polymers and synthetic electrospun nanofibers as two distinct components. This approach has been considered one of the most exciting alternatives since the developed devices can benefit from the advantages of both compartments and their synergistic effects. In this frame, Nakielski et al.^[122] designed and produced a nanostructured system by combining two external layers of PLA electrospun nanofibers, loaded with a drug model,

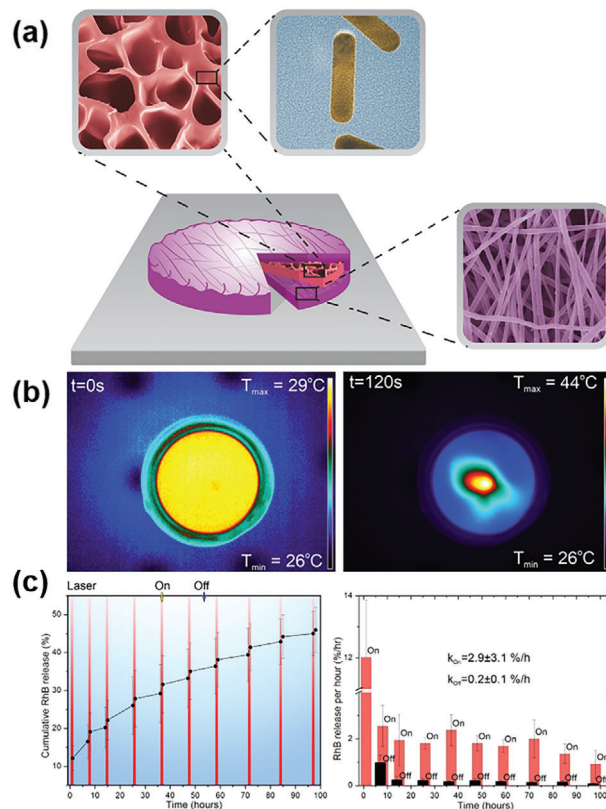


Figure 4. a) Schematic representation of a nanostructured platform composed of P(NIPAAm-co-NIPMAAm) hydrogel loaded with gold nanorods and incorporated between two layers of PLLA electrospun fibers loaded with a drug model. b) Thermographic images of the nanostructured pillow recorded during laser irradiation, showing the fast thermo-responsiveness of the proposed platform. c) Drug model delivery characteristics of the nanostructured pillow: cumulative (left) and hourly (right) release after 10 on-off laser irradiation cycles. Reproduced under the terms of the Creative Commons Attribution 4.0 International License (<http://creativecommons.org/licenses/by/4.0/>).^[122] Copyright 2020, American Chemical Society.

with an internal core of bulk thermo-responsive P(NIPAAm-co-NIPMAAm) hydrogel containing gold nanorods (Figure 4a). The authors demonstrated that the proposed pillow platform possessed fast photothermal responsiveness upon NIR light irradiation, allowing a controlled on-demand drug delivery. More in detail, the designed system-generated reversible cascade-like structural changes activated by NIR light, provoking the shrinkage of the platform and the increase of temperature up to 44 °C (Figure 4b). This led to the rapid expulsion of water from the inner structure, accelerating the drug model release kinetics (Figure 4c).

Evanghelidis et al. proposed to cover an electrospun microfibrillar structure made of gold-sputtered poly(methyl methacrylate) (PMMA) with a PNIPAAm thermo-responsive hydrogel layer and were able to create a flexible construct for transdermal drug release upon electrical heating.^[123] In another research, a combined system composed of PNIPAAm electrospun fibrous mesh and 3D printed PNIPAAm loaded with clays was developed. The 3D printed PNIPAAm/clay was deposited onto the electrospun structure, forming a layered construct. In this case, exploit-

ing the thermo-responsivity of PNIPAAm and the swelling mismatch between the layers, the authors could achieve the production of several hydrogel actuators with distinctive responsive behaviors.^[124] The same group prepared other thermal actuators by embedding P(NIPAAm-co-AA) fibers into a passive thermoplastic polyurethane (TPU), obtaining composites with a gradient concentration of TPU along with the thickness and capable of bending and rolling upon either a temperature or a pH variation.^[94]

2.3. Applications of Thermo-responsive Electrospun Fibers

The unique and outstanding properties of thermo-responsive polymer-based electrospun fibers make them great candidates to be exploited in several fields. Among others, biomedical, sensor, actuators, and filtration applications as well as separation processes have been widely explored.

In the biomedical field, bioactuators based on thermo-responsive electrospun fibers can be used for artificial muscle application,^[94,124] while the temperature sensitivity of the polymers can be valorized during cell culture passaging and expansion,^[110] anisotropic cell sheet formation,^[100] as well as cell isolation from body fluids and successive release.^[116,125] In one example, electrospun fibers of PLA blended with poly(di(ethylene-glycol) methyl ether methacrylate-co-poly(di(ethylene-glycol) thiol (PDEGMA/SH) surface-functionalized with a cell adherence peptide sequence were used to support the growth of human corneal stromal cells (hCSCs). The LCST-type behavior of PDEGMA enabled the detachment of adherent hCSCs cells from the scaffold when placed at 4 °C for 30 min as a consequence of scaffold swelling, thus avoiding the use of enzymatic treatments for cell passaging that can reduce cell quality.^[110] In another example, erythrocytes from blood were selectively captured by a mesh of core/shell fibers of PCL/crosslinked PNIPAAm conjugated with bovine serum albumin (BSA), thanks to the establishment of hydrophobic interactions between fibers and cells at 37 °C, whereas at 25 °C the hydrophilic surface of nanofibers determines the release of erythrocytes.^[116] Additionally, thermo-responsive P(NIPAAm-co-NMA) electrospun fibers have been combined with electrically conductive Ag particles in order to create devices able to generate an electrical response to temperature variations, suitable for the design and fabrication of wearable healthcare electronics.^[126]

Thermo-responsive polymers can be also designed as drug carriers, permitting the tunable on-demand drug release in dependence on temperature changes. In this frame, several kinds of drugs (e.g., antibiotics, anti-tumors, calcium channel blockers, and curcumin) and drug models (e.g., rhodamine) have been assessed.^[95,98,105,106,112,127,128] Researchers have demonstrated that the release rate can be controlled by optimizing a few key factors, such as the composition and concentration of the fibrous materials (i.e., concentration of polymers and loaded drug) as well as temperature and pH of the releasing medium.^[95,105,127] In a study conducted by Kin et al.,^[128] a crosslinked P(NIPAAm-co-NMA) fibrous matrix loaded with an anti-cancer drug (i.e., doxorubicin) and magnetic nanoparticles (MNPs), used as heating source, was developed (Figure 5a,b). By applying an alternating magnetic field (AMF), authors could achieve an “on-off” release of the drug,

leading to the death of about 70% of human melanoma cells in only 5 min application of AMF by a combined effect of heat and drug (Figure 5c,d).

In another study, P(VCL-co-MMA) fibers have been exploited for the release of a hydrophobic anticancer drug, Erlotinib, that was either incorporated in the fibers or introduced in a drug reservoir surrounded by the thermo-responsive mesh. In the first case, the drug was released below LCST, when the swollen polymer chains allowed the leaching out of Erlotinib, while above LCST the drug release was hampered by chain contraction and hydrophobic environment. The opposite behavior was found when the drug, incorporated in a reservoir, had to cross the mesh to be leached out. In this case, the swollen state of the mesh below LCST reduced the porosity and slowed down the drug release, while the collapsed state above LCST, characterized by bigger pores, allowed a faster drug release.^[98] In another example, water-soluble BSA was incorporated in fibers composed of PCL and a thermo-responsive multiblock PU.^[129] In this case, the protein release was faster at 37 °C than at 25 °C. Indeed, at 25 °C the swollen fiber is capable of retaining the hydrophilic BSA but at 37 °C the water is expelled from the nanofiber mat together with BSA.

Additionally, sensory devices based on thermo-responsive polymer fibers have also been largely explored. A few studies report the design of systems that can control and tune the photoluminescence of fluorophore covalently attached to PNIPAAm blocks: here the collapse of polymer chains above LCST induces the formation of fluorophore aggregates, accompanied by a decrease in the emission intensity, revealing their great potential for thermo-sensitive colorimetric sensor applications.^[130,61] On the other hand, electrospun thermo-responsive platforms have also been exploited to detect^[90,131,132] as well as to remove metal ions.^[107] In this frame, Chen et al. developed multifunctional fibrous fluorescent chemosensors made of P(NIPAAm-co-NMA-co-rhodamine derivative), demonstrating that the platform is not only temperature sensitive but can also detect pH variations and the presence of mercury ions. Thanks to these outstanding properties, authors could observe reversible changes in fluorescence in response to pH variations.^[90]

Finally, thermo-responsive polymers can also be used for oil/water separation purposes by switching from hydrophilic to lipophilic behavior in response to temperature variations.^[63,103,118] For instance, Li et al. have developed a thermo-responsive membrane of P(NIPAAm-*b*-MMA) capable of filtrating water from a mixture of water/*n*-hexane at a temperature below its LCST, while, being hydrophobic above LCST, *n*-hexane could cross the membrane pores.^[63] The same principle has been applied for capturing water at low temperature and releasing it at high temperature.^[113,114] As an example, core-shell fibers made of a core of PAN and a shell of P(VCL-co-AA) showed a temperature-triggered wettability change, with a water absorption capability of more than 200% at 25 °C that drops down to 20% at 50 °C (Figure 3c,d).^[113]

3. Shape Memory Electrospun Fibers

Among the thermally responsive polymers, one of the most studied classes is that featuring the so-called shape memory effect. Polymers belonging to this class are also known as shape mem-

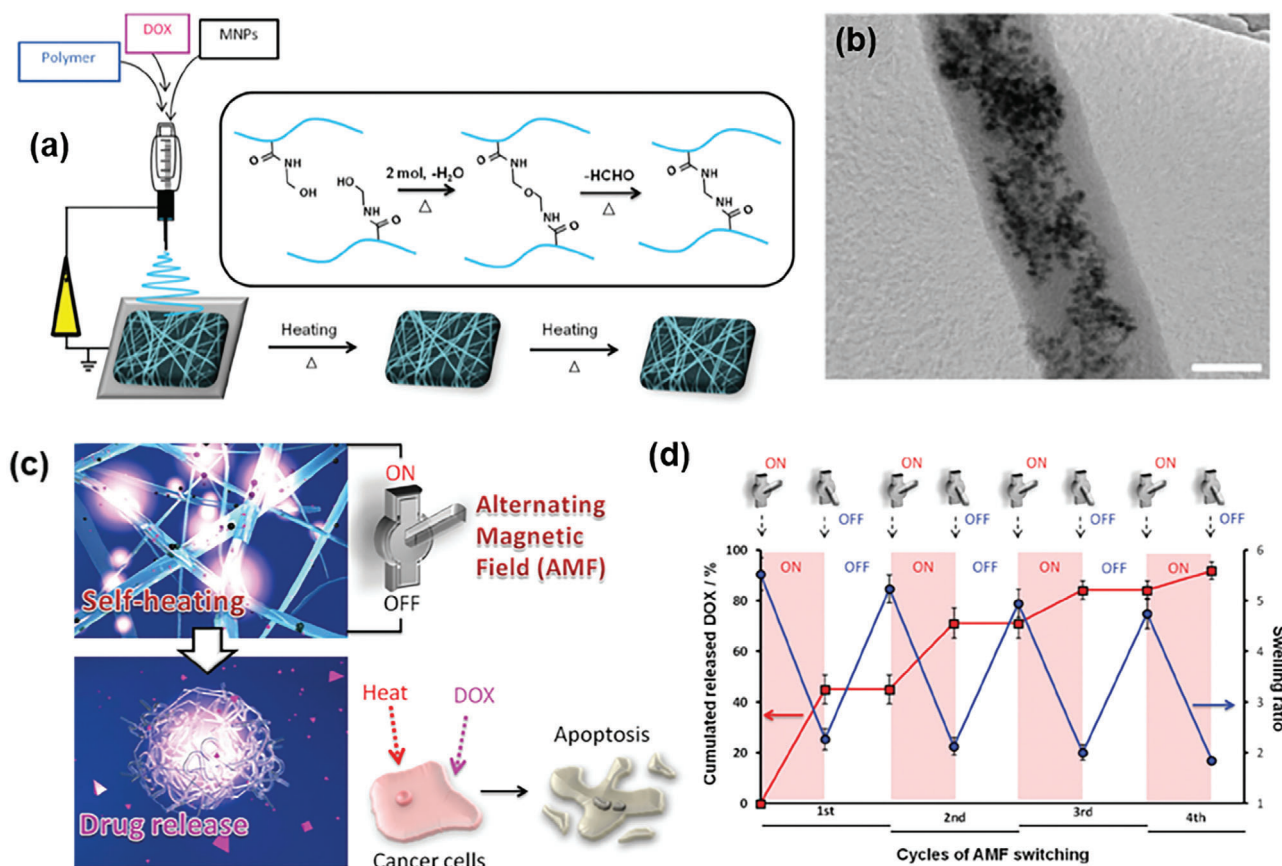


Figure 5. a) Preparation of thermally-crosslinkable temperature-responsive P(NIPAAm-co-NMA) nanofibers by ESP and thermal curing. b) TEM image of the MNPs-nanofibers with 31 wt% of MNPs after thermal curing (scale bars 200 nm). c) Design concept for the smart hyperthermia nanofiber system: AMF is turned “on” to thermally activate the MNPs in the nanofibers that induce collapsing of the polymer networks, allowing the “on–off” release of DOX. d) “On–off” switchable cumulative release of DOX and swelling ratio of crosslinked MNPs-nanofibers by applying of AMF cycles. Adapted with permission.^[128] Copyright 2013, Wiley Interscience.

ory polymers (SMPs) and they show the capability to significantly change their shape among various previously memorized, upon the application of a thermal stimulus. This effect is studied since the 60s, when it concerned crosslinked polyethylene shrinking tubes, it was revived in the 80s on PU systems for the car industry, but the most consistent efforts followed the seminal review of Lendlein and Kelch.^[134] The great interest toward the study of such peculiar materials relies on their ability to recover even large deformations, the relatively ease to tailor their shape memory response, and the wide spectrum of potential applications, ranging from aerospace to biomedical devices.^[135]

In the mid-2000, when ESP became more and more established among advanced manufacturing approaches, researchers started to employ SMPs for the realization of electrospun fiber structures with the aforementioned properties. The deriving advantages regard at first the possibility to extend the shape memory response to the micro/nanoscale, in order to obtain structures capable of changing simultaneously their macroscopical shape and their nanostructure (porosity, surface-to-volume ratio, fiber alignment); at the same time, it represents an improvement in the technological tools to realize shape memory polymer-based products and, in part, to finely control their response.^[11,136,137] Various fields may benefit from shape mem-

ory based electrospun materials: smart textiles and intelligent clothes, active membranes for filtration and catalysis, sensors and actuators, tissue engineering as biomimetic scaffolds and templates for cell growth, artificial skin and blood vessels, pharmaceutical devices for drug release. In this chapter, the different approaches pursuing the production of shape memory electrospun materials are reviewed and the specific types of shape memory effects that have been achieved are detailed, as well as the proposed possible applications.

3.1. Shape Memory Effects

The presence in the polymer macromolecular architecture of two functional domains, “hard” and “soft” domains, as sketched in **Figure 6a**, is the first essential characteristic of the fiber itself, to obtain materials featuring a shape memory response. Being “hard” or “soft” depends on the value of the domain transition temperature (that can be either a glass transition or a melting temperature) with respect to the thermal region identified to stimulate the shape memory effect: hard domains have transition far away from the stimulus temperature range, and thus remain unaffected by it; soft domains are activated by the ther-

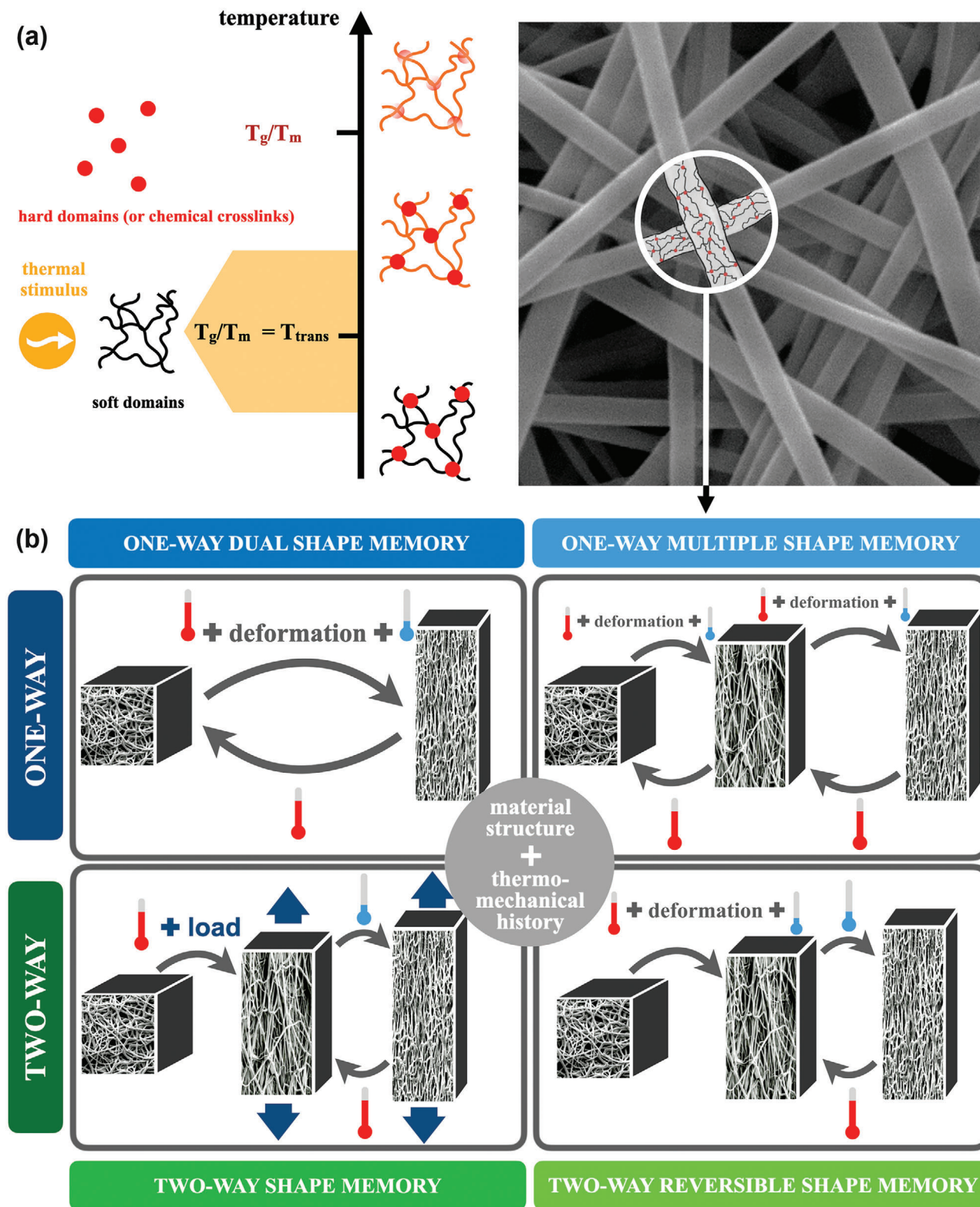


Figure 6. Scheme describing the shape memory effects in electrospun materials: a) a reliable shape memory behavior is achieved when each fiber presents a macromolecular architecture consisting of “soft” domains, whose mobility is activated by the thermal stimulus, and “hard” domains, which remains unaffected by the stimulus and preserve the memory of the shape; b) by combining such a structure to specific thermomechanical histories, the various types of shape memory behavior may be obtained, each one consisting in specific changes of the macro- and microstructure in response to a change in temperature.

mal stimulus, through a thermal transition that involves a significant change in the mobility of polymer chains. From a functional point of view, hard domains are responsible for preserving a “permanent” shape, while soft domains act as “thermal switches” on the transformation among the various shapes. Structurally, hard domains can be seen as net points in the macromolecular architecture, and they consist of chemical (i.e., covalent) or physical (i.e., noncovalent chain entanglement, crystalline domains, segregated phase in a copolymer) crosslinks, while soft domains are the chains connecting them and becoming active at their crystallization, melting, or glass transition temperature, usually labeled under the common term T_{trans} .

Depending on the combination of these functional domains, shape memory polymers are conventionally subdivided into four groups:^[138] I) covalently crosslinked amorphous polymers activated by T_g (e.g., thermosets); II) covalently crosslinked semicrystalline polymers activated by T_m , (e.g., semicrystalline networks); III) physically crosslinked polymers activated by T_g and IV) physically crosslinked polymers activated by T_m . Many types of polymers can be included into these two latter groups, such as neat semicrystalline polymers, amorphous polymers with high molecular weight, glassy and amorphous copolymers, and blends. Such a wide family of materials capable of shape memory response may reasonably suggest that polymers are intrinsically capable of such behavior. In fact, shape memory polymers have not to be considered as a specific class of polymers, but more as the result of the combination of a polymer architecture and of a specific thermomechanical history.^[134,138] Depending on the combination of these parameters, four main important types of shape memory response may be found, at least considering those studied in the literature on shape memory electrospun materials (schematically sketched in Figure 6b): 1) one-way dual shape memory effect; 2) one-way multiple shape memory effect; 3) two-way shape memory effect; 4) reversible two-way shape memory effect.

The one-way dual shape memory effect is the most studied response and may be defined as the ability of a polymer, that possesses a permanent shape, to be fixed in a secondary shape and to return to its pristine form in a thermally driven effect. This behavior is usually achieved through a four steps procedure consisting of: i) heating above T_{trans} ; ii) applying the temporary shape; iii) cooling below T_{trans} under fixed deformation; iv) reheating above T_{trans} . The steps (i–iii) are typically referred to as “programming” and are an effective way to fix the temporary shape; step iv) activates, through a stress-free heating, the shape memory effect.

When the polymer presents more than one transition temperature that may be successfully employed as T_{trans} , as in the case of immiscible blends or block copolymers, programming may be applied at each T_{trans} , from the highest to the lowest, and the recovery step will lead to a multistep recovery, in which each subrecovery process restores an amount of strain close to that applied in the corresponding subprogramming step.

The two-way shape memory effect consists in the possibility to achieve a reversible change between two configurations under the application of on–off stimuli, such as a heating-cooling cycle. This effect is not shown by all polymers, but only by semicrystalline networks (group II) and liquid crystalline elastomers. Also in this case, the two-way shape memory response involves typically a four-step procedure consisting of: i) heating above T_{trans} ;

ii) applying a given load; iii) under the fixed load, cooling below T_{trans} , and iv) reheating above T_{trans} .

Recently, in addition, it was shown that even in absence of the fixed load, a predeformed specimen may undergo elongation-contraction cycles, and such effect was termed “two-way reversible shape memory” or “stress-free two-way shape memory” effect.^[139,140]

3.2. Electrospinning Approaches for the Production of Shape-Memory Fibers

The realization of shape memory electrospun systems was variously pursued employing approaches that range from the conventional ESP of SMPs to more complex strategies, where the shape memory capabilities were achieved by resorting to postcrosslinking reactions or to the development of hybrid structures. A comprehensive list of the most relevant works is reported in Table 2.

3.2.1. Direct Electrospinning of SMPs

The early attempts were based on materials renowned for their shape memory response, as PU,^[141–143] or for their application as electrospun textiles, as Nafion.^[144] These works were fundamental for the technique itself, since they evidenced the versatility of the approach in achieving a good control on both the micro/nanofiber morphology and on the shape memory performances. Experiments on PUs shown the possibility to obtain an interconnected fibrous network with finely controlled fiber diameter on the basis of the solution viscosity (early works: 50–700 μm ;^[141] recent works: 0.08–2 μm ^[145]); similar findings were reported by Zhang et al.^[144] for Nafion fibers.

Starting from these encouraging results, conventional ESP approaches were extended to further polymer families, mainly chosen among those intended for biomedical applications [e.g., PLA-based fibers;^[146] poly(ω -pentadecalactone-*b*- ϵ -caprolactone);^[147] poly(ϵ -caprolactone)-poly(dimethylsiloxane) (PCL-PDMS);^[148] poly(D,L-lactide-*co*-trimethylene carbonate) [P(DLLA-*co*-TMC)]].^[149]

This approach was also applied to a solution of polymers and functional particles, aiming at producing shape memory mats of composite fibers with enhanced features: as an example, PU-based fibers with graphene oxide NPs in order to improve mechanical properties and wettability;^[150] hyperbranched PLA-cellulose nanocrystals in PLA to enhance the shape memory performances of the material;^[151] electrically conductive particles, such as nanotubes^[152] and carbon black nanofibers,^[148] to achieve electrical conductivity and the possibility of remote actuation.

3.2.2. Coaxial Electrospinning of Shape-Memory Fibers

A different approach to the realization of multifunctional fibers is represented by the production of core–shell fibrous structures via coaxial ESP of different polymers. As an example, Rana and Cho^[153] developed core–shell fibers with a neat PU core and a

Table 2. Types of temperature-responsive shape memory electrospun systems, classified in terms of ESP approach, SMP class, type of shape memory effect, and applications.

Fabrication strategy	Material	SMP class	T_{trans} [°C]	Shape memory effect	Application	Refs.
Direct ESP	PU block copolymer	(III)	T_g	One-way dual	Basic research	[141,166]
Direct ESP	PCL-based PU	(III)	T_g	One-way dual	Basic research	[142]
Direct ESP	Cycloaliphatic PU	(III)	T_g	One-way dual	Basic research	[145]
Direct ESP	PLA	(III)	T_g	One-way dual	Basic research	[146]
Direct ESP	Nafion®	(III)	T_g	One-way dual	Basic research	[144]
Direct ESP	PCL-based PU	(IV)	T_m	One-way dual	Basic research	[143,167]
Direct ESP	PU, Krystalflex PE-399	(IV)	T_m	One-way dual	Basic research	[169]
Direct ESP	Multiblock poly(ω -pentadecalactone)-poly(ϵ -caprolactone)	(IV)	T_m	One-way dual	Basic research	[147]
Direct ESP	PCL-based PU	(IV)	T_m	Two-way	Basic research/Filtration	[180]
Direct ESP	POSS – PLA/PCL copolymer	(IV)	T_m	One-way dual	Tissue engineering	[187]
Direct ESP	PCL-based PU	(IV)	T_m	One-way dual	Tissue engineering	[188]
Direct ESP	PCL/PDMS-based PU	(IV)	T_m	One-way dual	Tissue engineering—bone	[148]
Direct ESP	P(DLLA- <i>co</i> -TMC) ^{a)}	(IV)	T_m	One-way dual	Tissue engineering—bone	[149]
Direct ESP	P(LA- <i>co</i> -TMC) ^{b)}	(IV)	T_m	One-way dual	Tissue engineering—nerve conduit	[185]
Direct ESP	Biodegradable polyols	(IV)	T_m	One-way dual	Pharmaceuticals, drug delivery	[192]
Direct ESP + filler	PU + graphene oxide	(IV)	T_m	One-way dual	Basic research	[150]
Direct ESP + filler	PLA+ cellulose nanocrystals	(IV)	T_m	One-way dual	Basic research	[151]
Direct ESP + filler	PCL/PDMS + carbon-black	(IV)	T_m	One-way dual	Basic research	[152]
Direct ESP + filler	Ethylene-vinyl acetate copolymer + Fe nanowire	(IV)	T_m	One-way dual, remote actuation	Basic research	[170]
Direct ESP + filler	P(DLLA- <i>co</i> -TMC) + hydroxyapatite particles	(IV)	T_m	One-way dual	Tissue engineering—bone	[183]
Direct ESP + filler	PCL + hydroxyapatite	(IV)	T_m	One-way dual	Pharmaceuticals, drug delivery	[191]
Coaxial ESP	Multiblock (p-dioxanone)/(ϵ -caprolactone) + sacrificial PEG	(IV)	T_m	One-way dual	Basic research	[155]
Coaxial ESP	PU + PU pyridine	(IV)	T_m	One-way dual	Basic research	[154]
Coaxial ESP	PU + PU containing carbon nanotube	(IV)	T_m	One-way dual	Basic research	[153]
Coaxial ESP	PLA + PVAc	(IV)	T_m	One-way multiple	Basic research	[176]
Coaxial ESP	PU + sacrificial PEG	(IV)	T_m	One-way dual	Smart textiles	[195]
Coaxial ESP, crosslinking	PCL + epoxy	(II)	T_m	One-way dual	Basic research	[161]
Crosslinking	PCL	(II)	T_m	One-way dualTwo-way	Basic research	[156,179]
Crosslinking	PCL-based PU	(II)	T_m	One-way dual	Basic research	[157]
Crosslinking	PCL-based PU	(II)	T_m	Two way	Basic research	[158]
Crosslinking	PCL/epoxy blend	(II)	T_m	One-way dual	Basic research	[159,160]
Crosslinking	PCL	(II)	T_m	Two-way reversible	Basic research	[181]
Crosslinking + filler	PCL-based PU + gold NPs	(II)	T_m	One-way dual, remote actuation	Basic research, tissue engineering	[171]
Crosslinking + filler	PCL + Fe3O4-functionalized carbon nanotubes	(II)	T_m	One-way dual, remote actuation	Basic research	[170]
Hybrid (dual ESP)	PCL + Pellethane®	- ^{c)}	T_m	One-way dual	Basic research	[163]
Hybrid (dual ESP and multilayer ESP)	PCL + PEO	- ^{c)}	T_m	One-way dual	Basic research	[165]
Hybrid (composite)	PVA + polyether block amide	- ^{c)}	T_m	One-way dual	Basic research	[162]
Hybrid (dual ESP)	PVAc + PCL	(IV)	T_m	One-way dual	Basic research, self-healing	[164]

(Continued)

Table 2. (Continued).

Fabrication strategy	Material	SMP class	T_{trans} [°C]	Shape memory effect	Application	Refs.
Hybrid (composite)	Epoxy + graphene reinforced PCL	- ^{c)}	T_m	One-way multiple	Basic research	[175]
Hybrid (composite)	Epoxy-PMMA bend + PCL fibers	- ^{c)}	T_m , T_g	One-way multiple	Basic research	[177]
Hybrid (composite)	Nafion + carbonized PAN	(III)	T_g	One-way dual, remote actuation	Basic research	[173]
Hybrid (core-shell morphology)	PLA + polypyrrole	(IV)	T_m	One-way dual, remote actuation	Basic research	[172]
Hybrid (composite)	Nafion/silica nanofiber + carbon nanotube	(III)	T_g	One-way dual, remote actuation	Basic research	[174]
Hybrid (composite)	P(LA-co-TMC)	(III)	T_g	One-way dual	Tissue engineering— nerve conduit	[190]
Hybrid (composite)	PLA film + PCL-gelatin methacrylate	(IV)	T_m	One-way dual	Tissue engineering— vascular graft	[184]
Hybrid (composite)	Poly(lactide-glycolide-trimethylene carbonate) film + poly(lactide-glycolide)-chitosan	(IV)	T_m	One-way dual	Tissue engineering	[189]
Hybrid (blend ESP)	PU + chitosan + gelatin	(IV)	T_m	One-way multiple	Pharmaceuticals, smart patches	[194]
Hybrid (multilayer ESP)	PU + PU/berberine hydrochloride	(IV)	T_m	One-way multiple	Pharmaceuticals, drug release	[193]
Hybrid (composite)	Epoxy + PCL	- ^{c)}	T_m	One-way dual	Self-healing	[196,197]
Hybrid (blend ESP+ coating)	PLA/ thermoplastic PU + carbon nanotubes	(III)	T_g	One-way dual	Large strain sensor	[198]
Hybrid (blend ESP)	PU/PEG microfibers/spheres	(III)	T_g	One-way dual	Triboelectric generator	[199]
Hybrid (multiple ESP)	Poly(rac-lactide-co- glycolide)	(IV)	T_m	One-way multiple	Tissue engineering— nerve conduit	[186]

^{a)} P(DLLA-co-TMC): poly(D,L-lactide-co-trimethylene carbonate); ^{b)} P(LA-co-TMC): poly(lactide-co-trimethylene carbonate); ^{c)} a proper classification cannot be given, since soft/hard domain corresponds to the specific component and not to the macromolecular architecture.

shell of PU reinforced multiwalled carbon nanotubes (MWCNTs). The obtained material, thanks to the good nanotube dispersion and alignment, presented improved mechanical properties with respect to those obtained by the single spun components, and fast recovery response, due to a combined effect of high thermal conductivity and the increased internal stress stored in the core-shell system. Coaxial ESP was also employed for materials whose characteristics would prohibit spinning them alone and for the preparation of hollow fibers. In this context, Zhuo et al.^[154] were able to spin an otherwise unspinnable shape memory PU containing pyridine with antibacterial properties, and to prepare hollow fibers, while Zhang et al.^[155] used a poly(ethylene glycol) (PEG) sacrificial core on a copolyester shell to store drugs in smart pharmaceutical devices.

3.2.3. Crosslinking Approaches

In some works, to introduce stable hard domains, a crosslinking reaction was incorporated in the ESP process. Crosslinking, by strongly binding the fibers together and stabilizing the structure also at temperatures above melting, ensured an effective and fast shape memory response, or advanced effect, as two-way shape memory response. In some works^[156,157] crosslinking is obtained by sol-gel reaction from triethoxysilane-terminated

precursors. A preliminary crosslinking of the polymer is often required to achieve a solution viscosity enabling to spin bead free-fibers, but it is the later post-crosslinking of the electrospun mat that provides the proper crosslinked structure to the material. With a different approach, Kuang and Mather^[158] employed what they labeled “latent-crosslinkable” systems, adding pendent crosslinking sites to a PCL-based PU. The systems were conventionally electrospun from solvent and later crosslinked under compression molding conditions at a temperature able to activate crosslinking without melting the crystals. Others adopted diglycidyl ether of bisphenol A and a photoinitiator, blended with a high molecular PCL^[159,160] or coelectrospun as the core for a PCL shell,^[161] to finally postcrosslink by UV radiation.

3.2.4. Hybrid Systems

For the development of hybrid composite structures, complex strategies, in which the shape memory electrospun system is embedded in a matrix and acts as an inner vascular-like network, were explored. The approach reminds the idea to use the surrounding matrix as soft domains and thermal switch, and the fibers as hard domains, replicating at a nano/microlevel what in shape memory polymers occurs at a macromolecular scale. Impregnation of the fibers in the matrix may be considered the

most obvious approach, and it is made particularly easy in the work of Shirole et al.^[162] where an inner structure of electrospun poly(vinyl alcohol) (PVA) fibers are sandwiched between sheets of a thermoplastic elastomer (polyether block amide) and impregnated upon compaction melting. Crystallization/melting of the matrix is employed to fix a temporary shape and activate recovery, while the rubbery behavior of the fibers on such transition region allows to employ them as inner memory. Other approaches were based on simultaneously spinning different polymers from two separate syringes (in a process also called “dual ESP”) to obtain a hybrid membrane with finely interwoven fibers; subsequently, the two constituents are strongly bound together by melting either one^[163] or both polymers,^[164] or by crosslinking one of them.^[165] For example, Nejad et al.^[164] applied dual ESP with poly(vinyl acetate) (PVAc) and PCL, to obtain, after melting of both fibers, a stiff, non-porous film with shape memory and self-healing abilities; Robertson et al.^[163] created a shape memory composites material with a stiff fibrous structure (Pellethane fibers) embedded in an elastomeric PCL matrix. Interestingly, the approach allows to easily choose among different fibers and their weight ratio, to achieve a well-controlled and tightly interwoven hybrid fibrous structure.

3.3. Shape Memory Effects in Electrospun Fibers and Mats

Most of the works concentrated on the possibility to realize electrospun systems with a one-way response, often tested in more than one cycle. The results often reported good or excellent shape memory behavior, which means an effective fixing of the temporary shape (“shape fixity”) and the ability to recover a large fraction of the applied deformation (“shape recovery”). Sometimes a first training cycle was required to consolidate the permanent structure and led to an excellent response already at the second cycle. Further, early works on shape memory response focused on their response being much faster with respect to the corresponding bulk films,^[60] as a consequence of the higher surface area of fibers, determining a better interaction with the environment and a more uniform heating.

The shape memory performances were earlier thought to be mainly related to the material architecture (e.g., hard-soft segment concentration in PU systems),^[141] but recent systematic studies^[145,166,167] revealed an important role played also by the fiber morphology: shape fixity, which was overall good (>80%), increases for larger fibers, since the presence of more connection points enhances the stress transfer throughout the fiber networks;^[145,166,167] by contrast, shape recovery of larger fibers may also be very low (25%), and significantly increases for small diameter fibers, due to an effect of the molecular orientation.^[143,145,166]

This apparently inherent dual shapes ability of electrospun mats,^[168] as well as their intrinsic contraction tendency,^[169] was deepened by adopting PU systems as model material. Interestingly, it was shown that phase changing (i.e., crystal formation/melting) is not a strict requirement for shape fixing and recovery, which may be effectively supported by a change in chain mobility. The formation of a crystalline fraction, however, can provide an additional fixing/recovery mechanism.^[168] Further experiments and modeling suggested that the shape recovery pro-

cess can entirely occur in the amorphous state,^[169] and that the possible presence of a crystalline phase, developed through processing or annealing, alters the onsets and the kinetics of recovery in a sharper process close to the melting temperature of the switching phase. According to this interpretation, the characteristic recovery time may even simply regard the ability of the chains to disentangle and to revert back to their original position; in the case of electrospun fibers, whose production process tends to reduce the entanglement density, this should intrinsically lead to faster recovery.

Remote actuation through indirect heating promoted by electrical or light stimuli was often pursued. The most straightforward strategies for the preparation of such systems were the direct incorporation of fillers in the polymer solution before spinning. By this approach Yao et al.^[170] incorporated Fe nanowires in an ethylene-vinyl acetate copolymer, enabling actuation by light radiation, thanks to the ability of Fe nanowire to convert light energy into heat. Fast actuation (about 100ns) was achieved by exposure to a light source, at least at 40 cm from the specimen. Similarly, Zare et al.,^[171] starting from a solution of PCL dimethacrylate and gold particles, electrospun a 3D fibrous structure which may be activated under a near-infrared radiation, while Gong et al.,^[172] in a system electrospun from a solution of PCL and Fe₃O₄-functionalized nanotubes, demonstrated the possibility to apply remote actuation under alternating magnetic fields, due to the hysteresis loss of magnetic NPs.

With a different approach, Zhang et al.^[173] increased the system conductivity of an electrospun PLA through a vaporized coating of polypyrrole, obtaining a structure consisting of a conductive core over a shape memory shell, capable of uniform heating when electrically activated.

More complex structures were conceived in the works of Zhang et al.^[174] and Lu et al.^[175] In the former work, actuation was ensured by an electrospun PAN membrane, transformed in a carbon nanofiber membrane through carbonization at 1000 °C and encapsulated into Nafion, so to achieve fast recovery at a voltage of 14 V. In the latter work, a functionally graded paper, composed by carbon nanofibers and Nafion nanofibers containing silica and carbon nanotubes, was impregnated by an epoxy matrix, and thanks to the high carbon content, the recovery of the electrospun backbone was achieved via Joule effect at relatively low voltage (3–5 V).

One-way multiple shape memory response was also obtained with various strategies, mainly based on hybridization, instead of adoption of copolymer or blends with more transition temperatures: but, actually, hybrid structures create a sort of co-continuous phases blend or interpenetrated structure. Fejős et al.^[176] achieved a triple shape memory response by impregnating a mat of PCL nanofibers reinforced with graphene. The presence of two transition temperatures, i.e., epoxy's T_g and PCL's T_m , allowed to fix two different temporary shapes and to promote their recovery on distinguished temperature regions. A similar triple shape memory result was obtained by Sabzi et al.^[177] by co-ESP PLA fibers and PVAc fibers. This allowed to obtain an interwoven system with two thermal transitions and to overcome polymer miscibility which would have led to just one T_g . With a more articulated process, a quadruple shape memory effect was also obtained by introducing an electrospun mat of PCL in a blend of epoxy monomers and PMMA, which achieved phase

separation during epoxy crosslinking.^[178] The obtained system, a ternary composite with heterogeneous structure, shows three well-distinguished transitions temperatures for each phase.

If in the case of one-way shape memory response the crystallinity is not a strict requirement, however, it has a fundamental role in the case of the two-way and two-way reversible shape memory response. These peculiar shape memory responses are in fact entirely governed by crystallinity-driven phenomena taking place in the single fiber.^[179] Most of the works regard semicrystalline fibers that, according to the aforementioned approaches, were crosslinked, such as sol-gel crosslinked PCL fibers^[180] or a “latent-crosslinkable” reactive PCL.^[158] These systems were revealed to be capable of repeatable elongation-contraction cycles when subjected to cooling–heating cycles under a constant tensile stress of few hundreds of kPa. A similar behavior was also found for a PCL-based PU,^[181] without the need for postcrosslinking but employing the crystallization/melting transition of the soft segments to achieve the effects. For all these systems, the cyclic macroscopically changes led to significant and reversible changes of the fiber orientation and systems porosity. Finally, it is noteworthy to remark the case of mats, obtained by UV postcrosslinking of electrospun PCL fibers, showing a two-way reversible shape-memory effect,^[182] and thus being capable of self-actuation in the absence of stress and on a pure heating-cooling cycle, leading to an overall reversible change in porosity of about 11%.

3.4. Applications of Shape Memory Electrospun Fibers and Mats

Electrospun shape-memory systems were conceived, and in some cases studied, for a very wide spectrum of applications, whose broadness is a clear consequence of the combined advantages offered by such systems: the peculiar response to temperature, also apt for remote or self-regulated actuation; the nanostructured morphology, useful for specific fields, stemming from filtration to cell culturing; specific features of the material itself, such as biocompatibility, biodegradability, flexibility, and easy deformation.

The field that more intensively investigated this subject regards biomedical applications, as very well depicted in a specific literature review by Zare et al.,^[183] and in particular for the realization of scaffolds for tissue engineering: on one side the nanoscale topography of electrospun materials, similar to that of the extra cellular matrix (ECM), is regarded as a relevant advantage, biomimicking biological tissue, inducing cell alignment and affecting their motility, growth, and differentiation; in addition, shape memory response may lead to self-actuation at the human body temperature, meeting the needs of minimally invasive surgery, while a finely tuned biodegradability would permit to avoid second surgery for removal.

As an example, specific electrospun formulations revealed particularly capable as scaffold for bone tissue regeneration (PCL-PDMS^[148] and P(DLLA-co-TMC))^[149] also with hydroxyapatite nanocrystals^[184]. These systems, combining a microstructure similar to that of the bone ECM and the shape memory response, allowed minimally invasive insertion of the systems, easily filling the bone defect and creating good contact with the surrounding bone; interestingly, also the stress created upon expansion,

and enhanced by coelectrospun hydroxyapatite nanocrystals, is considered as further help towards bone regeneration through mechanotransduction.^[184] According to a similar approach, scaffolds with tubular permanent shape, that may be deformed in planar shapes in order to be more favorably seeded by endothelial cells and subsequently self-roll back at the physiological temperature, were investigated both for small vessel vascular grafts (Zhao et al.,^[185] as a hybrid structure made of coelectrospun PCL/gelatin methacrylate over a PLA film) and for peripheral nerve regeneration (Wang et al.,^[186] as multitubular P(LA-co-TMC)), as shown in **Figure 7**. Interestingly, for this latter field, also smart nerve conduits with multiple shape memory were studied by Chen et al.,^[187] who realized a multisegment scaffold through a sequential spinning of different poly(*rac*-lactide-co-glycolide)-based copolymers with different T_g . Finally, researchers have also aimed at the possibility to dynamically direct cell morphology through fiber alignment,^[188,189] as in the case of tubular scaffolds with the inner layer of aligned fibers, developing structures quite similar to those of vascular tissues,^[190] or of an injectable hydrogel-based composite scaffold for the treatment of the spinal cord injury.^[191]

The pharmaceutical field tried to provide new possible applications of electrospun systems for drug delivery, combining the possibility to incorporate large drug amounts in the electrospun system and to tune its release through their structure (PCL-based PU loaded with hydroxyapatite microfibers,^[192] PU-based materials for self-fitting medicating stents;^[193] PU loaded with antibacterial berberine hydrochloride^[194]). In Tan et al.,^[195] smart wound patches, incorporating an electrospun shape memory PU web in a chitosan/gelatin matrix, used the stress exerted through shape recovery to close the wound while releasing the drug, while in Yin et al.,^[194] the shape changing of a PU system was employed to better tune the release of antibacterial.

Electrospun materials with shape memory properties were also studied under various configurations for the realization of smart textiles, for different types of applications. In an interesting approach, schematically shown in **Figure 8**, a smart textile was conceived by Feng et al.^[196] to simultaneously display thermal regulation and a temperature-adaptive moisture permeability, by means of coaxial electrospun microfibers PEG as the core and PU as the shell). Both effects are based on polyethylene glycol, which upon melting can store energy and delay temperature increase, while through shape variation regulate moisture permeability and air filtration. A thermally selective filtration PU membrane was proposed by Ahn et al.,^[181] on the basis of the two-way shape memory effect: upon the application of a constant pressure, the membrane undergoes reversible changes in porosity as a response to temperature changes.

As mentioned above, smart electrospun fibers may be used for novel approaches to self-healing of materials. Electrospun systems were already considered for such an aim, thanks to the possibility to encapsulate a healing agent in coaxial electrospun fibers, to create a nanovascular healing networks in a polymer matrix; however, by adding shape memory ability, it is also possible to provide local closure of the cracks. Yao et al.^[197] incorporated an electrospun PCL microfiber mesh in an epoxy matrix, both serving as a toughening agent in epoxy and as an internal structure to guide self-healing. In another work,^[198] with the aim to provide surface protection towards scratches and corrosion, a

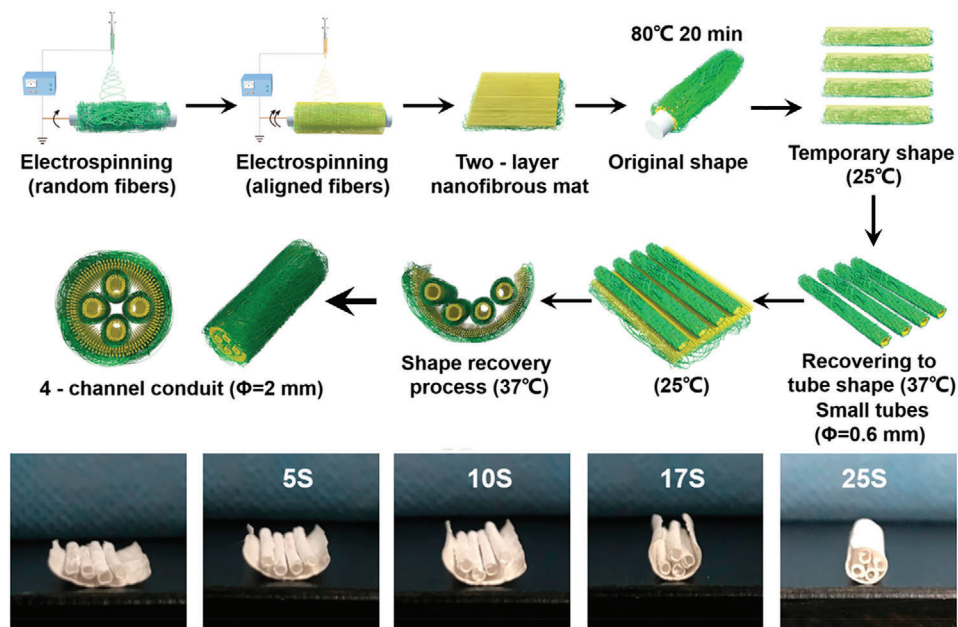


Figure 7. Production and self-forming multichannel conduit for nerve guidance and regeneration based on shape memory P(LA-co-TMC) nanofibrous mat: presenting a permanent tubular shape, it may be temporarily fixed in a planar one to achieve a uniform cellular growth; the initial tubular shape can be restored by heating to the human body temperature. Reproduced with permission.^[186] Copyright 2020, American Chemical Society.

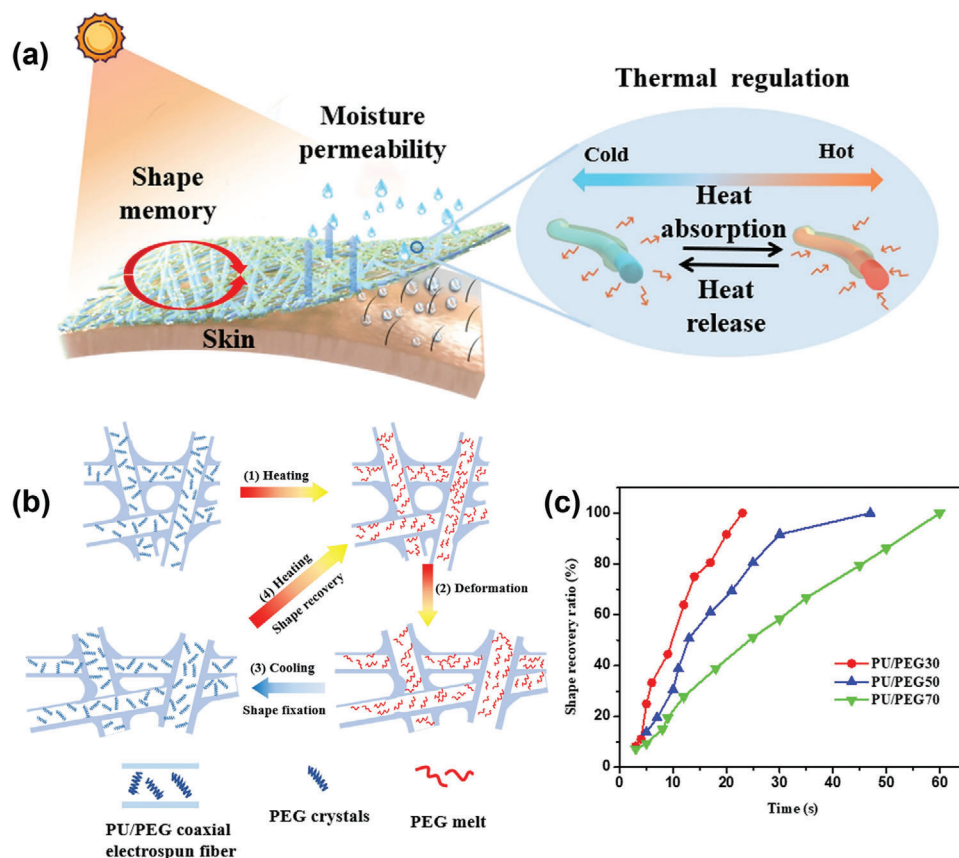


Figure 8. a) Schematic illustration of the PU/PEG coaxial electrospun membranes with both adaptive breathability and thermal regulation functions; b) microstructural evolution of the PU/PEG coaxial electrospun membranes during heating, shape deformation, shape fixation, and shape recovery processes; c) evolution of shape recovery ratio with increasing recovery time for different PU/PEG composition. Reproduced with permission.^[196] Copyright 2021, Elsevier.

composite coating, consisting of an electrospun PCL was embedded in an epoxy resin. The coating, after the formation of a crack, turned out to be able to repair the crack, upon heating above PCL melting temperature, by not only restoring the physical integrity, but also the initial corrosion resistance.

Finally, sensors and actuators based on conductive shape memory electrospun materials are particularly investigated for implantable electronics, e-skin, and wearable devices for rehabilitation. Kahlili et al.^[199] obtained flexible/stretchable sensors operating under large strain conditions starting from an electrospun mat made of a blend of cross-linked PLA and TPU, subsequently spray-coated with a homogeneous layer of carbon nanotubes. Sensing is achieved by a resistance variation due to changes in the nanotubes coating structure, and the deformability of the supporting material permits to achieve of large strains. The shape memory response of such networks allowed to obtain, also after application of large strains, recovery of the initial shape and also of the original electrical resistance by simply heating above 80 °C, overcoming the limitation of cumulative damaging and plastic deformation which would progressively affect sensor reading throughout its functioning. Xiong et al.^[200] exploited the combination of electrospun systems and of their shape memory ability to enhance the efficiency of triboelectric nanogenerators, used for energy harvesting and self-powered sensors, as displayed in **Figure 9**. These devices may in fact convert environmental mechanical energy, due to friction with water and fluids, into electricity. Electrospun nanostructured surfaces, by enhancing frictional effects, increased of about 20-times the power produced with respect to traditional ones obtained by photolithography. Furthermore, shape memory allowed to restore the original microstructure that may be affected by prolonged friction, extending the lifetime of the device.

4. Thermo-Optically Responsive Electrospun Fibers

Materials undergoing a color change induced by a variation of temperature are called thermochromic; on the other hand, when the change involves the luminescence properties, materials are named thermoluminescent. The color of a material is an easy-to-observe property and it can be detected at the macroscopical level, even without the help of any instrumentation. However, for a quantitative analysis, the detection of luminescence changes allows for much higher sensitivity and lower signal interferences than color detection. These kinds of molecular probes and materials^[201–203] are widely studied and suitable for different applications (e.g., temperature sensing, optoelectronic devices, and anticounterfeiting technologies^[204]); however the literature on thermochromic/thermoluminescent electrospun nanofibers is not too vast if compared to the research carried out on bulk materials having the same characteristics.^[201,205] In this frame, the processing of the materials into electrospun nanofibers presents further significant advantages, such as very high surface area and porosity, which are extremely attractive characteristics when it comes to the preparation of high-performance sensors. In this chapter, the most common approaches for obtaining either low temperature- or high temperature- optically responsive materials are described and critically discussed. Among others, the strategies include the careful selection of polymers and additives to tune the responsivity in the temperature range of interest, as well

as the optimization and customization of fabrication parameters to reach the desired sensitivity.

4.1. Thermochromic Electrospun Fibers

One of the simplest outputs obtainable by applying a change of temperature is a variation of material transparency, which relies on the temperature-induced transition in the material. Interesting examples are fibers doped with VO₂ NPs that, thanks to their temperature-dependent change in transmittance, not only in the visible but, above all, in the infrared range (1000–2500 nm), allow to prepare stealth materials able to hide hot objects from infrared cameras. These nanomaterials undergo a reversible crystallographic transition from a monoclinic structure to a tetragonal rutile one at about 68 °C, going from a transparent to a more light-reflective state. When VO₂ NPs were incorporated in polyacrylonitrile fibers stealth mats were obtained.^[206] The phase transition temperature was also tuned by doping the metal oxide NPs with tungsten embedded in Poly(vinylpyrrolidone) (PVP) fibers.^[207]

In general, however, the thermochromic effect can be more rigorously described with a change in the absorption properties in the visible range upon a variation of temperature (i.e., a color change of the material). The most straightforward approach to obtain thermochromic fibers is, therefore, the addition of thermochromic species to the polymer. In a first example, this species is a second polymer, i.e., polydiacetylene (PDA), obtained after photopolymerization of PEO electrospun fibers loaded with ethylene oxide-containing bisdiacetylenes as PDA precursor.^[208] The thermochromism of PDA, due to a first-order phase transition (blue/low to red/high temperature), is maintained in the fibrous mat and the reversible thermochromic behavior occurs in the range of 40–80 °C (**Figure 10a**), while the temperature range is narrower (i.e., 40–60 °C) in case of bispolydiacetylenes solution or when embedded in a PVA film. Following the same approach, Mapazi et al.^[209] investigated the effect of the inclusion of a PCDA-urea derivative on the thermal and thermochromic properties of PAN fibers. The authors obtained a high-temperature thermochromic electrospun mat presenting advantages in terms of reduced degradability and an improved reversibility ranging up to 220 °C (only 160 °C in the film) but with a lower thermochromic resolution.

De Oliveira Peres et al.^[210] have studied the potentialities of an electrospun mat obtained from a mixture of cobalt-doped hopeite ceramics [Co²⁺:Zn₃(PO₄)₂·4H₂O] and polyglycerol dendrimer host polymer to prepare a broad range temperature sensor based on the deposition of the thermochromic nanofibers on an optical fiber. The color change from blue to pink in the range 20–200 °C was quantitatively measured and presented good linearity. The authors explained the phenomenon by the difference in the coordination number of the Co²⁺, going from low temperatures (tetrahedral) to high temperatures (octahedral).

An alternative approach exploits the phase transition of polymers used as the core of a core-shell electrospun fiber. The phase-change medium acts as the “solvent” of a couple of reactants: a leuco dye, generally crystal violet lactone, and a developer (bisphenol A) able to donate a proton that takes the dye to its colored state via the formation of a reversible adduct. This process

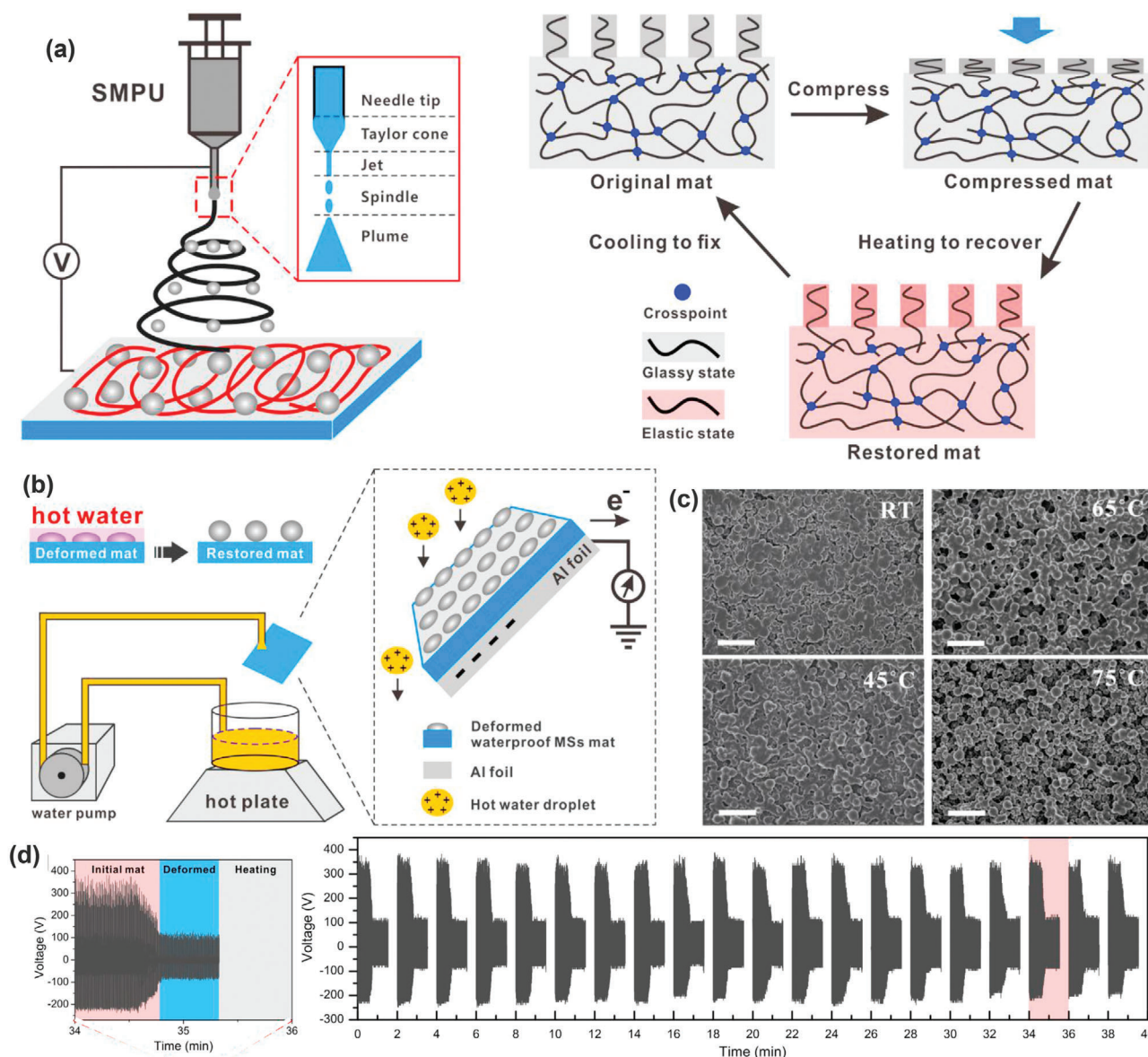


Figure 9. Triboelectric nanogenerator capable of high-power production and self-recovery. a) Schematic illustration of the ESP process of shape memory PU and of its deformation and heating-triggered recovering process; b) setup and working mechanism of a deformed mat based on water-triboelectric nanogenerator driven by hot water; c) representative SEM images of the deformed mat under impacting by hot water at different temperature for 40 s, scale bar, 10 μ m; d) 20 cycles of output voltage recorded when the triboelectric nanogenerator is compressed by a strong force (100 N) followed recovery by heating at 75 °C for 40 s. Reproduced with permission.^[200] Copyright 2019, Elsevier.

is controlled by melting and crystallization of the phase change material, which, therefore, defines the temperature range of color change.^[211–213] As an example, Wang et al.^[212] prepared core-shell fibers with 1-tetradecanol as the core and poly(vinylidene fluoride) (PVDF) as the fiber shell. The authors reported that the fibers turned from blue to white at around 38 °C, well matching the phase transition temperature of 1-tetradecanol, and presented good thermal stability and reversibility proved by 100 thermal cycle tests. All these characteristics, together with a transition temperature close to that of the human body, led the authors to envisage their potential applications as functional fibers in thermal protective clothing and thermoresponsive sensors. In

a variation of this approach, He et al.^[213] embedded microcapsules of 1-tetradecanol containing the crystal violet and bisphenol A, directly in a PVA/water-soluble PU solution, where a cross-linking agent was added to enhance the water resistance of the fibers. Then, the authors compounded a thermosensitive PU film with the fibrous mat to obtain a multifunctional composite film with temperature-dependent porosity and thermal storage, temperature-adjusting, and thermochromic properties.

Among the phase transition-based strategies, approaches that exploit cholesteric liquid crystals (CLCs) are also worth to be mentioned. Enz and Lagerwall^[214] used coaxial ESP to encapsulate short-pitch cholesteric liquid crystal in the core of PVP mi-

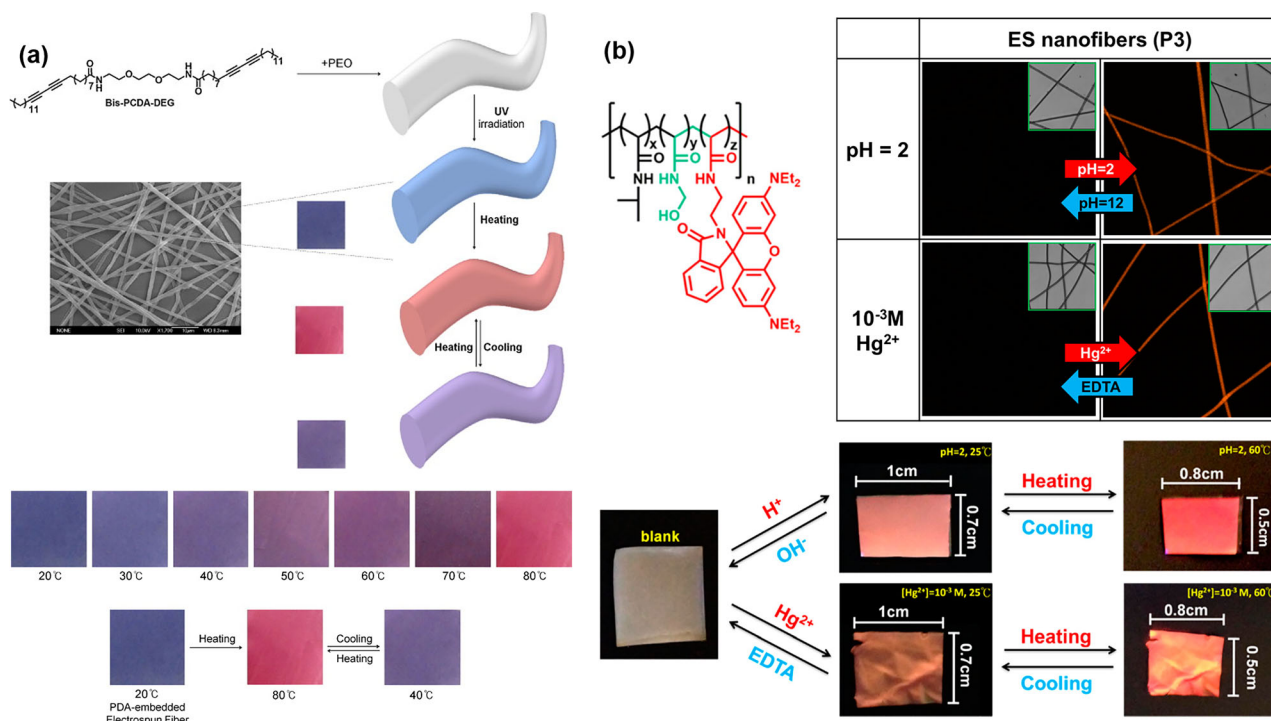


Figure 10. a) Thermochromic PEO fibers containing PDA:PDA structure, schematic representation of the preparation and thermochromism of PDA-based fibers, and color switch upon temperature change. Reproduced with permission.^[208] Copyright 2012, Elsevier. b) Thermoluminescence of P(NIPAAm-co-NMA-co-rhodamine derivative) fibers with high sensitivity toward pH, Hg²⁺, and temperature: confocal microscopy of nanofibers at pH 2 and in aqueous solutions with Hg²⁺ ions (top); photos of the membrane for sensing Hg²⁺ at pH 2 and various temperatures (bottom). Reproduced under terms of the CC-BY license.^[90] Copyright 2018, MDPI.

crofibers. The CLCs presented a temperature-dependent iridescence under a polarized optical microscopy due to a selective reflection of a narrow band of the visible spectrum that also causes an evident change of color. The authors showed that the relative flow rate of the core and shell solutions affected the core diameter, and consequently the reflected color. This was more deeply investigated by Enz et al.^[215] who observed selective light reflection also for liquid crystal cores smaller than one micrometer. At this scale, small variations in dimension and shape correspond to strong changes in the reflection, since only a few or even half of one turn of the helix can be formed. The iridescence temperature sensitiveness of analogous fibers, containing N-(4-methoxybenzylidene)-4-butylaniline in the core, was studied by Bertocchi et al.,^[216] highlighting a significant reversible change in the temperature range of 30–42 °C. Nguyen et al.^[217] compared fibers obtained by blending a liquid crystal formulation with PS and by using coaxial ESP to incorporate LC in the core of a PEO fiber. They obtained, however, thermochromic fibers only with the coaxial ESP method.

4.2. Thermoluminescent Electrospun Fibers

The literature on this topic is limited and there is still a large room for further investigation. The described thermoluminescent behavior covers the temperature range between 10 °C and 60 °C, with materials that undergo a change in intensity and/or

a change in the emission spectrum. The latter is often obtained by exploiting the metal complexation ability of some polymers to get multistimuli-responsive (e.g., pH, metal ions, temperature) mats. However, even though metal ion complexation enhances the luminescence changes caused by temperature, the process is often irreversible.

In the works of Chen and co-workers—already mentioned in Chapter 2.3—different multifunctional block copolymers^[61] and random copolymers^[218,219] presenting a fluorescent probe are proposed as thermoresponsive luminescent electrospun nanofibers. As an example, nanofibers of conjugated triblock polyfluorene-*b*-PNIPAAm-*b*-PNMA copolymers, with good wettability and dimension stability in aqueous solution, presented a structured emission band centered at about 450 nm, with a significant and reversible on–off intensity variation (circa 80%) going from 10 °C to 50 °C, ascribable to a different state of fluorophore aggregation and light absorption determined by the swollen and the collapsed states of thermoresponsive PNIPAAm blocks. A comparison with the corresponding drop-cast film in the same conditions evidenced a similar behavior, just with a much smaller variation (less than 30%).^[61] To make a further step forward, the same authors prepared random copolymer containing fluorophores carrying chelating units able to complex different metal ions and thus changing the emission spectrum and intensity. In this way, they were able to successfully couple thermoresponsivity with metal sensing.^[218,219]

Other authors have investigated the thermoresponsiveness of metal ion-sensitive electrospun nanofibers. Electrospun fibers were obtained blending either 1,10-phenanthroline-based fluorescent sensor^[62] or a 1,8-naphthalimide-based colorimetric derivative^[220] into P(NIPAAm-co-NMA) and P(NIPAAm-co-NMA-co-AA), respectively. In the first case, Chen et al. found that, in the absence of the target copper ions, the increase of temperature from 10 °C to 60 °C induced a decrease of the luminescence intensity (residual emission less than 20%) and a blue shift. This is because, above LCST, water molecules are squeezed out from the fibers, thus changing the environment of the 1,10-phenanthroline emitting moieties. In the second case, Kuo et al. investigated the thermoresponsivity only in the presence of the mercury target ions, showing a minor on-off effect on the luminescence intensity at 450 nm is minor (residual emission circa 60%). Some of the same authors,^[90] however, have presented another system where a P(NIPAAm-co-NMA) was covalently functionalized with a rhodamine B derivative. In this case, an intensity increase of the red luminescence centered at 585 nm could be observed either upon protonation or Hg²⁺ ions complexation, but most interestingly, in both cases, the mat shows a further increase in emission intensity upon heating from 27 to 55 °C (Figure 10b). Even in this case, this is the consequence of the transition from the swollen to the shrunk state of the PNIPAAm-based materials. However, it is worth mentioning that all the processes—including complexation, protonation, and thermoresponse—are reversible.

5. Phase Change Materials in Electrospun Fibers

In the last decade, due to the growing global energy consumption, novel thermal energy storage (TES) devices have attracted the attention of researchers. These platforms are designed to increase the efficiency of renewable energy sources, by developing technologies to reduce the overall energy demand through passive thermal regulation.^[221,222] TES technology enables the storage of excess thermal energy, which can be released and reused at a later time during peak demand, thus addressing the mismatch between the supply and demand of energy. TES technologies can rely on: i) sensible heat storage, ii) latent heat storage, and iii) thermochemical energy storage. Among them, the use of latent heat storage systems is particularly interesting. It is based on the heat absorbed or released by a storage material during a phase transition (Figure 11). Latent heat storage materials are known as phase change materials (PCMs). In this chapter, PCMs are briefly introduced and the most recent and remarkable researches on electrospun Phase Change Fibers (PCFs) are reviewed, classifying them according to the types of solid–liquid PCMs incorporated into the fibers. The main characteristics of the described phase change electrospun systems are summarized in Table 3. For a complete and detailed review on this topic, we recommend the comprehensive paper of Chen et al.^[223]

5.1. Phase Change Materials

PCMs have the advantages of high-energy storage density and can absorb and release heat at a nearly constant temperature corresponding to the phase transition temperature of the

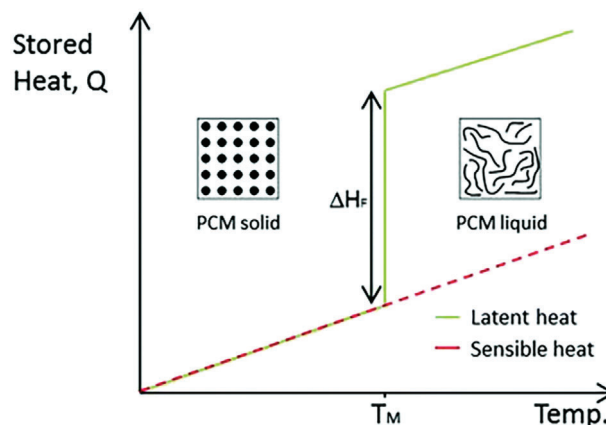


Figure 11. Comparison between sensible heat and latent heat in a PCM system (ΔH_f is the latent heat of fusion during melting, T_m is the melting temperature). Reproduced under terms of the CC-BY license.^[222]

PCM. Phase transitions include melting and solidification (solid–liquid), evaporation and condensation (liquid–gas), or change in crystalline structure (solid–solid), being solid–liquid transitions the most attractive ones from a practical point of view. Indeed, albeit displaying smaller latent heat than liquid–gas transition, solid–liquid transitions involve only a small change in volume (about 10%). A large number of PCMs, that melt and solidify at different ranges of temperatures, are available for several applications.^[221,222,224] They can be classified into organic, inorganic, and eutectic materials: organic PCMs comprise hydrocarbons and paraffin waxes, fatty acids, esters, glycols, and PEG; inorganic PCMs list salt hydrates, salts, or metals; eutectic PCMs consist of a mixture of at least two other organic or inorganic PCMs. More details on the different types of PCMs can be found in a few review articles dedicated to this topic.^[222–225] PCMs find applications in two main fields: i) TES for efficient use and conservation of the waste heat and solar energy in industrial processes and buildings; ii) thermal regulation, to prevent temperature fluctuations with no energy input. For these purposes, PCMs can be used either encapsulated into micro- and nanocapsules or as “form-stable” PCMs.^[222,226] In the first case, the physical containment prevents PCM leakage during the solid–liquid transition, protects the PCM against degradation during heat uptake/release cycles, and increases PCMs surface area and heat conductivity. In the case of form-stable PCMs, the latent heat storage component is incorporated either in a polymer or in an inorganic porous/lamellar material, with the great advantage of being fabricated in the desired shape/dimension.^[222,223] Examples of form-stable PCMs are phase change fibers (PCFs), which are extremely attractive to develop textiles for clothing and packaging. ESP technology was used for the first time in 2006 to fabricate ultrafine PCFs with sub-micrometric diameters as high-performance fabrics.^[227,228] Since then, a rapid rise in the research of electrospun PCFs has been registered, where the use of coaxial ESP has enabled to achieve high PCM loading, high phase change enthalpy, and retention of physical, mechanical, and structural properties of the fibers.

Table 3. Types of phase change electrospun systems, classified in terms of composition, electrospinning approach, and properties.

Types of PCMs	Components of PCFs (PCM/ supporting polymer)	Electrospinning approach	Properties	Refs.
Long-chain aliphatic hydrocarbons and paraffin waxes	Hexadecane, octadecane, eicosane/PVP/TiO ₂	Coaxial ESP	Octadecane/PVP/TiO ₂ : PCM 45 wt%, T_m 27 °C, ΔH_m 114 J g ⁻¹	[227]
	Octadecane/PVB	Coaxial ESP	T_m 27 °C, ΔH_m 96.9 J g ⁻¹	[229]
	Octadecane/PVP, PVDF, PAN	Coaxial ESP	Octadecane/PVP: EE 36%, T_m 31 °C, ΔH_m 80 J g ⁻¹ , good thermoregulating properties in body simulated conditions	[230]
	Paraffin wax/PMMA/MWCNTs	Coaxial ESP	T_m 52–54 °C, EE 45%, ΔH_m 58.25 J g ⁻¹	[231]
	Octadecane and silk	O/W emulsion ESP	T_m 23 °C, EE 20%, ΔH_m 40 J g ⁻¹	[232]
Long-chain fatty acids and their eutectics	RT4/RT-4 blend and RT5 / PCL, PS, HIPS	Single needle ESP	RT5/PS: EE 78%, T_m 5 °C, ΔH_m 107 J g ⁻¹ . Melting and crystallization enthalpies decreased with time of storage: \approx 56–58% and \approx 30–40% decrease in samples stored at 25 °C and 4 °C, respectively	[233,234]
	LA/PS	Encapsulation in nanochannel fibers	PCM 81.5 wt% LA, T_m 42–53 °C, ΔH_m of 147.1 J g ⁻¹	[235]
	LA/PA eutectic + PVA / PA6	Coaxial ESP	T_m 32 °C, ΔH_m 93.12 J g ⁻¹ . Improved thermal characteristics of PCFs to control body temperature fluctuations	[236]
	MP/LA eutectic/PAN/Cu NPs	Single needle ESP	T_m 21 °C, ΔH_m 85.07 J g ⁻¹ . The addition of Cu NPs significantly augmented the heat storing and releasing rates of the phase change fibers	[237]
	CA/PA/SA eutectic/PAN/MWCNTs-COOH	Physical absorption	Phase change temperatures and enthalpies of PCFs were about 7 °C–32 °C and 130–138 J g ⁻¹ , respectively	[238]
	BS, CA/MA eutectic, CA/PA/SA eutectic/PAN/Ag-NPs	Physical absorption	Melting temperatures and enthalpies of the PCFs were in the range 23–29 °C and 138–157 J g ⁻¹ , respectively	[239]
	CA/PA/LA eutectic/PLA + CFP and graphene	Single needle ESP + electrospinning	T_m 14–17 °C, ΔH_m 7–24 J g ⁻¹ . The electrically conductive PCFs have unique features such as near-ambient phase change temperature	[240]
PEG-based form-stable PCMs	PEG/CA	Single needle ESP	ΔH_m , T_m , ΔH_c and T_c were about 86 J g ⁻¹ , 58 °C, 65 J g ⁻¹ , 39 °C, respectively	[228]
	PEG/PA6/HNTP	Coaxial ESP	Incorporation of 3 wt% HNT-P increased the tensile modulus value by 25%, the latent heat of melting from 68 J g ⁻¹ to up to 82 J g ⁻¹ , and PEG encapsulation efficiency from 78% to 96%	[244,245]
	PEG/PVA/Ag	Single needle ESP	T_m 46 °C, ΔH_m 67.5 J g ⁻¹ . Excellent thermal, chemical, and morphological stability after 2000 thermal cycles	[246]
Fatty acid alkyl esters	Dodecanol dodecanoate/ PVA/GA	Emulsion ESP	EE 33% T_m 25–30 °C, ΔH_m 65 J g ⁻¹	[248]
	MP and IPP/PAN and PMEA	Coaxial ESP	PAN-MP and PMEA-MP: ΔH_m 71 J g ⁻¹ and 86 J g ⁻¹ respectively; T_m 28–32 °C; EE: 49% and 69% respectively. PAN-IPP and PMAE-IPP: ΔH_m 72 J g ⁻¹ and 60 J g ⁻¹ respectively; T_m 7–15 °C; EE 77% and 87% respectively	[249]
Ionic liquid	1-hexadecyl-3-methylimidazolium bromide/CoPA/AlN	Single needle ESP	PCM 57 wt% and 5 wt% of AlN: T_m 63 °C, ΔH_m 86.4 J g ⁻¹ .	[250]

5.2. Hydrocarbons-Based Phase Change Electrospun Fibers

Long-chain aliphatic hydrocarbons and paraffin waxes have been widely investigated as solid–liquid PCMs incorporated in electrospun fibers, due to their low cost, high latent heat, as well as good chemical and thermal stability.^[222–224] In 2006, McCann

et al.^[227] were among the first researchers describing the fabrication of PCFs by a combination of solution and melt coaxial ESP (Figure 12a). Hexadecane, octadecane, and eicosane, with melting points (T_m) close to room temperature (27 °C for octadecane) and body temperature (37 °C for eicosane), were loaded into the fiber core as PCMs, while a composite made of PVP and TiO₂ was

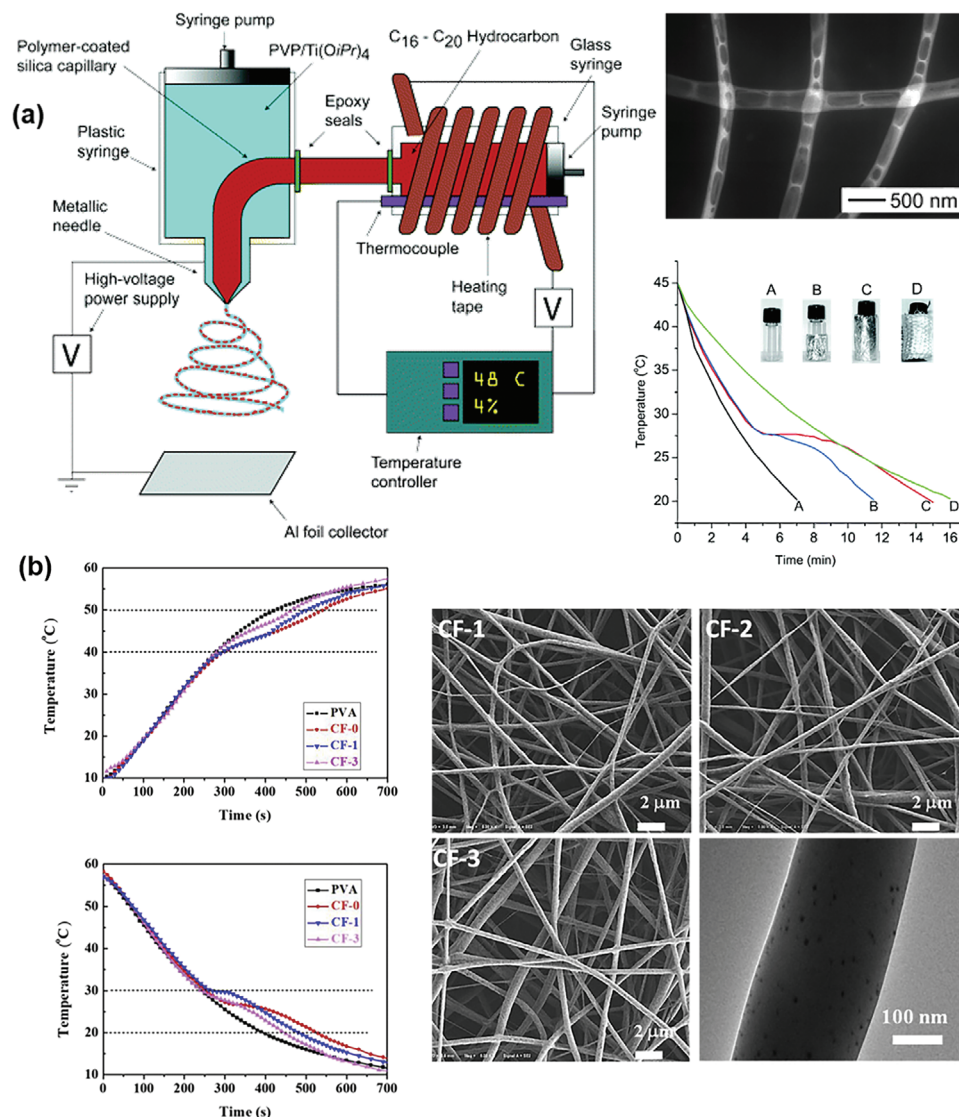


Figure 12. a) PVP–TiO₂ nanofibers loaded with hydrocarbon PCMs: schematic of the melt coaxial electrospinning setup, TEM image of the resulting fibers after removal of octadecane PCM and demonstration of thermal insulation capability of octadecane@TiO₂-PVP nanofibers, where 1 cm³ of water at 60 °C was allowed to cool in a 4 °C environment in glass vials covered with different insulation jackets (A: no insulation; B: half-covered with the PCM nanofiber jacket; C: fully covered by the PCM nanofiber jacket; D: covered by a jacket of conventional fiberglass). Reproduced with permission.^[227] Copyright 2006, American Chemical Society; b) PEG/PVA/Ag composite fiber: heating (top left) and freezing (bottom left) curves of PVA, CF-0, CF-1, and CF-3 (left); SEM images of CF-1, CF-2, and CF-3 fibers and TEM image of a CF-3 fiber (right). Reproduced with permission.^[246] Copyright 2020, Elsevier.

used as the sheath supporting material. The hydrocarbons were successfully incorporated along the fiber axis with a maximum content of 45 wt% (in the case of octadecane) and a corresponding melting enthalpy (ΔH_m) of 114 J g⁻¹, and the resulting PCFs demonstrated to efficiently stabilized temperature (Figure 12a). A similar instrumental set-up was recently used by Yi et al.^[229] to fabricate core–sheath PCFs with polyvinylbutyral (PVB) as the sheath and octadecane as the core of the fibers. Optimization of the PVB solution concentration and of the core feed rate allowed to maximize the encapsulation rate, resulting in a latent heat of 96.9 J g⁻¹. Additionally, the incorporation of a near-infrared absorber demonstrated the possibility to improve the efficiency of converting solar to thermal energy, and a 100 thermal cycles test

showed the good stability of the PCFs. In a recent systematic study published by Haghghat et al.,^[230] coaxial ESP was optimized to incorporate octadecane into PCFs by using PVP, PVDF, and PAN as fiber shell; among those, PVP showed the best results in terms of ΔH_m and ΔH_c . Indeed, PCM-PVP mat, with an encapsulation efficiency (EE) of around 36%, showed ΔH_m and ΔH_c of about 80 J g⁻¹, and good thermoregulating properties in body simulated conditions were reported. In another interesting study, Lu et al.^[231] successfully encapsulated paraffin wax (PW, $T_m = 52–54$ °C) as PCM in a sheath of PMMA through solution coaxial ESP. To improve the thermal conductivity, MWCNTs were also added to the sheath layer. The authors proved that the highest tested feed rate of the core solution led to the highest PW EE

(around 45%), with a latent heat of 58.25 J g^{-1} and a solidifying enthalpy of -56.49 J g^{-1} . After 200 thermal cycles, there was little change in latent heat, thus demonstrating the advantage of PCM encapsulation to prevent its leakage and enhance its thermal stability.

Single needle ESP has been used, in addition to coaxial ESP, by several researchers to fabricate ultrafine PCFs containing aliphatic hydrocarbons, or paraffin waxes. As an example, Zhao et al.^[232] prepared environmental-friendly octadecane/silk ultrafine PCFs from O/W emulsion ESP using hexadecyltrimethylammonium bromide (CTAB) as emulsifier. The phase change enthalpy of the fibers was around 40 J g^{-1} with a PCMs EE of about 20%. PCFs of interest in food packaging were systematically investigated by Chalco-Sandoval et al.^[233,234] The authors electrospun two PWs (RT4/RT-4 blend, $T_m = -1.5 \text{ }^\circ\text{C}$ and RT5, $T_m = 5 \text{ }^\circ\text{C}$) blended with different polymers (i.e., PCL, PS, and high impact PS) by means of single needle ESP, after optimization of the solvent systems. The most interesting results were obtained in the case of RT5 encapsulated in PS, which showed a particularly good EE ($\approx 78\%$). Additionally, the storage temperature influenced the reduction of melting and crystallization enthalpies over time, showing a decrease of $\approx 56\text{--}58\%$ and $\approx 30\text{--}40\%$ in samples stored at $25 \text{ }^\circ\text{C}$ and $4 \text{ }^\circ\text{C}$, respectively. Furthermore, the thermal buffering capacity of RT5 was investigated by recording the temperature profiles of PS trays with and without blending with PCM, demonstrating that RT5 effectively extended the time needed to increase the temperature of food products when compared to the neat PS tray.^[234]

5.3. Long-Chain Fatty Acids-Based Phase Change Electrospun Fibers

Long-chain fatty acids and their eutectics are among the most commonly investigated types of solid-liquid PCMs loaded in electrospun fibers. An interesting approach for encapsulating lauric acid (LA), a natural food-grade PCM, in PS fibers was presented by Lu et al.^[235] Via vapor-induced phase separation during ESP, the authors produced PS fibers with internal nanochannels that were subsequently filled by thermally heated LA through nanocapillary forces. Authors were thus able to encapsulate 81.5 wt% of LA, showing a ΔH_m of 147.1 J g^{-1} , which corresponded to 81.6% of the heat storage capacity of pristine LA. The LA-PS fibers showed a robust cycling stability and reusability without a significant decrease in thermal storage capacity during 100 continuous heating-cooling cycles. The eutectic mixture of two fatty acids, i.e., LA and palmitic acid (PA), was encapsulated in polyamide 6 (PA6) fibers through coaxial ESP by Hemmatian et al.^[236] PVA was added to the eutectic mixture to facilitate the ESP of the core material. The eutectic T_m was measured at $32 \text{ }^\circ\text{C}$ and the eutectic ΔH_m was 93.12 J g^{-1} . Thermal imaging demonstrated improved thermal characteristics of PCFs to control body temperature fluctuations. PAN has been used by several researchers as a supporting polymer with fatty acids eutectics.^[237-239] Xie et al.^[237] used single-needle ESP to electrospun blends of PAN and eutectic of methyl palmitate (MP) and LA with the addition of copper NPs to improve thermal conductivity. The obtained PCFs, with a phase transition at $21 \text{ }^\circ\text{C}$ and enthalpy of 85.07 J g^{-1} , showed an outstanding thermal reliability

and maintained their phase change properties even after long-time thermal cycles. The addition of copper NPs significantly augmented the heat-storing and releasing rates of the phase change fibers. Ke and Wei^[238] used PAN/MWCNTs-COOH composite fibrous membranes as supporting matrix for the physical absorption of the molten capric-palmitic-stearic acid ternary eutectic mixture (CA-PA-SA). The addition of 10% of MWCNTs-COOH decreased the melting and freezing times of the PCFs by about 52% and 56%, respectively, when compared to values of plain PCFs. The phase change temperatures and enthalpies of PCFs were about registered at $7 \text{ }^\circ\text{C}\text{--}32 \text{ }^\circ\text{C}$ and $130\text{--}138 \text{ J g}^{-1}$, respectively. In a similar study published by the same authors, PAN/Ag-NPs electrospun membranes have been used as supporting materials for the physical absorption of butyl stearate (BS), capric-myristic acid binary eutectic (CA-MA), and CA-PA-SA eutectic introduced as PCMs. Melting temperatures and enthalpies of the PCFs were measured in the range $23\text{--}29 \text{ }^\circ\text{C}$ and $138\text{--}157 \text{ J g}^{-1}$, respectively.^[239] In a recent study by Darzi et al.,^[240] PLA was used as supporting material for the PCM. ESP of a blend of CA-PA-LA fatty acid ternary eutectic and PLA (0.8:1 ratio) was simultaneously carried out together with the electro-spraying of carbon fiber powder (CFP) and graphene to fabricate nanofibers with improved thermal and electrical properties. The average T_m of graphene and CFP composites were detected at 14.5 and $16.9 \text{ }^\circ\text{C}$, respectively. The electrically conductive form-stable PCFs have shown unique features such as near-ambient phase change temperature as well as suitable matrix structure and physical properties required for energy storage/retrieval applications.

5.4. PEG-Based Phase Change Electrospun Fibers

PEG is a typical solid-liquid PCM with outstanding properties, including nontoxicity, corrosion resistance, and relatively large enthalpies. For these reasons, it has been widely used in the production of several electrospun PCF systems. One of the first studies on PEG-based PCFs was carried out by Chen et al.^[228] reporting the fabrication of PEG/cellulose acetate (1:1 w/w) ultrafine PCFs by ESP. Morphological analysis revealed that PEG was distributed both at the surface and within the core of the fibers. The obtained electrospun PCFs showed high latent heats of fusion and crystallization, with ΔH_m , T_m , ΔH_c and T_c of about 86 J g^{-1} , $58 \text{ }^\circ\text{C}$, 65 J g^{-1} , $39 \text{ }^\circ\text{C}$, respectively. The thermal properties and morphology of the fibers were well retained after 100 heating/cooling cycles, demonstrating good thermal stability and reliability. In addition to cellulose acetate, other polymers, such as PVDF,^[223,241] PAN,^[242] PLA,^[243] PVP,^[223] and PA6^[223,244,245] have been investigated as the fibrous supporting matrix for the encapsulation of PEG. In a recent paper by Yilmaz et al.,^[245] core-shell PCFs were fabricated by using coaxial ESP of PEG containing halloysite nanotubes (HNTs) as the core material and PA6 as fiber shell. Surface activation of HNTs was also conducted by piranha etching, in order to increase the affinity between etched nanotubes (HNT-P) and PEG. Results showed that the incorporation of 3 wt% HNT-P increased the tensile modulus value by 25%, the latent heat of melting from 68 J g^{-1} to up to 82 J g^{-1} , and PEG encapsulation efficiency from 78% to 96%. Another interesting PEG-based system was recently reported by Song et al.^[246] that de-

veloped eco-friendly PEG/PVA/Ag electrospun PCFs by ESP an aqueous solution of PEG/PVA/AgNO₃, followed by UV irradiation to generate Ag-NPs through photoreduction. The optimized ESP process was carried out with 45 wt% of PEG. The electrospun fibers with 0, 5, 10, and 15 w% of AgNO₃, were labeled as CF-0, CF-1, CF-2, and CF-3, respectively (Figure 12b). The fibers melted at 46 °C, had a latent heat of 67.5 J g⁻¹, and exhibited excellent thermal, chemical, and morphological stability after 2000 thermal cycles. The thermal energy storage times of CF-1 and CF-3 were 16% and 23% lower than that of CF-0, respectively, whereas the thermal energy release times of CF-1 and CF-3 were about 21% and 26% lower than that of CF-0, respectively.

5.5. Phase Change Electrospun Fibers Based on Other Types of PCMs

In addition to the PCMs described above, other commercial and synthesized solid-liquid PCMs were also employed in electrospun PCFs. Among those, fatty alcohols^[247] and fatty acid alkyl esters^[223,248,249] have recently become of interest as PCMs. Zhou et al.^[248] used emulsion ESP to prepare PCFs where dodecanol dodecanoate oil-in-water emulsion was mixed with PVA solution to yield polymer emulsion. This was then treated with glutaraldehyde to crosslink the polymer before the ESP process. Both the PVA/PCM nanofibers and the crosslinked ones presented a core-shell structure. Crosslinked fibers displayed excellent water resistance, good thermal stability, and improved mechanical properties. Endothermic peaks of the PCFs were measured in the range of 25–30 °C with a melting enthalpy of 65 J g⁻¹, indicating a PCM encapsulation efficiency of around 33%. In another recent article published by Onder and Sarier^[249] methyl palmitate (MP) and isopropyl palmitate (IPP) esters, were electrospun, through coaxial ESP, using either PAN or poly(methacrylic acid-co-ethyl acrylate) (PMEA) as supporting shell material. The phase change enthalpies of PAN-MP and PMEA-MP fibers were 71 J g⁻¹ and 86 J g⁻¹ at 28–32 °C, indicating an encapsulation efficiency of 49% and 69% respectively. Those of PAN-IPP and PMAE-IPP fibers were 72 J g⁻¹ and 60 J g⁻¹ at 7–15 °C, indicating an encapsulation efficiency of 77% and 87%, respectively. A very recent research article worth of mention is the study performed by Lin et al.^[250] The authors developed an innovative PCF material based on ionic liquid/aluminum nitride/copolyamide composite fabricated through ESP using HFIP as a common solvent. The ionic liquid 1-hexadecyl-3-methylimidazolium bromide (IL) was selected as phase change material, nano aluminum nitride (AlN) was chosen as additive, while copolyamide 6/12 (CoPA) was used as supporting matrix. IL crystallizes at 40 °C and displays two melting peaks at 61 °C and 65 °C. The latent heat of melting of IL was found to be 158.60 J g⁻¹, while that of freezing 133.91 J g⁻¹. IL/AlN/CoPA fibers with different compositions were studied. Fibers with 57 wt% of IL and 5 wt% of AlN showed a melting temperature of 63 °C and an enthalpy of 86.4 J g⁻¹, corresponding to an encapsulation efficiency of 57%. The authors demonstrated that new hydrogen bonds were formed between IL and CoPA, resulting in a beneficial effect on the thermal performance of the composite fibers.

6. Thermoelectric Electrospun Fibers

Thermoelectric materials are smart materials able to induce electrons and holes diffusion from a temperature gradient through p- and n-type semiconductors (also called Seebeck effect, discovered in 1821).^[251] The converse effect, that is the application of voltage to induce a temperature gradient across a thermoelectric material, was discovered by Jean Peltier^[251] in 1834, and it is thus called the Peltier effect.

The Seebeck effect may be interestingly exploited to convert waste heat into electricity, potentially improving the efficiency of energy usage in both industry and everyday life.^[252] The efficiency of thermoelectric materials is commonly described by the figure of merit ($zT = S^2\sigma T/k$), where S is the Seebeck coefficient (that in turn is the ratio of the induced voltage over the thermal gradient across the thermoelectric device), σ the electrical conductivity, T the absolute temperature and k the thermal conductivity. For many years, the benchmark for a good thermoelectric material has been to show a zT of order unit.^[252] Thermoelectric response may belong to two material classes: inorganic and organic materials: the first class includes oxides, chalcogenides, iodates, and nitrides; while the second one is mainly represented by the conjugated polymers.^[253] Recently, new materials and strategies have been exploited to reach higher values of figure of merit. In the framework of bulk solids, a successful route for improving zT is the reduction of lattice thermal conductivity; moreover, several studies have proposed that the reduction of the linear dimensions of the thermoelectric materials, transforming them in 1D structures, can induce an increase of zT .^[254–257] This can be ascribed to an increase of the Seebeck coefficient with respect to the bulk materials, due to the occurrence of a 1D electrons transport, and to a decrease of the thermal conductivity, k , probably linked to the boundary scattering of the phonons. In this context, ESP turned out to be a very promising strategy for the preparation of 1D nanostructures (mainly nanowires and nanofibers) potentially exploitable as thermoelectric materials. In the following paragraphs, we present and discuss studies proposing the use of the ESP technique to obtain inorganic, organic, and organic-inorganic thermoelectric nanostructures.

6.1. Inorganic Electrospun Fibers

Metal oxides were disregarded as potential candidates for the development of thermoelectric materials until the last two decades, when scientists discovered novel oxide thermoelectric materials. Among them, cobalt-based and zinc oxides, which do not experience oxidation problems under environmental conditions, have been widely investigated.^[258]

Qiu et al.^[259] used ESP to synthesize 1D Ca₂Co₂O₅ fibers, according to the procedure schematized in **Figure 13a**. The resulting fibers were composed of nanoplates that pile up to build-up a 1D hierarchical structure. The resulting materials were characterized by a Seebeck coefficient of 133 μV K⁻¹ at 305 K, which further increased to 191 μV K⁻¹ at 963 K. According to the authors, the presence of a high content of grains boundaries significantly contributes to the increase of the Seebeck coefficients. Furthermore, the hierarchical nanostructure plays a relevant role in reducing the lattice thermal conductivity of the materials due to the effective scattering of phonons at the grains' boundaries and in-

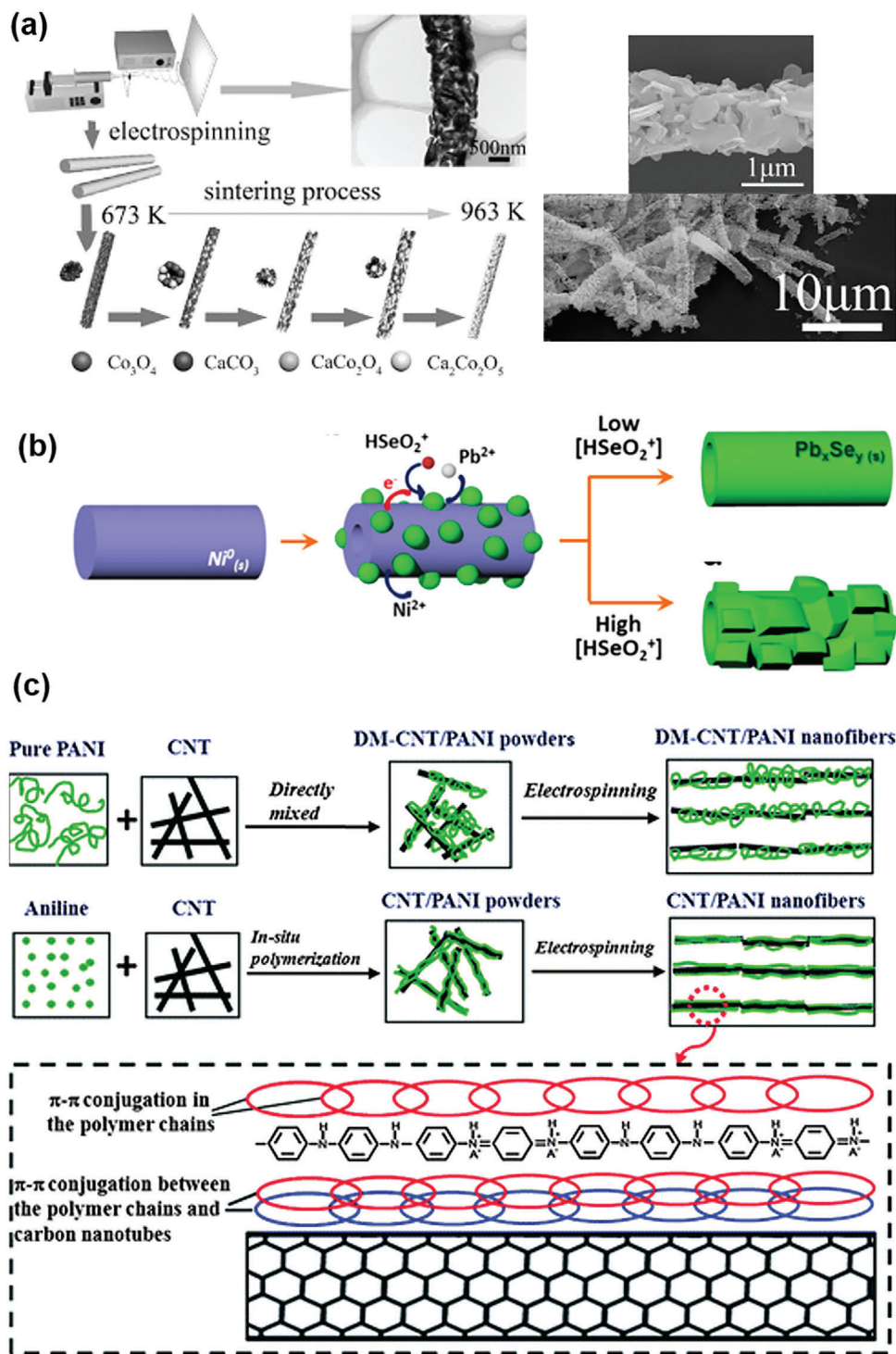


Figure 13. a) Scheme of the formation and morphological evolution of 1D hierarchical $\text{Ca}_2\text{Co}_2\text{O}_5$ fibers (left) and corresponding SEM image of $\text{Ca}_2\text{Co}_2\text{O}_5$ (right). Reproduced with permission.^[259] Copyright 2015, Elsevier. b) Schematic illustration of the galvanic displacement reaction of Ni nanofibers to form Pb_xSe_y hollow nanofibers. Reproduced with permission.^[267] Copyright 2014, American Chemical Society. c) Schematic representations of the formation mechanism of DM-CNT/PANI and CNT/PANI nanofibers: the enlarged part shows the highly ordered arrangement of the PANI backbone chains on the surface of the CNTs. Reproduced with permission.^[271] Copyright 2012, Royal Society of Chemistry.

interfaces. Xu et al.^[260] carried out studies devoted to measure the Seebeck coefficient and thermal conductivity of $\text{La}_{0.95}\text{Sr}_{0.05}\text{CoO}_3$ nanofibers. The Seebeck coefficient was measured for fibers with a diameter around 35 nm and it turned out to reach the high value of $650 \mu\text{V K}^{-1}$ in environmental conditions, able to provide a voltage output of 1.7 mV. In a following paper, the thermal conductivity^[261] was investigated for $\text{La}_{0.95}\text{Sr}_{0.05}\text{CoO}_3$ fibers showing a diameter of 140 and 290 nm; values of $0.7 \text{ W m}^{-1} \text{ K}^{-1}$ and $2.1 \text{ W m}^{-1} \text{ K}^{-1}$ were reached respectively, confirming the dramatic effect of fiber diameter on the thermal conductivity. Besides the fiber diameter, the grain scale turned up to be an important parameter for thermoelectric properties. In this frame, Lee et al.^[262] produced ZnO/PVP electrospun nanofibers, which were sintered at 550°C for 30 min under a nitrogen atmosphere and that presented different morphology depending on the applied cooling rate. The quenched nanofibers consisted of mesoscale grains linked along the fiber's axis and showed Seebeck coefficient of $-313.7 \mu\text{V K}^{-1}$, while slowly cooled fibers, with a Seebeck coefficient of only $-82.1 \mu\text{V K}^{-1}$, showed a smooth surface.

Besides metal oxides, other metal compounds were investigated for the production of thermoelectric electrospun materials. Among them, lead telluride (PbTe) has been object of study: it is a V–VI semiconductor with a narrow bandgap energy of 0.31 eV at room temperature and with a rock salt crystal structure. By adjusting its composition, PbTe can be either an n-(Pb rich PbTe) or a p-type (Te rich PbTe) semiconductor.^[263] Zhang et al.^[264] proposed the fabrication of PbTe thermoelectric hollow nanofibers by means of a galvanic displacement process carried out onto sacrificial cobalt nanofibers. First, the cobalt nanofibers were obtained from ESP a solution containing cobalt, citric acid, and PVP followed by calcination. Then, the galvanic displacement process was performed by immersing the freestanding cobalt nanofibers into a solution containing lead nitrate, tellurium oxide, and nitric acid: Co fibers acted as a template for PbTe deposition and slowly dissolved into Co^{2+} . The morphology of the resulting hollow PbTe nanotubes was adjusted by acting on the Pb^{2+} concentration in the electrolyte, while their diameter was tuned by modifying the diameter of the cobalt nanofibers. PbTe-based hollow nanofibers for thermoelectric applications were also synthesized by Park et al.^[265] via a three-step sequential process consisting of: i) production of silver nanofibers by ESP, ii) electrodeposition of Te, in order to obtain silver telluride nanotubes, and iii) cationic exchange reaction in $\text{Pb}(\text{NO}_3)_2$ solution. Polycrystalline PbTe nanotubes with an average diameter of 100 nm and with 20 nm of wall thickness were thus produced. Variation of the Ag-to-Pb ratio in the $\text{Ag}_x\text{Te}_y\text{-PbTe}$ nanocomposites during the cationic exchange reaction enabled to control the thermoelectric properties of resulting 1D hollow nanofibers. Indeed, the highest value of Seebeck coefficient ($433 \mu\text{V K}^{-1}$ at 300 K) was achieved for a remaining Ag content of around 30%.

Lead selenide (PbSe), a material similar to PbTe, has not been exploited for thermoelectric applications for several years, due to its smaller bandgap energy and the expected higher thermal conductivity.^[266] Recently, significant progresses have been carried out by reducing the dimensions of PbSe devices, in order to increase the Seebeck coefficient and to reduce the thermal conductivity. The combination of ESP and galvanic displacement was employed for the development of ultralong hollow $\text{Pb}_x\text{Se}_y\text{Ni}_z$ nanofibers.^[267] The concentration of cations (HSeO_4^- in this

study), controls the formation of protrusions onto the surface of nanotubes, as schematized in Figure 13b, as similarly observed in the previously reported work on PbTe.

6.2. Organic Electrospun Fibers

Polymers have attracted great attention for the realization of thermoelectric devices, mainly due to their easy fabrication processes and low material costs. Furthermore, thanks to the possibility of easily tune their physical and chemical properties, it is possible to properly design the most suitable polymer for a specific application. Conjugated polymers turn out to be particularly suitable for thermoelectric applications; having a backbone containing sp^2 hybridized carbons, able to delocalize electrons. These organic semiconductors are typically doped to increase their conductivity by 7–9 orders of magnitude.^[268] Furthermore, also in this context, conjugated polymers, nanowires, and nanotubes have been considered particularly intriguing, due to their frequent higher molecular order and improved charge-carrier transport compared to more conventional structures, such as thin films.^[269,270]

With the aim to obtain ordered nanostructures exploitable for thermoelectric applications, Wang et al.^[271] produced CNTs/polyaniline (PANI) composites through a combination of in situ polymerization and ESP. Raman spectroscopy and X-ray diffraction demonstrated that PANI nanofibers were aligned along the CNTs axis, due to the presence of strong chemical interactions between PANI and CNTs. This arrangement contributed to reduce the $\pi\text{-}\pi$ conjugated defects in the polymer backbones and to relevantly increase the effective degree of electron delocalization, with a consequent improvement of conductivity. As a comparison, composites obtained by ESP a mixture of already formed PANI macromolecules and CNTs (DM-CNT/PANI) was reported. The schematic representation of the two distinct strategies is reported in Figure 13c; the enlarged part of the figure highlights the highly ordered structure achieved when aniline was polymerized in situ to form PANI chains on the CNTs surface. The electrical conductivity (σ) and Seebeck coefficient (S) of the CNT/PANI composites were measured along and perpendicularly to the fibers' axis. DM-CNT/PANI turned out to show an isotropic behavior, with σ and S increasing at the increase of CNTs content, in accordance with the simple rule of mixture of composite materials. For the in situ fabricated CNT/PANI nanofiber composites, σ and S also increased with the increase of CNTs content and a more anisotropic behavior was detected. Biobased carbon nanofibers, potentially suitable for thermoelectric applications, were also developed by ESP PAN and lignin.^[272] The presence of lignin, with a content of 70% w/w, contributed to increase the p-type power factor of 34.5 folds with respect to the one registered in absence of lignin. By subjecting the samples to a hydrazine treatment, an increase of the n-type power factor around 11 folds was registered for nanofibers containing lignin with respect to those containing only polyacrylonitrile.

6.3. Organic–Inorganic Electrospun Fibers

With the final aim to develop wearable thermoelectric devices, able to convert the heat from the human body into electric en-

ergy, the production of organic–inorganic electrospun materials has been investigated. This strategy has been pursued in order to combine the typical characteristics of conjugated polymers, such as cost-effectiveness, high flexibility, low intrinsic thermal conductivity, and outstanding potential for use on the human body, with the high output power density of inorganic thermoelectric materials.

Tin oxide NPs and vanadium oxide/tin oxide nanocomposites were prepared using a simple sol-gel method followed by ESP process, using PVA as a carrier.^[273] PVA–SnO₂ nanofibers were characterized by the presence of beads, which were not detectable in PVA–V₂O₅/SnO₂ nanofibers. The produced nanofibers showed interesting thermoelectric properties, with a Seebeck coefficient in the range 20–100 V K⁻¹ evaluated from room temperature to 400 K. Ryu et al.^[274] reported the use of dual-ESP for the fabrication of PAN and sodium cobalt oxide precursors. The obtained fibers were heat-treated to simultaneously induce carbonation and calcination. The EDS analysis confirmed the presence of both PAN-derived carbon nanofibers and NaCo₂O₄-based ceramic nanofibers. The Seebeck coefficient increased from 27 to 73 μV K⁻¹ and from 15 to 41 μV K⁻¹ with the increase of the NaCo₂O₄ content inside the nanofibers fabricated at 700 and 800 °C, respectively. However, an opposite trend was detected for the electrical conductivity, which turned out to increase with the reduction of NaCo₂O₄ inside the fibers as well as with the increase of thermal treatment temperature. Mohammadi et al.^[275] prepared through ESP nanocomposite structures composed of PVP/CNTs/ CuO NPs. The resulting nanofibers, containing 20:20 w/w (CuO: CNT) NPs, showed a Seebeck coefficient up to 29.13 μV K⁻¹ and an electrical conductivity of 2.114 × 10⁻⁴ S cm⁻¹. This result paves the way to the development of multilayer composites, employable as energy-saving devices.

7. Pyroelectric Electrospun Fibers

In the context of thermal energy harvesting, while thermoelectric materials have been widely employed to convert temperature gradients (dT/dx) into electrical energy; pyroelectricity, namely the potential of certain materials to convert temperature fluctuations (dT/dt) in electrical energy,^[276] is still less exploited, although this property, typical of ferroelectric materials, has been object of study since 1960s.^[277–279] Pyroelectrics are characterized by a crystal structure that displays a spontaneous polarization (P_s) in the absence of an applied electric field.^[280] The pyroelectric effect is based on the change of polarization with temperature that generates charges at the material surface; therefore, when pyroelectric materials are heated ($dT/dt > 0$) or cooled ($dT/dt < 0$), the overall polarization is decreased or increased, respectively, causing current to flow in the circuit.^[276] Pyroelectric properties are typically associated with piezoelectricity, namely the ability of the material to convert mechanical energy into electrical energy.

Pyroelectric materials can be classified into inorganic, organic, and organic–inorganic materials. The class of inorganic materials is definitely the widest one and it includes: i) lead-based and lead-free single crystals; ii) metal oxide materials; iii) nanostructures, such as the halloysite nanotubes, naturally occurred materials formed by the rolling of aluminosilicate kaolin sheet. Pyroelectric materials can be classified into inorganic, organic, and organic–inorganic materials. The class of inorganic materi-

als is definitely the widest one and it includes: In the frame of organic materials, PVDF and poly(vinylidene fluoride-co-trifluoroethylene) P(VDF-TrFE) copolymers are the most important examples. Concerning the organic–inorganic materials, they are developed with the aim to combine the pyroelectricity of the inorganic component with the flexibility and the low permittivity of the polymeric matrix.^[276]

Among the process for the fabrication of pyroelectric materials, ESP has revealed a big potential for the development of fiber-based organic and organic–inorganic pyroelectric materials. Conversely, to the best of our knowledge, no studies have so far reported the development of pure inorganic electrospun nanofibers.

Indeed, ESP has been widely investigated to obtain PVDF nanofibers membranes suitable for energy harvesting without any additional treatment: during the ESP process, the applied high voltage, rapid evaporation of the solvent, and high stretching ratio of the PVDF solution jet induce the crystallization in the β -phase,^[281,282] which shows the most promising piezo- and pyroelectric properties. Furthermore, in organic–inorganic nanofibers, the presence of the inorganic nanofillers turns out to play an important role in improving the piezoelectric and pyroelectric properties of PVDF. Indeed, the intimate interface between PVDF and nanofillers suggests a strong electrostatic interaction, with a resulting increase of the β -phase content.^[283]

7.1. Pyroelectric Organic Nanofibers

Pyroelectric organic nanofibers were exploited by Roy et al. for the fabrication of self-powered, flexible, piezo- and pyro-electric hybrid nanogenerator (NG) device capable to work as a pyroelectric breathing sensor.^[284] The strategy was based on the incorporation of organic nanofiller, i.e., graphene oxide, inside PVDF nanofibers and the resulting device was obtained according to the scheme reported in **Figure 14a**. The device turned out to reach a pyroelectric output power density around 1.2 nW m⁻², and was able to sense temperature changes during respiration thanks to the generation of an output voltage when mounted on a N95 mask at the location where most of the airflow during the respiration process is condensed, with temperature fluctuations of almost 5 K. Isakov et al. reported the fabrication of electrospun PVA and 1,4-diazabicyclo[2.2.2]octane perchlorate (dabcoHReO₄) and their suitability for energy microharvesting and thermal sensing.^[285] DabcoHReO₄ is characterized by NH–N hydrogen-bonded cations aligned along the [001] polar axis. These hydrogen bond networks directly contribute to the existence of a P_s at room temperature. XRD analysis reported that dabcoHReO₄ nanocrystals are oriented in order that the NH–H interactions are parallel to the fiber mat plane. The authors investigated the pyroelectric current obtained from 1 cm² of electrospun mat as a function of the temperature. The pyroelectric response turned out to be nearly symmetrical with respect to heating/cooling and the current followed the shape of the temperature fluctuations over time. De Matos Gomes et al. proposed an interesting study in which the pyroelectric properties of PEO nanofibers embedding DL-alanine and L-lysine amino acids were investigated.^[286] Polar crystalline amino acids, apart from glycine, are chiral and, therefore, when crystallized they dis-

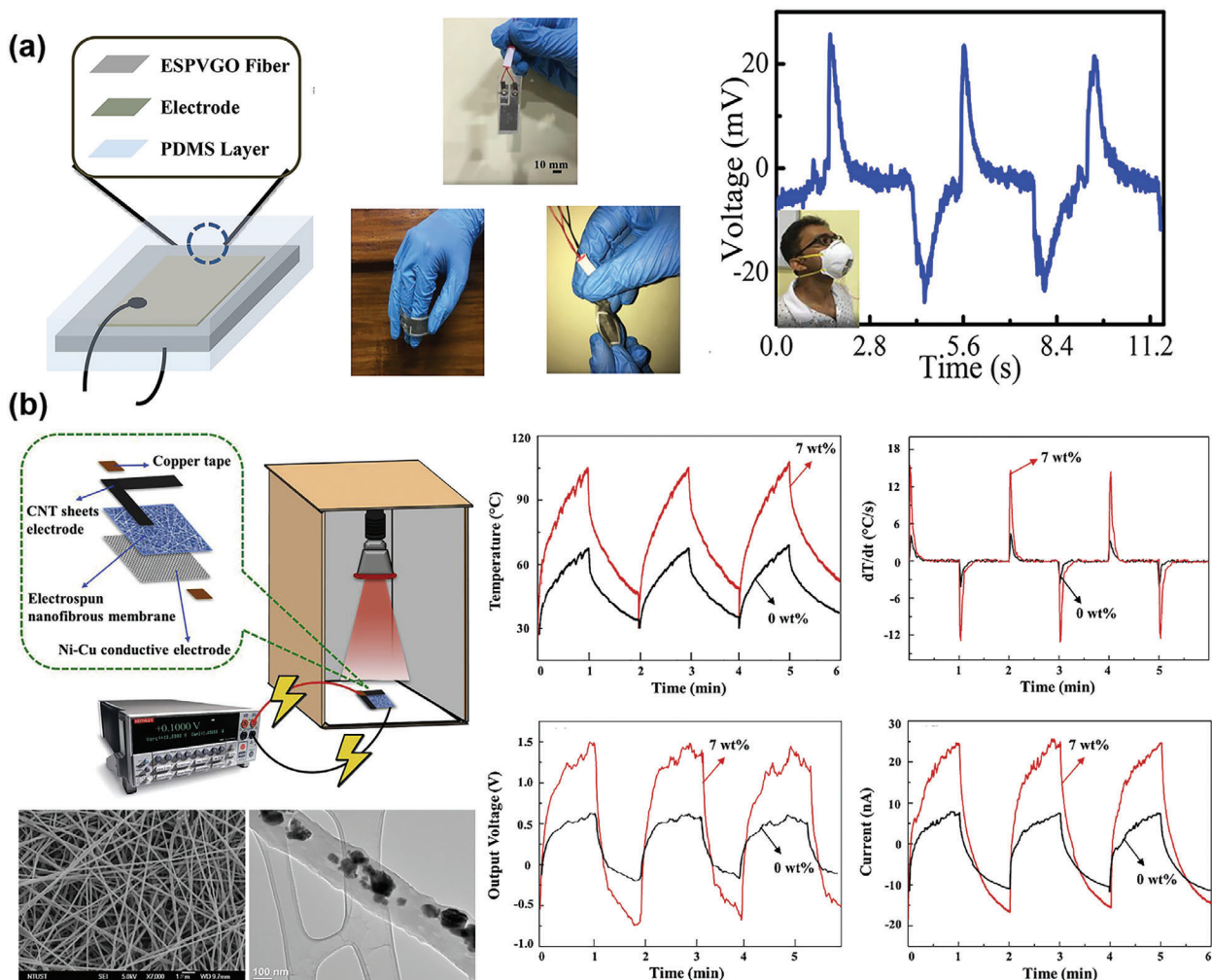


Figure 14. a) A sketch of the nanogenerator stack composed of PVDF nanofibers containing graphene oxide NPs and images of the fabricated flexible sensor and its bending and twisting ability (left); open-circuit voltage of the PVDF/graphene oxide nanofibers driven by human respiratory at room temperature. Reproduced with permission.^[284] Copyright 2019, American Chemical Society. b) Schematic illustration for the measurement of pyroelectricity PVDF/ $\text{WO}_{2.72}$ nanofibers irradiated by a NIR lamp; SEM and TEM images of the nanofibers are reported (left, scale bars: 1 μm , 100 nm). Temperature variation in time, corresponding differential curve, output voltage, and output current of $\text{WO}_{2.72}$ -free PVDF and 7 wt% PVDF/ $\text{WO}_{2.72}$ pyroelectric composites (right). Reproduced with permission.^[283] Copyright 2019, Elsevier.

play piezoelectricity and pyroelectricity.^[287] The pyroelectric coefficient, defined as the differential change of spontaneous polarization at a constant electric field and stress due to a temporal change in temperature, turned out to be 150 and 1.4 $\mu\text{C m}^{-2} \text{K}$ for electrospun mats containing L-lysine hemihydrate and DL-alanine, respectively. The pyroelectric coefficient exhibited by L-lysine hemihydrate nanofibers is remarkably high, showing the same order of magnitude of those displayed by some bulk semiorganic ferroelectric crystals, such as the triglycine sulfate (TGS), which lies within 158–350 $\mu\text{C m}^{-2} \text{K}$ at 25 $^{\circ}\text{C}$.^[288]

7.2. Pyroelectric Organic–Inorganic Nanofibers

In recent years, efforts have been devoted to the development of organic–inorganic electrospun materials with the aim to increase the pyroelectric performances of electrospun PVDF.

In this regard, Abbasipour et al.,^[289] to increase the piezoelectric and pyroelectric performances of PVDF nanofibers, introduced specific fillers inside the fibers. Among them also inorganic fillers, i.e., halloysites nanotubes, were tested with different concentrations. The incorporation of halloysites nanotubes simultaneously improved the piezoelectric and pyroelectric properties of the electrospun nanofibers, due to the enhancement of electroactive β -phase. In particular, the presence of nanofillers turned out to have a greater impact on the pyroelectric coefficient (increase of 31% with respect to the one of PVDF) than on the piezoelectric one (increase of 25% with respect to the one of PVDF). Finally, the presence of the inorganic nanofillers also conferred greater thermal and mechanical stability to the resulting fibers, as a consequence of the interactions between the polymer chains and the fillers. In another example, Wu et al.^[283] incorporated tungsten oxide ($\text{WO}_{2.72}$) photothermal NPs inside PVDF nanofibers to obtain a near-infrared (NIR) driven noncontact py-

roelectric generator (Figure 14b). When NIR radiation struck the PVDF/ $\text{WO}_{2.72}$ ($\text{WO}_{2.72}$ concentration = 7% wt) and $\text{WO}_{2.72}$ -free PVDF pyroelectric composites, a rapid increase of the temperature to 107.1 °C for PVDF/ $\text{WO}_{2.72}$ after 60 s was reached. This value was 41.5 °C higher than that of the PVDF nanofibers. As a result, the voltage and current output values of PVDF/ $\text{WO}_{2.72}$ composites reached 1.5 V and 25 nA, which represented a significant increase of 200% compared to the $\text{WO}_{2.72}$ -free PVDF (0.5 V and 8 nA). The results highlighted the significant improvement of the pyroelectric properties through the introduction of photo-thermal inorganic particles inside the PVDF nanofibers.

Sultana et al.^[290] developed a piezoelectric nanogenerator based on electrospun PVDF nanofibers incorporating methylammonium lead iodide (MAPI), able to harvest mechanical and thermal energies. The presence of MAPI in the nanofibers improved the fraction of the electroactive phase, which reached 95%. When subjected to a periodic compressive contact force at a frequency of 4 Hz, the device was able to generate an output voltage around 220 mV. Moreover, upon exposure to cyclic heating and cooling, a pyroelectric output current of 18.2 pA and a voltage of 41.78 mV were reached. Finally, the fast response and reset times, jointly with a pyroelectric coefficient around 44 pC m⁻² K⁻¹, demonstrated the potential of the material to be employed as a self-powered pyroelectric temperature sensor.

8. Concluding Remarks and Perspectives

An important contribution to the field of “intelligent” materials is given by the creativity of researchers, who can develop new stimuli-responsive systems by playing with chemical units and functional groups. However, a good control of the kinetics and the sensitivity of the response needs also a proper selection of the processing technology to control polymer solid-state properties and morphology. In this framework, electrospinning, enabling the accomplishment of high polymer chain orientation, high anisotropy, and high surface to volume ratio, offers outstanding advantages to tailor and exploit material responsiveness. In this review, we have presented the recent advancements of research on smart active materials produced by electrospinning, focusing exclusively on systems responsive to temperature. All categories of thermo-active materials processed by this technique have been discussed, describing their working principles, the electrospinning fabrication approaches, and their customized properties.

This literature overview shows that several different functions can be accomplished by thermo-active smart fibers, including actuation, drug release, separation processes, energy storage and conversion, sensing, self-healing, etc. However, much more research is still needed to fully exploit the possible benefits provided by electrospinning technology.

First, a more consolidated fundamental knowledge on the effects of polymer chain conformation, nanodimension, fiber alignment, and surface-to-volume ratio on the temperature responsiveness must be acquired. For instance, it is expected that fiber diameter, which in turns defines the surface-to-volume ratio of the fibers and affects the degree of chain orientation, has a massive influence on both the kinetics and the extent of the response. This know-how will conceivably allow to smartly tune

and control the electrospinning parameters to produce smart fibers with improved performance.

Other relevant advancements are expected when the versatility of the technology to produce-multilayer structures and composites will be fully exploited. Some steps in this direction have been already made but an infinite number of possible combinations of morphologies, fiber spatial organization, and polymers, arranged either as separated layers or to create gradient structures, can be developed and exploited to accomplish specific performances not achievable with the single components.

All these developments are expected to lead a better control of the material properties. On the other hand, the fine tuning of the stimulus both in time and in space, can be obtained by doping the fibers with internal heating sources in order to induce the thermal stimulus in an indirect way but with reliable sources, such as light as well as electrical and magnetic fields. This approach will allow to remotely and accurately control the material properties, exploring complex responses. Additionally, this strategy will benefit the freedom in the design of stimuli-responsive textiles. Moreover, the integration of several responsive materials will allow the production of multifunctional and multi-tasking systems, thus broadening the range of applications to meet practical needs.

Recently, scientific research has been very active in this field and we strongly believe that all these goals are not far to come, soon allowing electrospun materials to take over important roles in the broad framework of smart materials. We are entering, in fact, a new era in which smart materials will be increasingly applied in manufacturing, automotive, aerospace, and construction sectors, packaging, energy advertising, coating, soft robotics, water treatments and in the biomedical fields. Thus, we hold our hope that this review might be of some help and inspiration for scientists and engineers working in many different fields.

Acknowledgements

C.R. and F.P. acknowledge the First TEAM programme of the Foundation for Polish Science (POIR.04.04.00-00-5ED7/18-00), and the financial support from the Polish Ministry of Science and Higher Education through scholarships for outstanding young scientists. C.R. was partially supported by the Foundation for Polish Science (FNP). C.G. and N.Z. acknowledge MIUR through the PRIN project “Functional supramolecular polymers for self-diagnostic materials”, project n° 20179BJNA2, for financial support.

Open Access Funding provided by Università degli Studi di Bologna within the CRUI-CARE Agreement.

Conflict of Interest

The authors declare no conflict of interest.

Keywords

electrospinning, phase change materials, pyroelectric materials, shape memory polymers, thermoelectric materials, thermo-optically responsive materials, thermoresponsive materials

Received: October 16, 2021

Revised: December 15, 2021

Published online:

- [1] F. Liu, M. W. Urban, *Prog. Polym. Sci.* **2010**, *35*, 3.
- [2] Z.-Q. Cao, G.-J. Wang, *Chem. Rec.* **2016**, *16*, 1398.
- [3] M. D. Hager, S. Bode, C. Weber, U. S. Schubert, *Prog. Polym. Sci.* **2015**, *49*, 3.
- [4] C. J. Kloxin, T. F. Scott, B. J. Adzima, C. N. Bowman, *Macromolecules* **2010**, *43*, 2643.
- [5] L. Hines, K. Petersen, G. Z. Lum, M. Sitti, *Adv. Mater.* **2017**, *29*, 1603483.
- [6] M. C. Koetting, J. T. Peters, S. D. Steichen, N. A. Peppas, *Mater. Sci. Eng., R* **2015**, *93*, 1.
- [7] M. Karimi, A. Ghasemi, P. Sahandi Zangabad, R. Rahighi, S. M. Moosavi Basri, H. Mirshekari, M. Amiri, Z. Shafaei Pishabad, A. Aslani, M. Bozorgomid, D. Ghosh, A. Beyzavi, A. Vaseghi, A. R. Aref, L. Haghani, S. Bahrami, M. R. Hamblin, *Chem. Soc. Rev.* **2016**, *45*, 1457.
- [8] Y. Zhu, B. Yang, S. Chen, J. Du, *Prog. Polym. Sci.* **2017**, *64*, 1.
- [9] Z.-C. Jiang, Y.-Y. Xiao, Y. Kang, M. Pan, B.-J. Li, S. Zhang, *ACS Appl. Mater. Interfaces* **2017**, *9*, 20276.
- [10] D. Wang, Y. Jin, X. Zhu, D. Yan, *Prog. Polym. Sci.* **2017**, *64*, 114.
- [11] J. Xue, T. Wu, Y. Dai, Y. Xia, *Chem. Rev.* **2019**, *119*, 5298.
- [12] J. F. Cooley, US 692,631, **1902**.
- [13] W. J. Morton, US 705,691, **1902**.
- [14] J. Doshi, D. H. Reneker, *J. Electrostat.* **1995**, *35*, 151.
- [15] H. Fong, I. Chun, D. H. Reneker, *Polymer* **1999**, *40*, 4585.
- [16] D. H. Reneker, A. L. Yarin, H. Fong, S. Koombhongse, *J. Appl. Phys.* **2000**, *87*, 4531.
- [17] R. Jaeger, M. M. Bergshoef, C. M. I. Batlle, H. Schönherr, G. Julius Vancso, *Macromol. Symp.* **1998**, *127*, 141.
- [18] M. M. Hohman, M. Shin, G. Rutledge, M. P. Brenner, *Phys. Fluids* **2001**, *13*, 2221.
- [19] A. Haider, S. Haider, I.-K. Kang, *Arabian J. Chem.* **2018**, *11*, 1165.
- [20] D. Mailley, A. Hébraud, G. Schlatter, *Macromol. Mater. Eng.* **2021**, *306*, 2100115.
- [21] H. M. Ibrahim, A. Klingner, *Polym. Test.* **2020**, *90*, 106647.
- [22] M. Richard-Lacroix, C. Pellerin, *Macromolecules* **2013**, *46*, 9473.
- [23] D. Papkov, N. Delpouve, L. Delbreilh, S. Araujo, T. Stockdale, S. Mamedov, K. Maleckis, Y. Zou, M. N. Andalib, E. Dargent, V. P. Dravid, M. V. Holt, C. Pellerin, Y. A. Dzenis, *ACS Nano* **2019**, *13*, 4893.
- [24] D. Papkov, Y. Zou, M. N. Andalib, A. Goponenko, S. Z. D. Cheng, Y. A. Dzenis, *ACS Nano* **2013**, *7*, 3324.
- [25] I. Greenfeld, X. Sui, H. D. Wagner, *Macromolecules* **2016**, *49*, 6518.
- [26] C. Lu, S. W. Chiang, H. Du, J. Li, L. Gan, X. Zhang, X. Chu, Y. Yao, B. Li, F. Kang, *Polymer* **2017**, *115*, 52.
- [27] X.-X. He, J. Zheng, G.-F. Yu, M.-H. You, M. Yu, X. Ning, Y.-Z. Long, *J. Phys. Chem. C* **2017**, *121*, 8663.
- [28] W. E. Teo, S. Ramakrishna, *Nanotechnology* **2006**, *17*, R89.
- [29] D. Crespy, K. Friedemann, A.-M. Popa, *Macromol. Rapid Commun.* **2012**, *33*, 1978.
- [30] D.-G. Yu, M. Wang, X. Li, X. Liu, L. - M. Zhu, S. W. A. Blich, *Wiley Interdiscip. Rev. Nanomed. Nanobiotechnol.* **2020**, *12*, e1601.
- [31] P. Rathore, J. D. Schiffman, *ACS Appl. Mater. Interfaces* **2020**, *13*, 48.
- [32] O. Akampumuza, H. Gao, H. Zhang, D. Wu, X.-H. Qin, *Macromol. Mater. Eng.* **2018**, *303*, 1700269.
- [33] L. Persano, A. Camposeo, C. Tekmen, D. Pisignano, *Macromol. Mater. Eng.* **2013**, *298*, 504.
- [34] S. Thakkar, M. Misra, *Eur. J. Pharm. Sci.* **2017**, *107*, 148.
- [35] C. Gualandi, A. Zucchelli, M. Fernández Osorio, J. Belcari, M. L. Focarete, *Nano Lett.* **2013**, *13*, 5385.
- [36] Y. Liao, C.-H. Loh, M. Tian, R. Wang, A. G. Fane, *Prog. Polym. Sci.* **2018**, *77*, 69.
- [37] L. M. Valencia-Osorio, M. L. Álvarez-Láinez, *Macromol. Mater. Eng.* **2021**, *306*, 2100278.
- [38] G. Yang, X. Li, Y. He, J. Ma, G. Ni, S. Zhou, *Prog. Polym. Sci.* **2018**, *81*, 80.
- [39] Y. Ding, W. Li, F. Zhang, Z. Liu, N. Zanjanzadeh Ezazi, D. Liu, H. A. Santos, *Adv. Funct. Mater.* **2019**, *29*, 1802852.
- [40] S. Chen, R. Li, X. Li, J. Xie, *Adv. Drug Delivery Rev.* **2018**, *132*, 188.
- [41] J. Liu, X. Liu, D. Li, G. Yue, H. Li, S. Li, S. Gao, N. Wang, Z. Cui, J. Bai, Y. Zhao, *ChemNanoMat* **2020**, *6*, 1149.
- [42] D. Bonincontro, F. Frascchetti, C. Squarzone, L. Mazzocchetti, E. Maccaferri, L. Giorgini, A. Zucchelli, C. Gualandi, M. L. Focarete, S. Albonetti, *Processes* **2020**, *8*, 45.
- [43] T. Yang, L. Zhan, C. Z. Huang, *TrAC, Trends Anal. Chem.* **2020**, *124*, 115813.
- [44] H.-J. Cho, Y. H. Kim, S. Park, I.-D. Kim, *ChemNanoMat* **2020**, *6*, 1014.
- [45] A. Zucchelli, M. L. Focarete, C. Gualandi, S. Ramakrishna, *Polym. Adv. Technol.* **2011**, *22*, 339.
- [46] R. Palazzetti, A. Zucchelli, *Compos. Struct.* **2017**, *182*, 711.
- [47] Q. Wei, F. Xiong, S. Tan, L. Huang, E. H. Lan, B. Dunn, L. Mai, *Adv. Mater.* **2017**, *29*, 1602300.
- [48] X. Lu, C. Wang, F. Favier, N. Pinna, *Adv. Energy Mater.* **2017**, *7*, 1601301.
- [49] T. A. Arica, T. Isik, T. Guner, N. Horzum, M. M. Demir, *Macromol. Mater. Eng.* **2021**, *306*, 2100143.
- [50] L. Liu, W. Xu, Y. Ding, S. Agarwal, A. Greiner, G. Duan, *Compos. Commun.* **2020**, *22*, 100506.
- [51] J. D. Fox, S. J. Rowan, *Macromolecules* **2009**, *42*, 6823.
- [52] A. E. Felber, M.-H. Dufresne, J.-C. Leroux, *Adv. Drug Delivery Rev.* **2012**, *64*, 979.
- [53] A. W. Jackson, D. A. Fulton, *Polym. Chem.* **2012**, *4*, 31.
- [54] R. J. Wojtecki, M. A. Meador, S. J. Rowan, *Nat. Mater.* **2011**, *10*, 14.
- [55] T. Liu, T. Zhou, Y. Yao, F. Zhang, L. Liu, Y. Liu, J. Leng, *Composites, Part A* **2017**, *100*, 20.
- [56] H. K. Bisoyi, A. M. Urbas, Q. Li, *Adv. Opt. Mater.* **2018**, *6*, 1800458.
- [57] S. Nikazar, M. Barani, A. Rahdar, M. Zoghi, G. Z. Kyzas, *Chemistry-Select* **2020**, *5*, 12590.
- [58] W. Wang, Y. Liu, J. Leng, *Coord. Chem. Rev.* **2016**, *320*, 38.
- [59] B. T. Mai, S. Fernandes, P. B. Balakrishnan, T. Pellegrino, *Acc. Chem. Res.* **2018**, *51*, 999.
- [60] J.-N. Zhang, Y.-M. Ma, J.-J. Zhang, D. Xu, Q.-L. Yang, J.-G. Guan, X.-Y. Cao, L. Jiang, *Mater. Lett.* **2011**, *65*, 3639.
- [61] Y.-C. Chiu, Y. Chen, C.-C. Kuo, S.-H. Tung, T. Kakuchi, W.-C. Chen, *ACS Appl. Mater. Interfaces* **2012**, *4*, 3387.
- [62] H.-J. Lin, C.-Y. Chen, *J. Mater. Sci.* **2015**, *51*, 1620.
- [63] J.-J. Li, L.-T. Zhu, Z.-H. Luo, *Chem. Eng. J.* **2016**, *287*, 474.
- [64] M. Onoda, T. Ueki, R. Tamate, A. M. Akimoto, C. C. Hall, T. P. Lodge, R. Yoshida, *ACS Macro Lett.* **2018**, *7*, 950.
- [65] A. S. Holehouse, R. V. Pappu, R. V. Pappu, *Nat. Mater.* **2015**, *14*, 1083.
- [66] L. Tang, L. Wang, X. Yang, Y. Feng, Y. Li, W. Feng, *Prog. Mater. Sci.* **2021**, *115*, 100702.
- [67] T. Kertsomboon, S. Agarwal, S. Chirachanchai, *Macromol. Rapid Commun.* **2020**, *41*, 2000243.
- [68] Y. Xu, O. Ghag, M. Reimann, P. Sitterle, P. Chatterjee, E. Nofen, H. Yu, H. Jiang, L. L. Dai, *Soft Matter* **2018**, *14*, 151.
- [69] M. Najafi, M. Habibi, R. Fokkink, W. E. Hennink, T. Vermonden, *Soft Matter* **2021**, *17*, 2132.
- [70] Q. Zhang, C. Weber, U. S. Schubert, R. Hoogenboom, *Mater. Horiz.* **2017**, *4*, 109.
- [71] B. A. Humphreys, S. W. Prescott, T. J. Murdoch, A. Nelson, E. P. Gilbert, G. B. Webber, E. J. Wanless, *Soft Matter* **2019**, *15*, 55.
- [72] J.-W. Jang, J.-H. Park, I.-J. Kim, J.-H. Sim, S.-G. Yu, D.-J. Lee, Y.-H. Lee, S.-H. Park, H.-D. Kim, *J. Appl. Polym. Sci.* **2021**, *138*, 49788.
- [73] Y. Guo, X. Dong, W. Ruan, Y. Shang, H. Liu, *Colloid Polym. Sci.* **2017**, *295*, 327.
- [74] I. V. Stokrov, S. S. Abramchuk, E. E. Makhaeva, *Colloid Polym. Sci.* **2019**, *297*, 387.

- [75] L. Frenzel, I. Lokteva, M. Koof, S. Narayanan, G. Grübel, F. Lehmkuhler, *ChemPhysChem* **2020**, *21*, 1318.
- [76] C. Zhao, Z. Ma, X. X. Zhu, *Prog. Polym. Sci.* **2019**, *90*, 269.
- [77] X. He, R. Zhou, C. Ge, Y. Ling, S. Luan, H. Tang, *Eur. Polym. J.* **2019**, *112*, 547.
- [78] S. Ashraf, H.-K. Park, H. Park, S.-H. Lee, *Macromol. Res.* **2016**, *24*, 297.
- [79] D. Kim, H. Kim, E. Lee, K. S. Jin, J. Yoon, *Chem. Mater.* **2016**, *28*, 8807.
- [80] J. Seuring, S. Agarwal, *Macromol. Rapid Commun.* **2012**, *33*, 1898.
- [81] A. Saad, R. Mills, H. Wan, M. A. Mottaleb, L. Ormsbee, D. Bhat-tacharyya, *J. Membr. Sci.* **2020**, *599*, 117821.
- [82] S. Sun, J. Hu, H. Tang, P. Wu, *J. Phys. Chem. B* **2010**, *114*, 9761.
- [83] M. Lehmann, P. Krause, V. Miruchna, R. Von Klitzing, *Colloid Polym. Sci.* **2019**, *297*, 633.
- [84] F. Pierini, A. Guglielmelli, O. Urbanek, P. Nakielski, L. Pezzi, R. Buda, M. Lanzi, T. A. Kowalewski, L. De Sio, *Adv. Opt. Mater.* **2020**, *8*, 2000324.
- [85] D. N. Rockwood, D. B. Chase, R. E. Akins, J. F. Rabolt, *Polymer* **2008**, *49*, 4025.
- [86] H. Okuzaki, K. Kobayashi, H. Yan, *Synth. Met.* **2009**, *159*, 2273.
- [87] Y. Konosu, H. Matsumoto, K. Tsuboi, M. Minagawa, A. Tanioka, *Langmuir* **2011**, *27*, 14716.
- [88] J. Wang, A. Sutti, X. Wang, T. Lin, *Soft Matter* **2011**, *7*, 4364.
- [89] W.-J. Chuang, W.-Y. Chiu, *Polymer* **2012**, *53*, 2829.
- [90] B.-Y. Chen, Y.-C. Lung, C.-C. Kuo, F.-C. Liang, T.-L. Tsai, D.-H. Jiang, T. Satoh, R.-J. Jeng, *Polymers* **2018**, *10*, 1259.
- [91] E. Niiyama, K. Uto, C. Lee, K. Sakura, M. Ebara, *Polymers* **2018**, *10*, 1018.
- [92] Y. Zhang, A. L. Yarin, *J. Mater. Chem.* **2009**, *19*, 4732.
- [93] H. Okuzaki, K. Kobayashi, F. Hishiki, S.-J. Su, H. Yan, *J. Nanosci. Nanotechnol.* **2011**, *11*, 5193.
- [94] L. Liu, H. Bakhshi, S. Jiang, H. Schmalz, S. Agarwal, *Macromol. Rapid Commun.* **2018**, *39*, 1800082.
- [95] Z. Wei, Q. Lin, J. Yang, S. Long, G. Zhang, X. Wang, *Mater. Sci. Eng.: C* **2020**, *115*, 111050.
- [96] N. A. Cortez-Lemus, A. Licea-Claverie, *Prog. Polym. Sci.* **2016**, *53*, 1.
- [97] E. González, M. W. Frey, *Polymer* **2017**, *108*, 154.
- [98] Z. Yu, H. Gu, D. Tang, H. Lv, Y. Ren, S. Gu, *RSC Adv.* **2015**, *5*, 64944.
- [99] F. Liu, S. Jiang, L. Ionov, S. Agarwal, *Polym. Chem.* **2015**, *6*, 2769.
- [100] A. C. B. Allen, E. Barone, C. O.' Crosby, L. J. Suggs, J. Zoldan, *Biomater. Sci.* **2017**, *5*, 1661.
- [101] S.-Y. Gu, Z.-M. Wang, J.-B. Li, J. Ren, *Macromol. Mater. Eng.* **2010**, *295*, 32.
- [102] F. Song, X.-L. Wang, Y.-Z. Wang, *Colloids Surf., B* **2011**, *88*, 749.
- [103] F. Sun, H.-T. Ren, T.-T. Li, S.-Y. Huang, Y. Zhang, C.-W. Lou, J.-H. Lin, *Environ. Res.* **2020**, *186*, 109494.
- [104] X. Lin, D. Tang, S. Gu, H. Du, E. Jiang, *New J. Chem.* **2013**, *37*, 2433.
- [105] X. Lin, D. Tang, Z. Yu, Q. Feng, *J. Mater. Chem. B* **2014**, *2*, 651.
- [106] P. Slemming-Adamsen, J. Song, M. Dong, F. Besenbacher, M. Chen, *Macromol. Mater. Eng.* **2015**, *300*, 1226.
- [107] C.-H. Huang, T.-H. Hsieh, W.-Y. Chiu, *Carbohydr. Polym.* **2015**, *116*, 249.
- [108] J. Wang, A. Sutti, X. Wang, T. Lin, *MRS Online Proc. Libr.* **2012**, *1403*, 143.
- [109] M. Webster, J. Miao, B. Lynch, D. Green, R. Jones-Sawyer, R. J. Linhardt, J. Mendenhall, *Macromol. Mater. Eng.* **2013**, *298*, 447.
- [110] F. A. A. Ruiter, L. E. Sidney, K. L. Kiick, J. I. Segal, C. Alexander, F. R. A. J. Rose, *Biomater. Sci.* **2020**, *8*, 2611.
- [111] Z. Mahdieh, A. Holian, *J. Appl. Polym. Sci.* **2020**, *137*, 49786.
- [112] S. Pawłowska, C. Rinoldi, P. Nakielski, Y. Ziai, O. Urbanek, X. Li, T. A. Kowalewski, B. Ding, F. Pierini, *Adv. Mater. Interfaces* **2020**, *7*, 2000247.
- [113] S. Kim, H. Choi, *ACS Sustainable Chem. Eng.* **2019**, *7*, 19870.
- [114] N. Thakur, A. Sargur Ranganath, K. Sopiha, A. Baji, *ACS Appl. Mater. Interfaces* **2017**, *9*, 29224.
- [115] M. Chen, M. Dong, R. Havelund, V. R. Regina, R. L. Meyer, F. Besenbacher, P. Kingshott, *Chem. Mater.* **2010**, *22*, 4214.
- [116] Q. Shi, J. Hou, X. Xu, J. Gao, C. Li, J. Jin, S.-C. Wong, J. Yin, *Adv. Mater. Interfaces* **2016**, *3*, 1500652.
- [117] H. Yang, Q. Zhang, B. Lin, G. Fu, X. Zhang, L. Guo, *J. Polym. Sci., Part A: Polym. Chem.* **2012**, *50*, 4182.
- [118] Y. Wang, C. Lai, H. Hu, Y. Liu, B. Fei, J. H. Xin, *RSC Adv.* **2015**, *5*, 51078.
- [119] A. E. Özçam, K. E. Roskov, J. Genzer, R. J. Spontak, *ACS Appl. Mater. Interfaces* **2012**, *4*, 59.
- [120] Y.-G. Ko, Y.-J. Kim, W. H. Park, D. Cho, H. Y. Chung, O. H. Kwon, *J. Biomater. Sci., Polym. Ed.* **2018**, *29*, 1026.
- [121] K. Arroub, I. Gessner, T. Fischer, S. Mathur, *Adv. Eng. Mater.* **2021**, *23*, 2100221.
- [122] P. Nakielski, S. Pawłowska, C. Rinoldi, Y. Ziai, L. De Sio, O. Urbanek, K. Zembrzycki, M. Pruchniewski, M. Lanzi, E. Salatelli, A. Calogero, T. A. Kowalewski, A. L. Yarin, F. Pierini, *ACS Appl. Mater. Interfaces* **2020**, *12*, 54328.
- [123] A. Evangelidis, M. Beregoi, V. C. Diculescu, A. Galatanu, P. Ganea, I. Enculescu, *Sci. Rep.* **2018**, *8*, 17555.
- [124] T. Chen, H. Bakhshi, L. Liu, J. Ji, S. Agarwal, *Adv. Funct. Mater.* **2018**, *28*, 1800514.
- [125] Y.-J. Kim, M. Ebara, T. Aoyagi, *Angew. Chem., Int. Ed.* **2012**, *51*, 10537.
- [126] L. Deng, *Int. J. Electrochem. Sci.* **2018**, *13*, 7347.
- [127] H. Guo, J. H. Jeong, J.-C. Kim, *Colloids Surf., A* **2016**, *495*, 1.
- [128] Y.-J. Kim, M. Ebara, T. Aoyagi, *Adv. Funct. Mater.* **2013**, *23*, 5753.
- [129] X. J. Loh, P. Peh, S. Liao, C. Sng, J. Li, *J. Controlled Release* **2010**, *143*, 175.
- [130] P. Tzeng, C.-C. Kuo, S.-T. Lin, Y.-C. Chiu, W.-C. Chen, *Macromol. Chem. Phys.* **2010**, *211*, 1408.
- [131] H.-J. Lin, C.-Y. Chen, *J. Mater. Sci.* **2016**, *51*, 1620.
- [132] W. C. Wu, H. J. Lai, *J. Polym. Res.* **2016**, *23*, 223.
- [133] J. Li, C. Peng, Z. Wang, J. Ren, *RSC Adv.* **2018**, *8*, 17551.
- [134] A. Lendlein, S. Kelch, *Angew. Chem., Int. Ed.* **2002**, *41*, 2034.
- [135] Y. Xia, Y. He, F. Zhang, Y. Liu, J. Leng, *Adv. Mater.* **2021**, *33*, 2000713.
- [136] F. Zhang, Z. Zhang, T. Zhou, Y. Liu, J. Leng, *Front. Mater.* **2015**, *2*, 62.
- [137] Y. Yao, Y. Xu, B. Wang, W. Yin, H. Lu, *Pigm. Resin Technol.* **2017**, *47*, 47.
- [138] X. Luo, P. T. Mather, *Curr. Opin. Chem. Eng.* **2013**, *2*, 103.
- [139] J. Hui, H. Xia, H. Chen, Y. Qiu, Y. Fu, Q.-Q. Ni, *Mater. Lett.* **2020**, *258*, 126762.
- [140] L. F. Fan, M. Z. Rong, M. Q. Zhang, X. D. Chen, *Macromol. Rapid Commun.* **2018**, *39*, 1700714.
- [141] D. I. Cha, H. Y. Kim, K. H. Lee, Y. C. Jung, J. W. Cho, B. C. Chun, *J. Appl. Polym. Sci.* **2005**, *96*, 460.
- [142] H. Zhuo, J. Hu, S. Chen, *Mater. Lett.* **2008**, *62*, 2074.
- [143] S. E. Chung, C. H. Park, W.-R. Yu, T. J. Kang, *J. Appl. Polym. Sci.* **2011**, *120*, 492.
- [144] F. Zhang, Z. Zhang, Y. Liu, J. Leng, *Proc. SPIE* **2013**, *8687*, 86871Y.
- [145] T. Sauter, K. Kratz, M. Heuchel, A. Lendlein, *Mater. Des.* **2021**, *202*, 109546.
- [146] A. Leonés, A. Sonseca, D. López, S. Fiori, L. Peponi, *Eur. Polym. J.* **2019**, *117*, 217.
- [147] H. Matsumoto, T. Ishiguro, Y. Konosu, M. Minagawa, A. Tanioka, K. Richau, K. Kratz, A. Lendlein, *Eur. Polym. J.* **2012**, *48*, 1866.
- [148] D. Kai, M. P. Prabhakaran, B. Q. Yu Chan, S. S. Liow, S. Ramakrishna, F. Xu, X. J. Loh, *Biomed. Mater.* **2016**, *11*, 015007.
- [149] M. Bao, X. Lou, Q. Zhou, W. Dong, H. Yuan, Y. Zhang, *ACS Appl. Mater. Interfaces* **2014**, *6*, 2611.
- [150] L. Tan, L. Gan, J. Hu, Y. Zhu, J. Han, *Composites, Part A* **2015**, *76*, 115.
- [151] Q. Peng, J. Cheng, S. Lu, Y. Li, *Polym. Adv. Technol.* **2020**, *31*, 15.

- [152] D. Kai, M. J. Tan, M. P. Prabhakaran, B. Q. Y. Chan, S. S. Liow, S. Ramakrishna, X. J. Loh, *Colloids Surf., B* **2016**, *148*, 557.
- [153] S. Rana, J. W. Cho, *Fibers Polym.* **2011**, *12*, 721.
- [154] H. T. Zhuo, J. L. Hu, S. J. Chen, H. T. Hu, J. L. Chen, *eXPRESS Polym. Lett.* **2011**, *5*, 182.
- [155] Q. Zhang, K. Kratz, A. Lendlein, *Polym. Adv. Technol.* **2015**, *26*, 1468.
- [156] A. Merletтини, S. Pandini, S. Agnelli, C. Gualandi, K. Paderni, M. Messori, M. Toselli, M. L. Focarete, *RSC Adv.* **2016**, *6*, 43964.
- [157] H. Chen, X. Cao, J. Zhang, J. Zhang, Y. Ma, G. Shi, Y. Ke, D. Tong, L. Jiang, *J. Mater. Chem.* **2012**, *22*, 22387.
- [158] W. Kuang, P. T. Mather, *J. Mater. Res.* **2018**, *33*, 2463.
- [159] A. Iregui, L. Irusta, O. Llorente, L. Martin, T. Calvo-Correas, A. Eceiza, A. González, *Eur. Polym. J.* **2017**, *94*, 376.
- [160] A. Iregui, L. Irusta, L. Martin, A. González, *Polymers* **2019**, *11*, 475.
- [161] F. Zhang, Z. Zhang, Y. Liu, W. Cheng, Y. Huang, J. Leng, *Composites, Part A* **2015**, *76*, 54.
- [162] A. Shirole, J. Sapkota, E. J. Foster, C. Weder, *ACS Appl. Mater. Interfaces* **2016**, *8*, 6701.
- [163] J. M. Robertson, H. Birjandi Nejad, P. T. Mather, *ACS Macro Lett.* **2015**, *4*, 436.
- [164] H. B. Nejad, J. M. Robertson, P. T. Mather, *MRS Commun.* **2015**, *5*, 211.
- [165] Y. Yao, H. Wei, J. Wang, H. Lu, J. Leng, D. Hui, *Composites, Part B* **2015**, *83*, 264.
- [166] S. Budun, E. İsgören, R. Erdem, M. Yükses, *Appl. Surf. Sci.* **2016**, *380*, 294.
- [167] S. Banikazemi, M. Rezaei, P. Rezaei, A. Babaie, A. Eyvazzadeh-Kalajahi, *Polym. Adv. Technol.* **2020**, *31*, 2199.
- [168] A. Nissenbaum, I. Greenfeld, H. D. Wagner, *Polymer* **2020**, *190*, 122226.
- [169] D. Alhazov, C. Azra, E. Zussman, *J. Polym. Sci., Part B: Polym. Phys.* **2015**, *53*, 1590.
- [170] Y. Yao, Y. Luo, H. Lu, B. Wang, *Compos. Struct.* **2018**, *192*, 507.
- [171] M. Zare, N. Parvin, M. P. Prabhakaran, J. A. Mohandesi, S. Ramakrishna, *Compos. Sci. Technol.* **2019**, *184*, 107874.
- [172] T. Gong, W. Li, H. Chen, L. Wang, S. Shao, S. Zhou, *Acta Biomaterialia* **2012**, *8*, 1248.
- [173] F. Zhang, Y. Xia, L. Wang, L. Liu, Y. Liu, J. Leng, *ACS Appl. Mater. Interfaces* **2018**, *10*, 35526.
- [174] F. Zhang, Z. Zhang, Y. Liu, J. Leng, *Smart Mater. Struct.* **2014**, *23*, 065020.
- [175] H. Lu, Y. Yao, J. Yin, L. Lin, *Pigm. Resin Technol.* **2016**, *45*, 93.
- [176] M. Fejős, K. Molnár, J. Karger-Kocsis, *Materials* **2013**, *6*, 4489.
- [177] M. Sabzi, M. Ranjbar-Mohammadi, Q. Zhang, S. Kargoaz, J. Leng, T. Akhtari, R. Abbasi, *J. Appl. Polym. Sci.* **2019**, *136*, 47471.
- [178] S. L. Buffington, B. M. Posnick, J. Paul, P. T. Mather, *ChemPhysChem* **2018**, *19*, 2014.
- [179] Y. Liu, O. E. C. Gould, K. Kratz, A. Lendlein, *MRS Adv.* **2020**, *546*, 2391.
- [180] S. Pandini, S. Agnelli, A. Merletтини, F. Chiellini, C. Gualandi, K. Paderni, M. L. Focarete, M. Messori, M. Toselli, *Macromol. Mater. Eng.* **2017**, *302*, 1600519.
- [181] J.-S. Ahn, W.-R. Yu, J. H. Youk, H. Y. Ryu, *Smart Mater. Struct.* **2011**, *20*, 105024.
- [182] Q. Zhang, T. Rudolph, A. J. Benitez, O. E. C. Gould, M. Behl, K. Kratz, A. Lendlein, *Smart Mater. Struct.* **2019**, *28*, 055037.
- [183] M. Zare, P. Davoodi, S. Ramakrishna, *Nanomaterials* **2021**, *11*, 933.
- [184] M. Bao, X. Wang, H. Yuan, X. Lou, Q. Zhao, Y. Zhang, *J. Mater. Chem. B* **2016**, *4*, 5308.
- [185] Q. Zhao, J. Wang, H. Cui, H. Chen, Y. Wang, X. Du, *Adv. Funct. Mater.* **2018**, *28*, 1801027.
- [186] J. Wang, H. Xiong, T. Zhu, Y. Liu, H. Pan, C. Fan, X. Zhao, W. W. Lu, *ACS Nano* **2020**, *14*, 12579.
- [187] C. Chen, J. Hu, H. Huang, Y. Zhu, T. Qin, *Adv. Mater. Technol.* **2016**, *1*, 1600015.
- [188] L.-F. Tseng, P. T. Mather, J. H. Henderson, *Acta Biomater.* **2013**, *9*, 8790.
- [189] E. Niiyama, K. Tanabe, K. Uto, A. Kikuchi, M. Ebara, *Fibers* **2019**, *7*, 20.
- [190] M. Chen, L. Li, L. Xia, F. Zhang, S. Jiang, H. Hu, X. Li, H. Wang, *Macromol. Biosci.* **2020**, *20*, 1900312.
- [191] C. Wang, H. Yue, Q. Feng, B. Xu, L. Bian, P. Shi, *ACS Appl. Mater. Interfaces* **2018**, *10*, 29299.
- [192] H. Lv, D. Tang, Z. Sun, J. Gao, X. Yang, S. Jia, J. Peng, *Colloid Polym. Sci.* **2019**, *298*, 103.
- [193] M. Bil, E. Kijeńska-Gawrońska, E. Głodkowska-Mrówka, A. Manda-Handzlik, P. Mrówka, *Mater. Sci. Eng., C* **2020**, *110*, 110675.
- [194] X. Yin, P. Tan, H. Luo, J. Lan, Y. Shi, Y. Zhang, H. Fan, L. Tan, *Mater. Sci. Eng., C* **2020**, *109*, 110541.
- [195] L. Tan, J. Hu, H. Huang, J. Han, H. Hu, *Int. J. Biol. Macromol.* **2015**, *79*, 469.
- [196] W. Feng, Y.-S. Zhang, Y.-W. Shao, T. Huang, N. Zhang, J.-H. Yang, X.-D. Qi, Y. Wang, *Eur. Polym. J.* **2021**, *145*, 110245.
- [197] Y. Yao, J. Wang, H. Lu, B. Xu, Y. Fu, Y. Liu, J. Leng, *Smart Mater. Struct.* **2015**, *25*, 015021.
- [198] H. Birjandi Nejad, K. L. Garrison, P. T. Mather, *J. Polym. Sci., Part B: Polym. Phys.* **2016**, *54*, 1415.
- [199] N. Khalili, H. Asif, H. E. Naguib, *Smart Mater. Struct.* **2018**, *27*, 055002.
- [200] J. Xiong, H. Luo, D. Gao, X. Zhou, P. Cui, G. Thangavel, K. Parida, P. S. Lee, *Nano Energy* **2019**, *61*, 584.
- [201] A. Seeboth, D. Lötzsche, R. Ruhmann, O. Muehling, *Chem. Rev.* **2014**, *114*, 3037.
- [202] R. Li, F.-F. Xu, Z.-L. Gong, Y.-W. Zhong, *Inorg. Chem. Front.* **2020**, *7*, 3258.
- [203] M. M. Ogle, A. D. Smith McWilliams, B. Jiang, A. A. Martí, *ChemPhotoChem* **2020**, *4*, 255.
- [204] A. Abdollahi, H. Roghani-Mamaqani, B. Razavi, M. Salami-Kalajahi, *ACS Nano* **2020**, *14*, 14417.
- [205] Q. Zhang, Y. Jiang, L. Chen, W. Chen, J. Li, Y. Cai, C. Ma, W. Xu, Y. Lu, X. Jia, Z. Bao, *Adv. Funct. Mater.* **2021**, *31*, 2100686.
- [206] K. Y. Fang, Y. J. Wang, Y. C. Zhao, F. Fang, *Compos. Sci. Technol.* **2021**, *201*, 108483.
- [207] S. Li, Y. Li, K. Qian, S. Ji, H. Luo, Y. Gao, P. Jin, *ACS Appl. Mater. Interfaces* **2013**, *6*, 9.
- [208] S. Lee, J. Lee, H. N. Kim, M. H. Kim, J. Yoon, *Sens. Actuators, B* **2012**, *173*, 419.
- [209] O. Mapazi, K. P. Matabola, R. M. Moutloali, C. J. Ngila, *Polymer* **2018**, *149*, 106.
- [210] M. L. De Oliveira Peres, E. T. Wanderley Neto, A. A. A. E. De Queiroz, A. A. A. De Queiroz, *IEEE Sens. Lett.* **2021**, 2000304.
- [211] I. Malherbe, R. D. Sanderson, E. Smit, *Polymer* **2010**, *51*, 5037.
- [212] S. Wang, L. Yi, Y. Fang, L. Wang, J. Yao, J. Marek, M. Zhang, *J. Appl. Polym. Sci.* **2021**, *138*, 50465.
- [213] Y. He, S. Sun, N. Han, X. Zhang, W. Li, *J. Mater. Sci.* **2020**, *55*, 12921.
- [214] E. Enz, J. Lagerwall, *J. Mater. Chem.* **2010**, *20*, 6866.
- [215] E. Enz, V. La Ferrara, G. Scalia, *ACS Nano* **2013**, *7*, 6627.
- [216] M. J. Bertocchi, D. C. Ratchford, R. Casalini, J. H. Wynne, J. G. Lundin, *J. Phys. Chem. C* **2018**, *122*, 16964.
- [217] J. Nguyen, R. M. Stwodah, C. L. Vasey, B. E. Rabatin, B. Atherton, P. A. D'angelo, K. W. Swana, C. Tang, *Polymers* **2020**, *12*, 842.
- [218] L.-N. Chen, C.-C. Kuo, Y.-C. Chiu, W.-C. Chen, *RSC Adv.* **2014**, *4*, 45345.
- [219] L.-N. Chen, N.-K. Weng, W.-C. Wu, W.-C. Chen, *Mater. Chem. Phys.* **2015**, *163*, 63.
- [220] F.-C. Liang, Y.-L. Luo, C.-C. Kuo, B.-Y. Chen, C.-J. Cho, F.-J. Lin, Y.-Y. Yu, R. Borsali, *Polymers* **2017**, *9*, 136.

- [221] A. Sharma, V. V. Tyagi, C. R. Chen, D. Buddhi, *Renewable Sustainable Energy Rev.* **2009**, *13*, 318.
- [222] E. M. Shchukina, M. Graham, Z. Zheng, D. G. Shchukin, *Chem. Soc. Rev.* **2018**, *47*, 4156.
- [223] Y. Wu, C. Chen, Y. Jia, J. Wu, Y. Huang, L. Wang, *Appl. Energy* **2018**, *210*, 167.
- [224] M. F. Demirbas, *Energy Sources, Part B* **2006**, *1*, 85.
- [225] K. Faraj, M. Khaled, J. Faraj, F. Hachem, C. Castelain, *Renewable Sustainable Energy Rev.* **2020**, *119*, 109579.
- [226] C. Liu, Z. Rao, J. Zhao, Y. Huo, Y. Li, *Nano Energy* **2015**, *13*, 814.
- [227] J. T. Mccann, M. Marquez, Y. Xia, *Nano Lett.* **2006**, *6*, 2868.
- [228] C. Chen, L. Wang, Y. Huang, *Polymer* **2007**, *48*, 5202.
- [229] L. Yi, Y. Wang, Y. Fang, M. Zhang, J. Yao, L. Wang, J. Marek, *RSC Adv.* **2019**, *9*, 21844.
- [230] F. Haghighat, S. A. Hosseini Ravandi, M. Nasr Esfahany, A. Valipouri, *J. Mater. Sci.* **2017**, *53*, 4665.
- [231] Y. Lu, X. Xiao, Y. Zhan, C. Huan, S. Qi, H. Cheng, G. Xu, *ACS Appl. Mater. Interfaces* **2018**, *10*, 12759.
- [232] L. Zhao, J. Luo, Y. Li, H. Wang, G. Song, G. Tang, *J. Appl. Polym. Sci.* **2017**, *134*, 45538.
- [233] W. Chalco-Sandoval, M. J. Fabra, A. López-Rubio, J. M. Lagaron, *Eur. Polym. J.* **2015**, *72*, 23.
- [234] W. Chalco-Sandoval, M. J. Fabra, A. López-Rubio, J. M. Lagaron, *J. Food Eng.* **2017**, *192*, 122.
- [235] P. Lu, W. Chen, J. Fan, R. Ghaban, M. Zhu, *ACS Sustainable Chem. Eng.* **2018**, *6*, 2656.
- [236] B. Hemmatian, N. Heidarzadeh, G. C. Fard, L. Maleknia, *Mater. Chem. Phys.* **2020**, *245*, 122738.
- [237] N. Xie, J. Niu, X. Gao, Y. Fang, Z. Zhang, *Int. J. Energy Res.* **2020**, *44*, 8567.
- [238] H. Ke, Q. Wei, *Polym. Eng. Sci.* **2019**, *59*, E403.
- [239] H. Ke, Q. Wei, *Thermochim. Acta* **2019**, *671*, 10.
- [240] M. E. Darzi, S. I. Golestaneh, M. Kamali, G. Karimi, *Renewable Energy* **2019**, *135*, 719.
- [241] T. T. Dang, T. T. T. Nguyen, O. H. Chung, J. S. Park, *Macromol. Res.* **2015**, *23*, 819.
- [242] Z. Esmailzadeh, B. Rezaei, A. Mousavi Shoushtari, M. R. M. Mojtaheidi, *Adv. Polym. Technol.* **2018**, *37*, 185.
- [243] C. Chen, K. Liu, H. Wang, W. Liu, H. Zhang, *Sol. Energy Mater. Sol. Cells* **2013**, *117*, 372.
- [244] A. Babapoor, G. Karimi, S. I. Golestaneh, M. A. Mezjin, *Appl. Therm. Eng.* **2017**, *118*, 398.
- [245] R. B. Yilmaz, G. Bayram, U. Yilmazer, *Thermochim. Acta* **2020**, *690*, 178673.
- [246] S. Song, H. Ai, W. Zhu, F. Qiu, Y. Wang, J. Zhou, *Renewable Energy* **2020**, *148*, 504.
- [247] E. Baştürk, D. Yüksel Deniz, M. V. Kahraman, *J. Macromol. Sci., Part A: Pure Appl. Chem.* **2019**, *56*, 708.
- [248] L. Zhou, F. Shi, G. Liu, J. Ye, P. Han, G. Zhang, *Sol. Energy* **2021**, *213*, 339.
- [249] E. Onder, N. Sarier, *Thermochim. Acta* **2020**, *690*, 178698.
- [250] C. Lin, W. Li, Y. Yan, H. Ke, Z. Liu, L. Deng, Z. Qiu, *Sol. Energy Mater. Sol. Cells* **2021**, *223*, 110953.
- [251] D. K. C. MacDonald, *Thermoelectricity: An Introduction to the Principles*, John Wiley & Sons, Inc., New York **1962**.
- [252] X. Lu, D. T. Morelli, Y. Xia, F. Zhou, V. Ozolins, H. Chi, X. Zhou, C. Uher, *Adv. Energy Mater.* **2013**, *3*, 342.
- [253] (Eds: T. Mele, P. Narducci, D. Ohta, M. Biswas, K. Morante, J. Saini, S. Endo), *Thermoelectric Thin Films*, Springer International Publishing, Berlin **2019**.
- [254] C. J. Vineis, A. Shakouri, A. Majumdar, M. G. Kanatzidis, *Adv. Mater.* **2010**, *22*, 3970.
- [255] M. S. Dresselhaus, G. Chen, M. Y. Tang, R. G. Yang, H. Lee, D. Z. Wang, Z. F. Ren, J.-P. Fleurial, P. Gogna, *Adv. Mater.* **2007**, *19*, 1043.
- [256] L. D. Hicks, M. S. Dresselhaus, *Phys. Rev. B: Condens. Matter Mater. Phys.* **1993**, *47*, 16631.
- [257] Y. Tian, M. R. Sakr, J. M. Kinder, D. Liang, M. J. Macdonald, R. L. J. Qiu, H.-J. Gao, X. P. A. Gao, *Nano Lett.* **2012**, *12*, 6492.
- [258] Z. Dong, S. J. Kennedy, Y. Wu, *J. Power Sources* **2011**, *196*, 4886.
- [259] Z. Qiu, J. Pei, G. Chen, C. Lv, Y. Zhang, Y. Yu, Q. Zhang, *Mater. Lett.* **2015**, *158*, 182.
- [260] W. Xu, Y. Shi, H. Hadim, *Nanotechnology* **2010**, *21*, 395303.
- [261] W. Xu, E. Nazaretski, M. Lu, H. Hadim, Y. Shi, *Nano Res.* **2014**, *78*, 1224.
- [262] D. Lee, K. Cho, J. Choi, S. Kim, *Mater. Lett.* **2015**, *142*, 250.
- [263] Z. H. Dughaiash, *Phys. B: Condens. Matter* **2002**, *322*, 205.
- [264] M. Zhang, S.-D. Park, J. Kim, M. Nalbandian, S. Kim, Y. Choa, J. Lim, N. V. Myung, *Front. Chem.* **2018**, *6*, 436.
- [265] K.-R. Park, H.-B. Cho, Y. Song, S. Kim, Y.-T. Kwon, S. H. Ryu, J.-H. Lim, W.-J. Lee, Y.-H. Choa, *Appl. Surf. Sci.* **2018**, *436*, 785.
- [266] H. Wang, Y. Pei, A. D. Lalonde, G. J. Snyder, *Adv. Mater.* **2011**, *23*, 1366.
- [267] M. Zhang, J. Kim, S. Kim, H. Park, H. Jung, N. G. Ndifor-Angwafor, J. Lim, Y. Choa, N. V. Myung, *Chem. Mater.* **2014**, *26*, 2557.
- [268] M. A. Kamarudin, S. R. Sahamir, R. S. Datta, B. D. Long, M. F. Mohd Sabri, S. Mohd Said, *Sci. World J.* **2013**, *2013*, 713640.
- [269] O. Bubnova, Z. U. Khan, H. Wang, S. Braun, D. R. Evans, M. Faretto, P. Hojati-Talemi, D. Dagnelund, J.-B. Arlin, Y. H. Geerts, S. Desbief, D. W. Breiby, J. W. Andreasen, R. Lazzaroni, W. M. Chen, I. Zozoulenko, M. Fahlman, P. J. Murphy, M. Berggren, X. Crispin, *Nat. Mater.* **2014**, *13*, 190.
- [270] L. Persano, A. Camposeo, D. Pisignano, *Prog. Polym. Sci.* **2015**, *43*, 48.
- [271] Q. Wang, Q. Yao, J. Chang, L. Chen, *J. Mater. Chem.* **2012**, *22*, 17612.
- [272] N. Dalton, R. P. Lynch, M. N. Collins, M. Culebras, *Int. J. Biol. Macromol.* **2019**, *121*, 472.
- [273] M. P. Subramaniam, P. Veluswamy, A. Satheesh, G. Arunachalam, R. Kandaswamy, B. J. Cho, A. Alagiriswamy, *J. Sol-Gel Sci. Technol.* **2021**, *98*, 183.
- [274] K. M. Ryu, Y. H. Kang, S. Y. Cho, S. H. Lee, Y. C. Choi, M. S. Kim, Y. G. Jeong, *Sci. Rep.* **2020**, *10*, 9633.
- [275] A. Mohammadi, A. Valipouri, S. Salimian, *Diamond Relat. Mater.* **2018**, *86*, 54.
- [276] C. R. Bowen, J. Taylor, E. Leboulbar, D. Zabek, A. Chauhan, R. Vaish, *Energy Environ. Sci.* **2014**, *7*, 3836.
- [277] W. H. Clingman, R. G. Moore Jr, *J. Appl. Phys.* **2004**, *32*, 675.
- [278] A. Van Der Ziel, *J. Appl. Phys.* **2003**, *45*, 4128.
- [279] J. D. Childress, *J. Appl. Phys.* **2004**, *33*, 1793.
- [280] S. B. Lang, *Phys. Today* **2007**, *58*, 31.
- [281] J. Fang, X. Wang, T. Lin, *J. Mater. Chem.* **2011**, *21*, 11088.
- [282] S. Garain, S. Jana, T. K. Sinha, D. Mandal, *ACS Appl. Mater. Interfaces* **2016**, *8*, 4532.
- [283] C.-M. Wu, M.-H. Chou, T. F. Chala, Y. Shimamura, R.-I. Murakami, R. ichi Murakami, *Compos. Sci. Technol.* **2019**, *178*, 26.
- [284] K. Roy, S. K. Ghosh, A. Sultana, S. Garain, M. Xie, C. R. Bowen, K. Henkel, D. Schmeißer, D. Mandal, *ACS Appl. Nano Mater.* **2019**, *2*, 2013.
- [285] D. Isakov, E. De Matos Gomes, B. Almeida, A. L. Kholkin, P. Zelenovskiy, M. Neradovskiy, V. Y. Shur, *Appl. Phys. Lett.* **2014**, *104*, 032907.
- [286] E. De Matos Gomes, T. Viseu, M. Belsley, B. Almeida, M. M. R. Costa, V. H. Rodrigues, D. Isakov, *Mater. Res. Express* **2018**, *5*, 045049.
- [287] J. F. Nye, *Physical Properties of Crystals: Their Representation by Tensors and Matrices*, Oxford University Press, Oxford **2006**.
- [288] R. L. Byer, C. B. Roundy, *IEEE Trans. Sonics Ultrason.* **1972**, *19*, 333.

[289] M. Abbasipour, R. Khajavi, A. A. Yousefi, M. E. Yazdanshenas, F. Razaghian, A. Akbarzadeh, *Polym. Adv. Technol.* **2019**, *30*, 279.

[290] A. Sultana, S. K. Ghosh, M. M. Alam, P. Sadhukhan, K. Roy, M. Xie, C. R. Bowen, S. Sarkar, S. Das, T. R. Middy, D. Mandal, D. Mandal, *ACS Appl. Mater. Interfaces* **2019**, *11*, 27279.



Anna Liguori worked as postdoctoral researcher at the University of Bologna from January 2016 to September 2021. From September 2021 she is a Marie Skłodowska Curie Individual Fellow at KTH Royal Institute of Technology, Stockholm. Her research interests include the functional modification of polymeric materials by means of atmospheric pressure nonequilibrium plasma assisted processes; the electrospinning technology; green strategies for the synthesis of organic and inorganic coatings onto the surface of polymeric nanofibers; the thermal, chemical, and morphological characterization of polymeric materials. She is actually working on green approaches for the synthesis of bio-based self-healing and recyclable thermosets.



Stefano Pandini is associate professor at the University of Brescia. He received his Ph.D. in Materials Engineering at the University of Trento with a thesis entitled “Time-temperature correlation on deformation, yielding and fracture phenomena in thermoplastic polymers for engineering applications.” His field of research regards various aspects of the mechanical and functional behavior of polymers and composites, among which particular interest is reserved towards the investigation of the shape memory response of polymer-based systems.



Chiara Rinoldi received her M.Sc. degree in Biomedical Engineering from Politecnico di Milano, Italy in 2014, and her Ph.D. degree in Materials Science and Engineering from Warsaw University of Technology, Poland in 2020. In 2019, she has joined the Department of Biosystems and Soft Matter at the Institute of Fundamental Technological Research, Polish Academy of Sciences, Poland; where she is an assistant professor since 2020. Her research interests include the investigation of conductive and light-responsive hydrogels and fiber-based scaffolds for tissue engineering and drug delivery. Her activities also involve cell isolation and differentiation, as well as evaluation of cell-material interactions.



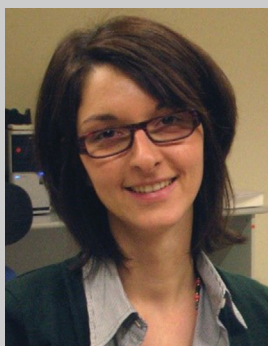
Nelsi Zaccheroni got her Master degree in Chemistry and Ph.D. (1997) in Chemical Sciences at the University of Bologna (Italy), where she is now associate professor in General and Inorganic Chemistry. She was postdoctoral fellow within a TMR-CEE project at the University College of Dublin (Ireland, 1997–98) and visiting professor in Australia and Canada. Her research focuses on luminescent systems for imaging and sensing, spanning from molecular to nanostructured materials, including stimuli responsive polymers, for biomedical and environmental applications.



Filippo Pierini is a professor and the head of the Pierini Research Group at the Institute of Fundamental Technological Research (IPPT PAN). He received his M.Sc. in Advanced Chemical Methodologies with the highest grades and honors (110/110 summa cum laude) in 2009, and his Ph.D. in Chemical Sciences at the University of Bologna (Italy) in 2013. His research interests include biomaterials, drug delivery, light-matter interaction, and the development of functional fibrous nanomaterials.



Maria Letizia Focarete received her M.S., and Ph.D. degrees from the University of Bologna in 1995 and 2000, respectively. She is currently full professor of Science and Technology of Polymeric Materials at the University of Bologna, where she leads the Polymer Science and Biomaterials research group. Her academic research interests include polymers for biomedical applications, hydrogels for 3D-bioprinting, innovative bioinspired scaffolds for tissue engineering and drug delivery, stimuli-responsive and smart, functional polymeric materials, bioplastics, and electrospinning technology.



Chiara Gualandi received her Ph.D. degree in Industrial Chemistry in 2010 from the University of Bologna. She worked as post-doc at the Advanced Mechanics and Materials Interdepartmental Center for Industrial Research of the University of Bologna. Currently, she is associate professor at the Chemistry Department (G. Ciamician), Bologna, Italy. Her research interests span from polymers for biomedical applications, where the technology of electrospinning is exploited to develop innovative nanostructure scaffolds, to stimuli-responsive and functional polymers, including mechano-responsive materials, thermoreversible polymeric systems and shape-memory polymers.